McDermott Technology, Inc.
Research and Development Division
Alliance, Ohio

Phase 1 Final Report for In-Situ Tritium Beta Detector

Prepared for:

U.S. Department of Energy

Prepared by:

J. W. Berthold
L. A. Jeffers
Research and Development Division
1562 Beeson St.
Alliance, Ohio 44601

Contract No. DE-AC21-96MC33128
Reporting Period Sept. 30, 1996 – March 31, 1998 April 15, 1998

Disclaimer

ABSTRACT

The objectives of this three-phase project were to design, develop, and demonstrate a monitoring system capable of detecting and quantifying tritium *in situ* in ground and surface waters, and in water from effluent lines prior to discharge into public waterways. The tritium detection system design is based on measurement of the low energy beta radiation from the radioactive decay of tritium using a special form of scintillating optical fiber directly in contact with the water to be measured. The system consists of the immersible sensor module containing the optical fiber, and an electronics package, connected by an umbilical cable. The system can be permanently installed for routine water monitoring in wells or process or effluent lines, or can be moved from one location to another for survey use. The electronics will read out tritium activity directly in units of pico Curies per liter, with straightforward calibration.

In Phase 1 of the project, we characterized the sensitivity of fluor-doped plastic optical fiber to tritium beta radiation. In addition, we characterized the performance of photomultiplier tubes needed for the system. In parallel with this work, we defined the functional requirements, target specifications, and system configuration for an *in situ* tritium beta detector that would use the fluor-doped fibers as primary sensors of tritium concentration in water. The major conclusions from the characterization work are:

A polystyrene optical fiber with fluor dopant concentration of 2% gave best performance. This fiber had the highest dopant concentration of any fibers tested.

Stability may be a problem. The fibers exposed to a 22-day soak in 120°F water experienced a 10x reduction in sensitivity. It is not known whether this was due to the build up of a deposit (a potentially reversible effect) or an irreversible process such as leaching of the scintillating dye.

Based on the results achieved, it is premature to initiate Phase 2 and commit to a prototype design for construction and test. Significant improvements must be made in fluor-doped fiber performance in order to use the method for *in situ* monitoring to verify compliance with current EPA drinking water standards. Additional Phase 1 fiber development work should be performed to increase the fluor dopant concentration above 2% until the self-absorption limit is observed. Continued fiber optimization work is expected to improve the sensitivity limits, and will enable application of the detector to verify compliance with the US EPA drinking water standard of 20,000 pico Curies per liter. However, if the need for monitoring higher levels of tritium in water at concentrations greater than 200,000 pico Curies per liter is justified, then prototype development and testing could proceed either as a Phase 2 stand-alone effort or in parallel with continued Phase 1 development work.

EXECUTIVE SUMMARY

NEED ADDRESSED

In the DOE complex, tritium (^3H) is one of the most commonly occurring radionuclide contaminants in ground, surface, and process effluent waters. This project addresses the need to continually monitor such waters for the presence and activity of tritium. Such monitoring is normally performed to demonstrate compliance with U.S. Environmental Protection Agency (EPA) regulations, DOE orders or other regulations, and to track the movement of tritium contaminated plumes in ground water. The present approach to this measurement is to sample water from a monitoring well, and send the sample to a laboratory for analysis, usually with liquid scintillation counting. This analysis method has good detection capability and precision. However the sampling, chain-of-custody paperwork and lab analysis are labor intensive and expensive, and there is frequently a long analysis turnaround time. Sampling and analysis must be performed at regular intervals to determine if and when changes have occurred, even when changes have not occurred, further increasing monitoring costs.

OBJECTIVES

The objectives of the three-phase program being conducted by McDermott Technology, Inc. (MTI) and B&W Services, Inc., (formerly Nuclear Environmental Services, Inc./NESI) are to design, develop, demonstrate and deliver a monitoring system capable of detecting and quantifying tritium *in situ* in ground and surface waters, and in water from effluent lines prior to discharge into public waterways. To meet these objectives with a system which is faster, better and cheaper than currently available methods, target characteristics of the tritium beta detector include:

- Compact, immersible sensor
- Large wetted sensor surface area
- High sensitivity to ^3H
- High specificity to ^3H
- Near real-time response
- Rugged, integrated electronics

This report summarizes project work completed in Phase 1 of the program.

DESCRIPTION OF TECHNOLOGY

The tritium detection system is based on measurement of the low energy beta radiation from the radioactive decay of tritium using a special form of scintillating optical fiber directly in contact with the water to be measured. The system consists of the immersible sensor module containing the optical fiber, and an electronics package, connected by an umbilical cable. The system can be permanently installed for routine water monitoring in wells or process or effluent

lines, or can be moved from one location to another for survey use. The electronics will read out tritium activity directly in units of pCi/L, with straightforward calibration. Compared to alternate methods of tritium detection and quantification, the proposed Tritium Beta Detector is:

- Faster: The use of this technology eliminates a significant portion of the time for sampling, chain-of-custody, and laboratory turnaround.
- Better: In situ monitoring permits measurements on demand, allowing more frequent measurements and identifying activity changes sooner.
- Cheaper: Costs associated with sampling protocols, sampling, chain-of-custody, shipping and laboratory analysis are significantly reduced.
- Safer: Likelihood of excursions over release limits is reduced, personnel exposure dose is reduced, and changes in activity are detected more quickly.

PHASE 1 PROJECT SUMMARY AND STATUS

In Phase 1 of the project, we characterized the sensitivity of fluor-doped plastic optical fiber to tritium beta radiation. In addition, we characterized the performance of photomultiplier tubes needed for the system. In parallel with this work, we have defined the functional requirements, target specifications, and system configuration for an in-situ tritium beta detector that would use the fluor-doped fibers as primary sensors of tritium concentration in water. The conclusions from the characterization work are summarized as follows:

– A polystyrene optical fiber with fluor dopant on the outside surface of the fiber performs better than a fiber that consists of a doped polystyrene core and polymethylmethacrylate (PMMA) clad.

– A polystyrene optical fiber with fluor dopant concentration of 2% gave best performance. This fiber had the highest dopant concentration of any fibers tested.

– Blue fluor dopants perform better than green fluor dopants.

– Because of energy loss experienced in water, the average beta energy incident on fibers immersed in water is much less than the 6keV average energy characteristic of tritium beta. This results in a low photon yield that makes the coincidence counting approach impractical.

– Stability may be a problem. The fibers exposed to a 22-day soak in 120°F water experienced a 10x reduction in sensitivity. It is not known whether this was due to the build up of a deposit (a potentially reversible effect) or an irreversible process such as leaching of the scintillating dye.

The characterization test results in water for the 2% doped fibers were used as input to the

system design and are tabulated in the accompanying table. We find that the immersible probe must contain approximately 34,000 optical fibers in order to achieve a detection sensitivity of 200,000 pCi/L tritium in water. Based on this predicted performance, possible applications can be identified which include:

– Real time, in-situ monitor of high levels of tritium in storage tanks at DOE sites.

– Real time, in-situ monitor to alarm near the lower detection limit for Canadian and World Health Organization drinking water standards.

Design Performance Summary

a (pCi/liter)	N (fibers)	Bundle Dia. (cm)
2000	3389002	24.9
20000	338900	7.9
200000	33890	2.49
1000000	6778	1.11

Applications to verify compliance with the US EPA drinking water standard of 20,000 pCi/L cannot be performed with an in-situ tritium beta detector system that uses fibers with 0.5% or 2% fluor dopant concentration, because the fiber bundle diameter is too large to interface with a single photomultiplier detector.

Based on the results achieved, B&W Services, Inc. (formerly NESI) and MTI believe it is premature to initiate Phase 2 and commit to a prototype design for construction and test. We believe it is more appropriate to perform further Phase 1 work first. MTI recommends further Phase 1 work and is willing to submit a detailed workscope and cost estimate, if requested by the DOE. However, if the need for monitoring higher levels of tritium in water at concentrations greater than 200,000 pCi/L is justified, then prototype development and testing could proceed either as a Phase 2 stand-alone effort, or in parallel with continued Phase 1 development work.

Based on the Phase 1 results obtained and information presently available, significant improvements must be made in fluor-doped fiber performance in order to use the method for in-situ monitoring to verify compliance with current EPA drinking water standards. Additional Phase 1 fiber development work should be performed to increase the fluor dopant concentration above 2% until the self-absorption limit is observed. Continued fiber optimization work is expected to improve the sensitivity limits.

DEVELOPMENT TEAM / CORPORATE COMMITMENT

The Babcock & Wilcox Company (B&W) has made a commitment to being involved in the cleanup of Government owned facilities and waste storage sites. In 1992, B&W's parent company, McDermott International Inc., formed the B&W Services, Inc. (formerly NESI) affiliate company which has the responsibility for remediating B&W owned contaminated sites, including a uranium conversion facility at Apollo, PA, the T-2 High Enriched Uranium (HEU) facility in Parks Township, PA, and the B&W Plutonium Facility in Parks Township, PA. B&W Services, Inc. also runs a Waste Volume Reduction Facility at the same location. B&W Services, Inc. has recently been or is currently involved in D&D activities in Weldon Spring, Fernald, Hanford, INEL, Savannah River, and other sites. In 1997, McDermott Technology, Inc. (MTI) was formed to provide research and development services to all business units of McDermott International and its customers

MTI and B&W Services, Inc. are uniquely qualified to develop the Tritium Beta Detector because of expertise in all of the areas required for development. B&W Services, Inc. brings real world experience and a detailed understanding of waste site operations, remediation and D&D activities by virtue of its on-going projects for the DOE and it's long-term commitment to supply remediation and characterization services to the DOE community. The Research and Development Division brings innovative technology, sensor development expertise and a proven track record in the development of radiation monitoring sensors and numerous product developments based on fiber optics.

Table of Contents

1.0 INTRODUCTION

In the DOE complex, tritium (^3H) is one of the most commonly occurring radionuclide contaminants in ground, surface, and process effluent waters. Monitoring of tritium is performed to demonstrate compliance with U.S. Environmental Protection Agency (EPA) regulations, DOE orders or other regulations, and to track the movement of tritium contaminated plumes in ground water.

Numerous applications require low level detection of tritium. The most recent publicized example of need is at Brookhaven National Laboratory, where elevated levels of tritium have been detected in ground water around the High Flux Beam Reactor. Over the past year, tritium has been found in monitoring wells and the measured tritium concentration has exceeded the EPA drinking water standard of 20,000 pCi/L.

Tritium has a half life of approximately 12.3 years and decays exclusively by emission of beta (β^-) particles. The tritium β^- emitted has a maximum energy of 18.6 keV and an average energy of 5.7 keV. The low energy of this emission makes penetration of the radiation very low, approximately 1 mm in air and about 1 μm in water or low molecular weight solids. One implication of this for detection is that the tritium bearing material must have a high degree of intimacy with the primary detector for detection to be possible; intervening absorbers such as window materials cannot be used. A second implication is that the measurements are essentially 2 dimensional (surface). The detector integration volume is affected primarily by detector surface area exposed, since for tritium in liquids or solids, self absorption insures that only β^- from tritium with a high degree of detector intimacy can reach the detector face. The low energy of the β^- also results in a low quantum efficiency, further complicating detection.

The present method used to measure tritium is to sample water from a monitoring well, and send the sample to a laboratory for analysis, usually with liquid scintillation counting (LSC). Samples are often pre-processed to remove major interfering nuclides. The tritiated water is mixed with a liquid scintillator and placed in a sample vial, insuring the intimacy of the tritium and detector. This "cocktail" is placed in a scintillation counter which employs multiple PMTs (photomultiplier tubes) to detect the optical scintillation photons, usually using coincidence techniques, energy discrimination and pulse shape discrimination as well as shielding to minimize the errors from background and from interferences. Correction techniques have been developed for the quenching effects of the sample on the scintillation liquid, and for chemiluminescence which may result from chemical interaction between the sample and the cocktail. After the count, the cocktail enters the waste stream. To minimize the waste volume, LCS manufacturers have developed systems which can reliably count 20 mL vials, with up to 50% of the volume as sample, as well as biodegradable cocktails. Even with high detection efficiencies, long count times are required. A 10 mL sample with 2000 pCi/L tritium contamination contains 20 pCi of tritium, roughly 0.74 Bq, requiring several hours of count time to accumulate the counts needed for a 2% accuracy peak area determination.

LSC has good detection capability and precision. However, the sampling, chain-of-custody paperwork and lab analysis are labor intensive and expensive, and there is frequently a long analysis turnaround time. Spent cocktail adds to the downstream waste stream. Sampling and analysis must be performed at regular intervals to determine if and when changes have occurred, even when changes have not occurred, further increasing monitoring costs.

K. J. Hofstetter at Savannah River Technology Center has made great strides in overcoming many of the limitations of LSC[1,2]. An automated prototype LSC-based system has recently been used in the field at Brookhaven National Laboratory to measure tritium contamination in ground water. The plume was tracked by measuring tritium concentration in samples pumped automatically to the prototype from ten different sampling wells. The prototype features remote controlled sample collection, purification, mixing with liquid scintillator, tritium measurement in an analytical cell, and finally flushing of the analytical cell prior to introduction of the next sample. The prototype characterizes 11 milliliter samples at 30-minute intervals (cycle time) with 200 pCi/L resolution. Spent sample/LSC mixtures are stored in special waste packages for subsequent disposal. Although the prototype does not operate in-situ, it is quasi real-time and on-line.

Low cost, reliable, long-term monitoring of tritium concentration could be achieved with an *in-situ,* on-line system designed around an immersible probe. Ideally, such a system would feature passive operation with no moving parts and could track tritium activity in monitoring wells or effluent lines on a near real-time basis. It would provide a prompt indication when significant changes in activity had occurred. The intent of the Tritium Beta Detector project summarized in this report was to investigate promising methods to provide this in-situ monitoring capability.

1.1 GENERAL INFORMATION

Tritium (T) may combine with hydrogen (H) and deuterium (D) in the molecular combinations listed below. The boiling points of these diatomic gases are also provided.

H2	20.39K
HD	22.14K
HT	22.92K
D2	23.66K
DT	24.38K
T2	25.04K

Besides H2O, the most common oxide forms are D20 and HT0. According to publicly available information from Los Alamos National Laboratory (LANL), HT0 may form whenever HT gas is exposed to oxygen or water vapor. The conversion reactions are oxidation and exchange:

---

[1] K.J. Hofstetter and H.T. Wilson, "Aqueous Tritium Monitor Development," Fusion Technology, Vol. 21, No. 2, 446 (1992).

[2] K.J. Hofstetter, "Continuous Aqueous Tritium Monitoring," Fusion Technology, Vol. 28, No. 3, 1527 (1995).

Oxidation	2HT + 02 ----> 2HTO
	2T2 + O2 ----> 2T20
Exchange	HT + H20 ----> H2 + HTO
	T2 + H2O ----> HT + HTO

These reaction rates are increased by radiation (from nearby tritium at high concentrations), heat, or the presence of metal catalysts (especially palladium or platinum). All chemical reactions involving hydrogen can also be performed with tritium, sometimes at higher rate if the tritium concentration is high enough to catalyze the reaction. One of the most important reactions occurs when a tritium atom exchanges with a loosely bonded hydrogen atom of an organic molecule. However, where HT is dissolved in water, the exchange process is fairly slow because the hydrogen is tightly bonded and the reaction is not catalyzed.

2.0 BACKGROUND

The method investigated in Phase 1 of the project is based on the detection of the low energy beta radiation from the radioactive decay of tritium using a special form of scintillating optical fiber directly in contact with the water to be measured. The conceptual system design consists of an immersible sensor module containing the optical fiber and detection electronics, and an electronics package for signal processing, interconnected by an umbilical cable. The system could be permanently installed for routine water monitoring in wells or process or effluent lines, or could be moved from one location to another for survey use. The electronics will read out tritium activity directly in units of pCi/L, with straightforward calibration.

Commercially available doped plastic optical fiber consists of a doped core plus cladding and buffer coatings. Photons or particles which deposit energy in the fiber core cause the fluor dopant incorporated into the core of the fiber to emit optical photons. The number of optical photons produced is proportional to the energy deposited. A portion of the photons generated are trapped within the numerical aperture (NA) of the fiber and are transmitted along the fiber length to detection electronics at one or both ends of the fiber. Such optical fibers have been configured into a wide variety of radiation detectors, including some for environmental beta detection, such as the "BetaScint" detector (developed at Pacific Northwest Laboratories under DOE-OTD funding and currently in commercialization) which detects beta emissions from ^{90}Sr and ^{238}U. Such commercially available optical fibers are not suitable for use in detecting the low energy β^- from tritium, because it is absorbed in the buffer or the cladding and never reaches the core. Prior to the start of Phase 1 of this project, MTI identified and evaluated two alternatives which can overcome the absorption problem and permit scintillating optical fiber to be used for the detection of low energy β^-.

2.1 FLUOR-DOPED UNCLAD FIBER

In the first method, a conventional undoped fiber core is used, but a fluor is incorporated in a thin fiber cladding layer and no outer protective buffer coating is used. Typically, the material and refractive indices of the core and cladding are the same. The cladding can directly contact the medium containing tritium providing the needed intimacy. Tritium β^- is absorbed in the clad layer and produces optical photons which are coupled into the undoped core. The fiber acts as a lightguide with the surrounding medium providing the optical confinement, as illustrated in Figure 2-1. With a polystyrene core and water as the surrounding medium, the NA of the fiber is nearly 0.89 and approximately 8.5% of the scintillation photons are optically confined within the fiber and transmitted along its length in both directions.

MTI performed tests on a bundle of experimental fibers ("original" fibers) fabricated by Nanoptics, Inc., a commercial fiber vendor. The fibers were 0.5 mm diameter polystyrene, with a polystyrene layer approximately 10 µm thick doped with a blue emitting scintillator. The tests were performed in air using a tritium beta detector planchet source with an emission rate of about 8.9 β/cm^2 second, using a 23 fiber flat ribbon in the test setup shown in Figure 2-2. Using a

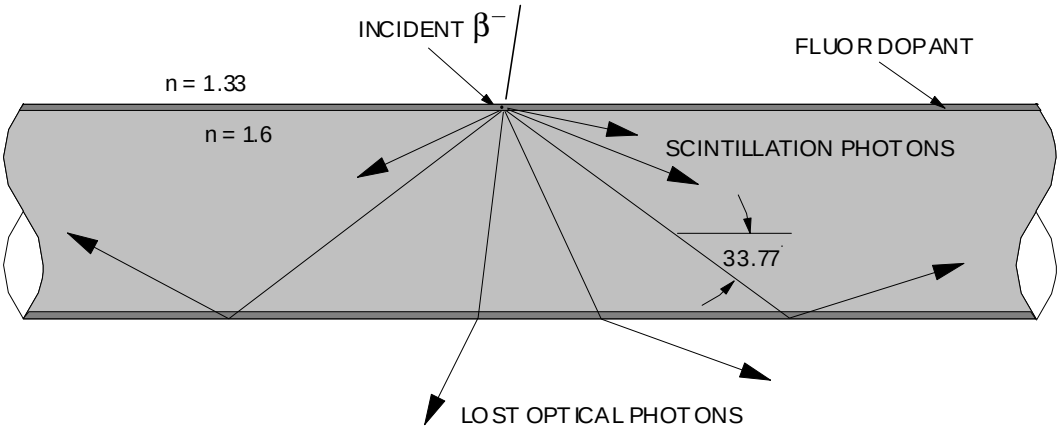

Figure 2-1. Fluor-Doped Unclad Fiber

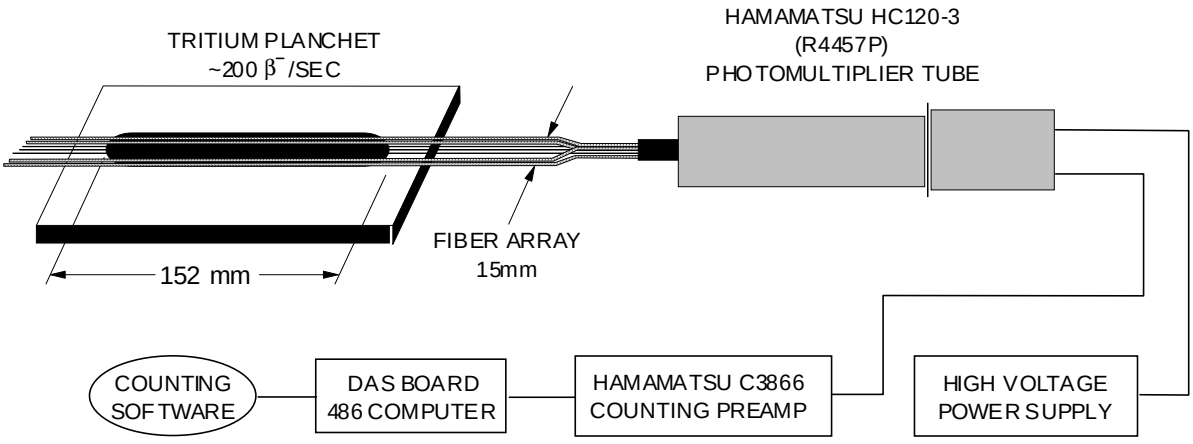

Figure 2-2. Fluor Doped Unclad Fiber: Counting Test Setup

room temperature bialkali PMT on one end of the fiber bundle, we counted this source at 95% confidence with count times from 800 to 1800 seconds against background count rates of 50 to 100 counts per second.

This approach has the benefit of insuring good intimacy between tritiated water and the scintillator. The fiber structure is simple and has a high numerical aperture, although the higher order modes are likely to be lossy in the presence of contaminants on the fiber OD, limiting the effective NA. The fiber cost will be low once commercialized. The polystyrene core material has relatively low fluorescence from gamma radiation and high transmission of gamma radiation, so this approach has high inherent rejection of gamma interference. The use of a blue emitting scintillator provides a good spectral match with a bialkali PMT, but the polystyrene core material is relatively lossy at blue wavelengths, limiting the length of fiber which can be used for a detector. The use of a thin doped layer (approximately the maximum range of tritium β) minimizes the losses of optical photons due to scattering or reabsorption.

β particles do not lose all of their energy in a single interaction with absorber atoms, but through multiple interactions along a path through it. The energy which is deposited is a function of the path length in the absorber and the particle's rate of energy loss with distance (dE/dx). For β particles with a maximum range shorter than the thickness of the doped layer, all of the energy of the incident β is deposited in this layer and produces scintillation photons. The number of optical photons produced is proportional to the total energy of the incident β. Higher energy β particles lose only a fraction of their energy within the doped layer and pass through into the undoped core. Scintillation photons are produced by the energy deposited in the doped layer, but not by the energy deposited in the core. The number of scintillation photons produced then is a function of the path length of the particle in the doped layer and of dE/dx, rather than of the total energy of the incident β. While both dE/dx and path length in the doped layer are functions of the incident β energy, the total number of optical photons generated in the doped layer is small, limiting the ability to characterize small differences in dE/dx.

At the time this work was done (prior to Phase 1 of the present contract), only a limited range of fiber parameters were evaluated to demonstrate the ability to detect the low energy tritium β. Efforts in Phase 1 were concentrated on optimization of the structure of a fiber detector to significantly improve the performance, resulting in a practical detector which can detect tritium β in the presence of interferences. Promising areas include optimizing the emission wavelength and dopant level of the fluor to increase quantum efficiency and minimize losses, optimizing the thickness of the dopant layer to provide a useful level of energy discrimination (the ability to reject higher energy β), consideration of alternate core materials which can minimize losses and provide good environmental immunity, matching of detector spectral response characteristics to fluor emission wavelength to improve detection quantum efficiency, use of coincidence counting to significantly decrease background count rates and the potential application of pulse shape discrimination or time resolved counting techniques to discriminate against α emitters.

2.2 UV FLUORESCENT CLAD WAVELENGTH SHIFTER

In the second method, an unbuffered clad fiber is used. Most optical fibers have an outer protective coating called a buffer coating, but for the present work, buffer coatings are not used because they would absorb beta energy without producing photons. The cladding material is selected as one which fluoresces in the near-UV when exposed to β. The use of an unbuffered fiber provides the intimacy needed for detection of low energy tritium β. The lower index of refraction of the surrounding water serves to confine some of the UV photons increasing the number which reach the core. The core material is chosen to have a higher index of refraction (as in conventional optical fiber) to provide optical confinement, and is doped with a wavelength shifting (WLS) fluor. The energy deposited in the cladding by an absorbed tritium β causes UV photons to be emitted; a portion of these UV photons enter the fiber core where they are absorbed causing the emission of optical photons at longer wavelengths. With PMMA cladding and a polystyrene core, the fiber NA is 0.58 and roughly 3.5% of the optical photons are confined (guided) in the fiber and transmitted to the ends for detection, as illustrated in Figure 2-3. The numerical aperture (NA) is defined as the sine of one-half the acceptance angle for light which is guided inside the fiber. Light which exceeds the fiber acceptance angle is not guided and is lost.

Prior to the start of Phase 1, MTI performed tests on single fibers fabricated by Bicron Corporation, a commercial fiber vendor. The fibers were 1.0 mm diameter polystyrene, with a PMMA clad layer approximately 5 μm thick. The core was doped with a WLS optimized to shift from the blue (410 nm) to the green (485 nm). The tests were performed in air with a variety of β emitters, using either a solid state single photon counting module or a room temperature bialkali PMT on one end of the fiber. The electronics used for the counting experiments was similar to those shown in Figure 2-2. The results of the tests showed that the sensitivity and count rate performance of this WLS fiber were comparable to that obtained with the fluor doped bare fiber described above. In addition, tests were performed to measure the pulse heights obtained with the WLS fiber. The pulse height tests showed that higher energy β which is not fully absorbed in the clad layer excites the WLS in the core directly, producing increased pulse heights which can be discriminated by pulse height.

During Phase 1 of the project, emphasis was placed on optimizing the unclad fiber configuration shown in Figure 1-1. The UV fluorescent clad fiber (Figure 1-3) was kept as a back-up approach, this fiber was tested in tritiated water, and the results were compared with the unclad fiber.

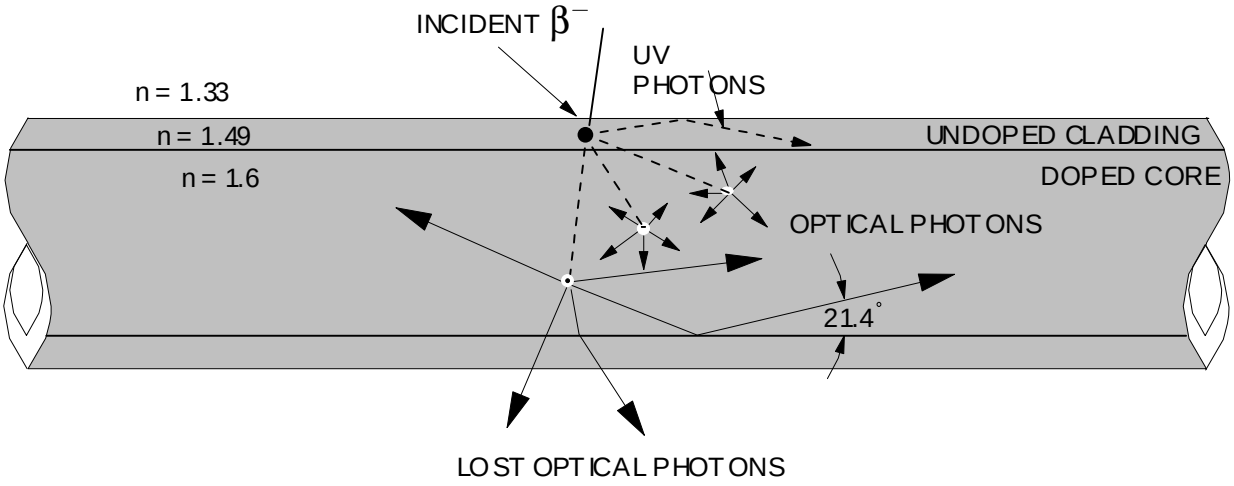

Figure 2-3. UV Fluorescent Cladding

3.0 GOALS AND ISSUES

3.1 OBJECTIVES

The objectives of Phase 1 of the project were to develop components and design a monitoring system capable of detecting and quantifying tritium *in situ* in ground and surface waters, and in water from effluent lines prior to discharge into public waterways. To meet these objectives with a system which is faster, better and cheaper than currently available methods, target characteristics of the tritium beta detector will include:

- Compact, immersible sensor
- Large wetted sensor surface area
- High sensitivity to ^{3}H
- High specificity to ^{3}H
- Near real-time response
- Rugged, integrated electronics

In follow-on Phases 2 and 3, MTI plans to carry the work through prototype development, field demonstration at a DOE site, and preliminary commercialization.

3.2 DESIGN ISSUES

The use of a fluor-doped polystyrene scintillation fiber for detection of tritium beta radiation in water raises a set of issues and concerns which must be addressed during method evaluation prototype design, and testing. These issues and concerns are summarized below. Not all of these issues were addressed in Phase 1.

A. Accommodate any memory effects in the fluor-doped polystyrene scintillation fibers –
   - Fibers must be kept in the dark because they phosphoresce.
   - Tritium, hydrogen, and also possibly tritium oxide, tend to adsorb preferentially on the surface of organics such as polystyrene.
   - What is the adsorption rate for tritium on the polystyrene fibers?
   - What is the exchange rate of absorbed water?
   - Is calibration or zero shift the result of memory effect?
   - What is the effect of acidic, alkaline, and/or organic environments on the scintillation fibers?

B. Concerns for the surface fluor are:
   - Aging, fouling and abrasion characteristics.
   - Does dissolved oxygen tend to quench the excited fluor?

C. Fiber bundle length issues –
- Sag of individual fibers due to inelasticity.
- If fibers touch each other, the effective surface for tritium detection is reduced and the overall bundle sensitivity may decrease. In addition, water may be trapped at the interface where the fibers touch and surface tension may tend to hold the fibers together at points of contact.
- Considering using Teflon spacer plates with holes to maintain fiber spacing along the length. How many spacer plates are needed?
- If spacer plates are used, then a flow manifold will be needed to maximize flow through the probe, minimize the refresh time and ensure the probe can be flushed out.

D. Provide magnetic shielding for photomultiplier tubes (PMTs).

E. Is the active area of commercial PMTs the limitation on how many fibers can be packed into a bundle?
- Possibly use multiple probes in parallel and sum the output signals from low-cost commercial PMTs.

F. The detection system must operate in the realm of small signals and long-term averaging (rather than pulse analysis) is important.
- Consider integration time compared to competing technology.

G. In addition to known beta emitters, identify other potential radiation interference effects that could give false signals –
- Cerenkov radiation can cause ultraviolet (UV) fluorescence in polystyrene. Polystyrene is a good UV absorber, but if UV is produced near the ends of the probe bundle, the detectors will see it. Coincidence detection should help.
- A high energy beta could give up just a small amount of energy to excite the fluor and produce a significant interference signal. (This problem should be minimal since with our approach, the fluor is contained in a thin layer on the outside surface of the fiber and is not present in the large volume core of the fiber.)

H. A key design issue is to determine if the scintillation fiber can be optimized to produce more than one photon per tritium beta electron.

4.0 SITE NEEDS AND TARGET SPECIFICATION

4.1 NEEDS

Site-specific needs for tritium detection and monitoring have been well documented. Five such needs that are representative within the DOE complex are listed below. Additional detail on these needs is provided in Appendix A.

Identifier	Description of Need
NV0013	A durable, reliable, accurate tritium monitor is needed for low level monitoring in deep wells at the Nevada Test Site.
CH-0005	Long-term monitoring of tritium is needed for use in monitoring wells at Brookhaven National Lab.
CH-0013	Argonne National Lab needs a tritium monitor to enable processing of 25,000 gallons of water prior to disposal.
ADS-1289	Groundwater monitoring for tritium at 460 ft. below surface must be performed at Sandia National Lab at Albuquerque.
SR-3006	Tritium monitor is needed at Savannah River site to track tritium concentration in large groundwater plumes over hundreds of acres.

A significant part of the present project work was to gather site specific information on needs for tritium monitoring and to use this information to help produce a target specification. To collect the information, B&W Services, Inc. (formerly NESI) prepared a questionnaire and sent it to nineteen participants at various DOE sites. The list of participants is provided in Appendix B, and included site personnel conducting monitoring and measurement activities as well as DOE personnel with jurisdiction over those activities. The sample questionnaire is also provided in Appendix B. Five surveys were returned. Additional information on needs was gathered by telephone interviews and was documented by B&W Services, Inc. in call reports.

4.2 TARGET SPECIFICATION

Information was obtained from DOE site personnel through telephone discussions and the questionnaire described in Section 4.1. The information was used to define desired operating characteristics for an in-situ tritium beta detector. The operating and performance characteristics were compiled by B&W Services, Inc. into a target specification which is provided in Appendix C. Copies of the complete target specification were sent to the survey participants listed in Appendix B.

5.0 TECHNICAL APPROACH

5.1 BASIS

The background work on fluor-doped plastic fiber described in section 2.0 provided the basis for defining a development program for an in-situ tritium beta detector. In Phase 1 of the project, a conceptual design was prepared and key components needed to support the conceptual design were procured and tested.

5.2 CONCEPTUAL DESIGN

The second generation conceptual design for the in-situ tritium beta detector is shown in Figure 5-1. This evolutionary design is based on two practical limits identified during the course of the project. These limits are:

- Total number of fibers less than 40,000
  Previous designs requiring more than 300,000 fibers would be difficult to manufacture into a probe of reasonable size. In addition, the fibers must be terminated to commercially available photomultiplier tubes with diameter of active area of 25 mm or less.

- Signal-to-noise ratio
  The conversion of tritium beta energy to measurable photoelectrons depends on many factors discussed in section 6. For example, the number of photons generated per beta event determines whether or not coincidence detection can be used to reduce noise and thus reduce counting time needed for low level measurement of tritium concentration. As indicated in the target specification (see Appendix C) a one-hour integration time is acceptable to potential users, although a faster response would be preferred if low end resolution and accuracy are not sacrificed.

One of the objectives for the second generation tritium beta detector is to improve the effective quantum efficiency of the original fibers tested (see Section 2). Improvements are expected by optimizing the fluor, reducing optical losses and improving the spectral match between the fluor emission wavelength and detector spectral response characteristics.

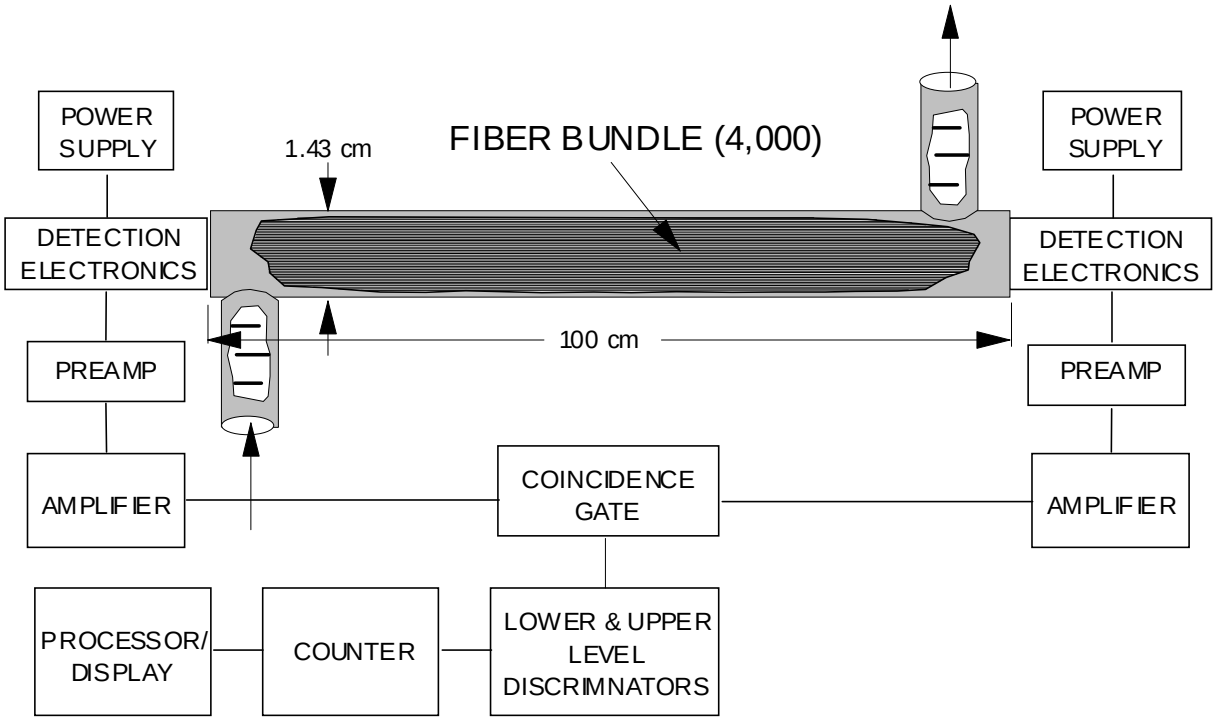

Figure 5-1. Second Generation Conceptual Design for In-situ Tritium Beta Detector

5.3 FIBER AND COMPONENT TESTS

A variety of off-the-shelf or readily manufactured components, including different scintillating fibers and electronic components were procured. The scintillating fibers were designed to improve on the performance of the original fibers. A table which summarizes the characteristics of all fibers tested is provided in Appendix D. Three types of photomultiplier tubes were tested and descriptions and specifications are provided in Appendices E and F. The photomultiplier tubes were characterized to determine the nature of the signals, to evaluate detection methods and signal-to-noise ratios, and to provide design information. The test results helped to determine the optimum detector configuration in terms of best spectral match between the scintillator and detector, as well as the optimum quantum efficiency. These results also helped support the conceptual design and provided input to estimates of system performance.

5.4 ESTIMATED SYSTEM PERFORMANCE

It is desirable that the tritium beta detector have a lower detection limit no greater than 10% of the EPA Drinking Water Standard (DWS) for tritium (20,000 pCi/L) and a precision of 5% or better at the DWS level, giving an LDL of 2000 pCi/L. The detector must be suitable for ground water immersion or for receiving water directly from a process line slipstream, and must

have a count time of one hour or less. Potential interferences will include α, β, and γ emitters, including ^{90}Sr, ^{60}Co, ^{99}Tc, ^{106}Ru, ^{129}I, ^{137}Cs, ^{40}K, U and Pu isotopes, and any others which may be found in the DOE complex, at DOE Derived Concentration Guideline (DCG) concentrations.

Because of the slight (1μm) penetration of tritium β in water, the detector needs a relatively large active surface area to obtain the good sensitivity needed for short count times. Surface area is provided by using multiple parallel fibers in an open bundle, which are in contact with the tritiated water on all sides and are optically in contact on their ends with a common detector. This configuration provides the large surface area needed in a relatively compact geometry (see Figure 5-1). A fiber diameter of 120 μm, fiber length of 60 cm, and fiber transmission of 43% were assumed. The fiber bundle would be housed in a light and liquid tight housing with light-baffled inlet and outlet ports for the tritiated water.

The performance of the detector design shown in Figure 5-1 is summarized in Table 5-1, which lists the number of fibers, N, and bundle diameter needed to detect various concentrations, a, of tritium in water. The system parameters used to generate this table are as follows:

Detector quantum efficiency	0.2
Detector dark count rate	5 counts/sec
Integration time	3600 sec
Generation rate of guided photons in fibers (from Section 9.2.7)	5.7×10^{-11} (photons/sec)$(pCi/L)^{-1}(cm^2)^{-1}$

Table 5.1 Design Performance Summary

a (pCi/liter)	N (fibers)	Bundle Dia. (cm)
2000	3389002	24.9
20000	338900	7.9
200000	33890	2.49
1000000	6778	1.11

Using commercially available electronics modules, a detector with 34,000 fibers could provide alarm capability near an LDL of 200,000 pCi/L tritium, and with relatively simple processing could read out directly in pCi/L. Based on current commercial pricing of similar fibers, it is expected that the total fiber cost would be less than $3000 for the needed 21 km of fiber. Fiber bundle diameters greater than 2.5 cm would not allow interface to a single photomultiplier detector, and thus would add significant system complexity and cost. However, alarm capability for an LDL of 200,000 pCi/L could be useful in applications to monitor drinking water for the Canadian Government and the World Health Organization, both of which require that tritium concentration be less than 200,000 pCi/L. However, an LDL of 200,000 pCi/L will not meet the DWS of the U.S. Environmental Protection Agency.

6.0 PHOTODETECTOR ANALYSIS

6.1 INTRODUCTION

The purpose of this section is to discuss the choice of detectors; both for the testing program and for incorporation in the prototype tritium beta detector.

6.2 REQUIREMENTS

There are several important considerations affecting the choice of the photodetector. The most important of these are:

- it must have a low dark count since the dark count is the primary noise limit.
- the detector must be capable of producing a detectable signal from the absorption of a single photon
- the quantum efficiency should be as high as possible
- the responsivity and dark noise must be stable since the detection strategy requires signal integration over extended time periods.

6.2.1 Dark Count

The purpose of the following analysis is to determine the parameters necessary for the fiber evaluation tests. The time required to achieve detection of a given activity level of ^3H is directly proportional to the dark count of the detector. We may write:

$$t = \frac{r^2 B}{\{ NRA\, p\, Q\, T\,[avg]\}^2} \tag{6.1}$$

where r is the signal-to-noise ratio
t is the time in seconds required to achieve a signal to noise ratio of r
B is the dark count rate in counts/sec
N is the number of fibers
R is the ^3H activity in $\beta/cm^2/sec$
A is the area of a single fiber that is exposed to the sample in cm^2
p is the probability that an incident β will result in at least one photon being captured in the fiber waveguide
Q is the quantum efficiency of the detector
T[avg] is the transmission of the fiber.

Assuming a bundle of fibers with 250μm diameter and pT[avg} = .135 (the same as the fiber we used in the feasibility study), we can write

$$A\ p\ T[avg] = \pi\ \text{x}\ .025\ell\ \text{x}\ .135 = 0.0106\ell \qquad (6.2)$$

where ℓ is the length of the bundle that is exposed to the sample.

Substituting Equation (6.2) into Equation (6.1), we get

$$t = \frac{8900\, r^2\, B}{(N\, \ell\, R Q)^2} \qquad (6.3)$$

Equation (6.3) shows that if we want to minimize the time required to get valid data:

- the dark count, B, should be minimized
- the detector's quantum efficiency, Q, should be maximized
- we should work with test samples having as high an activity, R, as possible
- the number of fibers, N, can be increased to reduce the time.

For testing, we could use tritiated water with an activity of 1 mCi/liter. Converted to our units this would be

$$R = 1\left(\frac{\text{mCi}}{\text{liter}}\right)10^{-3}\left(\frac{\text{liter}}{\text{cm}^3}\right)3.7\,\text{x}\,10^{7}\left(\frac{\beta}{\text{mCi}}\right)10^{-4}(\text{cm}) = 3.7\ \frac{\beta}{\text{cm}^2\ \text{sec}}$$

where we have assumed that the range of tritium beta in water is 10^{-4}cm.

A bundle size N = 50 fibers will

- be convenient to work with
- provide a large number in the denominator of Equation (6.3)

If we assume a detector with Q = 0.18 and use the above values for N and R in Equation (6.3), we get

$$t = \frac{8r^2 B}{\ell^2} \qquad (6.4)$$

We would like to make length resolved measurements with ℓ = 10 cm which, from Equation (6.3) will take

$$t = 8B \text{ (seconds)} \tag{6.5}$$

to achieve a signal to noise ratio, r = 10.

To provide convenient test times, we would therefore like to have a dark count of 100 c/sec or less.

6.2.2 Single Photon Detection

We do not know how many photons are delivered to the detector for each β absorption event. Based on the low energy of the β and on the results of threshold discrimination tests, we expect that many β events lead to the arrival of only one photon. It is therefore imperative that the detector be capable of producing a detectable signal from a single photoelectron.

The gain mechanism in a photomultiplier tube (PMT) provides high amplification (on the order of 10^6) with extremely low noise. Because of this, a PMT can produce a pulse that stands above the electronic noise when a single photon ejects an electron from the photocathode. In a silicon photodiode on the other hand (although it converts a higher percentage of incident photons to free-charge carriers), the signal resulting from a single photon event is buried by the noise in the subsequent amplifiers.

In a photon-counting PMT, the pulses produced by the absorption of a single photoelectron vary in height due to statistical fluctuations in the electron multiplication mechanism. Figure 6-1 shows the pulse height distribution for single photon pulses. Although the total number of noise pulses may far exceed the total number of signal pulses, the noise pulses are predominantly of low height. By providing an electronic threshold at the level marked LLD in Figure 6-1 and rejecting all pulses below the threshold, most of the noise can be eliminated.

Note that if each "event" produced two instead of one photon, the peak in this distribution would occur at twice the height and the threshold could be raised to reject an even higher fraction of the noise pulses.

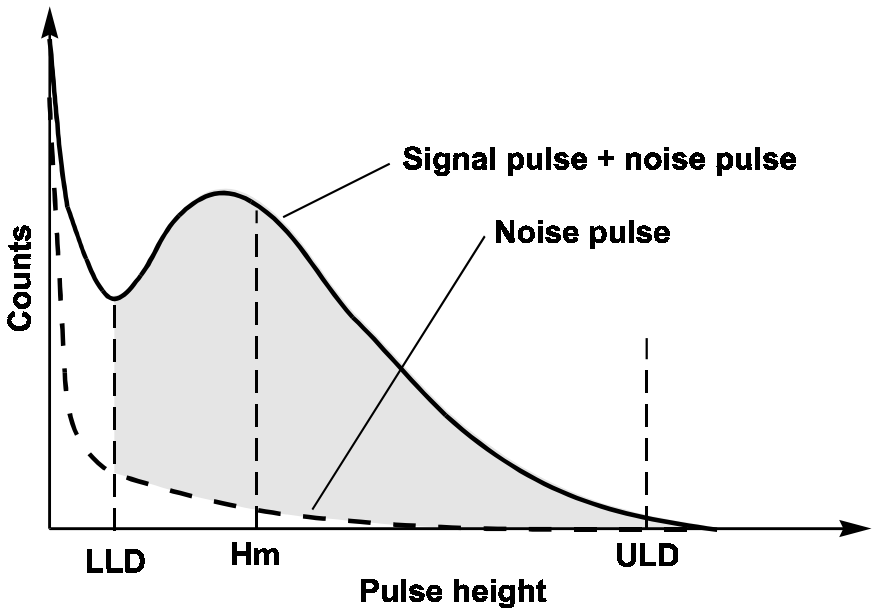

Figure 6-1. Typical Pulse Height Distribution. Taken from Hamamatsu "Photomultiplier Tubes" Booklet No. TPMO 0002E04

One of the important questions to be answered in our test program is "how many photons arrive at the detector for each β absorption event?" Note that the distribution in Figure 6-1 is rather broad. This means that the peaks for 1, 2, 3 ... photoelectrons all overlap to a considerable extent making it difficult to evaluate the individual contributions of the various peaks.

A new type of detector, the hybrid photomultiplier tube (HPMT) combines good features from PMTs and silicon detectors. Figure 6-2 shows a typical pulse height distribution from a HPMT. Note that the width of the peaks is small, allowing easy separation of the effects.

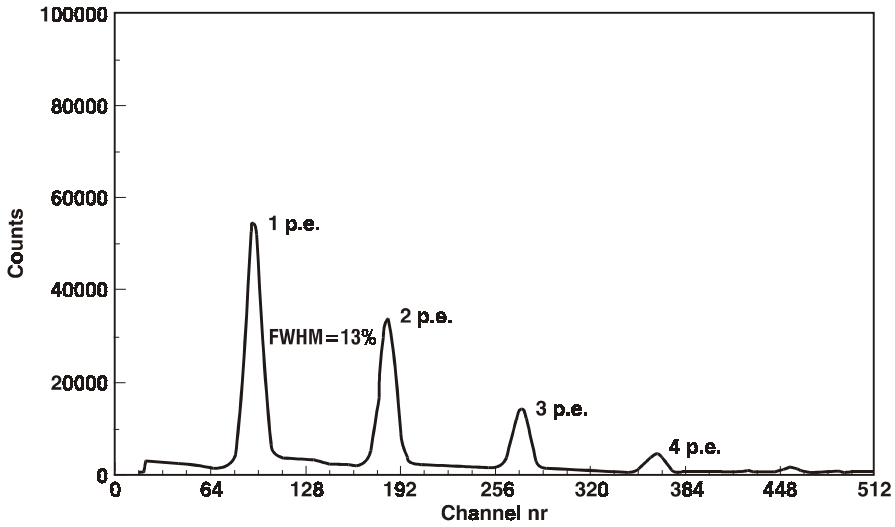

Figure 6-2. Pulse Height Distribution for an HPMT from Ziemer & Associates, who are the U.S. Representative for DEP Delft Instruments

6.2.3 Quantum Efficiency

The signal-to-noise ratio of the detector is directly proportional to the quantum efficiency, Q, defined as the fraction of incident photons that lead to the generation of a primary charge carrier, e.g., a photoelectron from the cathode of the PMT. Q is a wavelength dependent parameter dependent on the photosensitive material used.

Dozens of standard materials with a variety of spectral sensitivities have been developed over the years. Those with the highest Q's are shown in Figure 6-3. Note that the highest Q's tend to occur around 400 nm. Our prime candidate for fiber dopant dye was chosen to match this response, i.e., the dye emission peak is around 400 nm. Note also that the value of Q is relatively low. Few PMTs have a Q above about 20%.

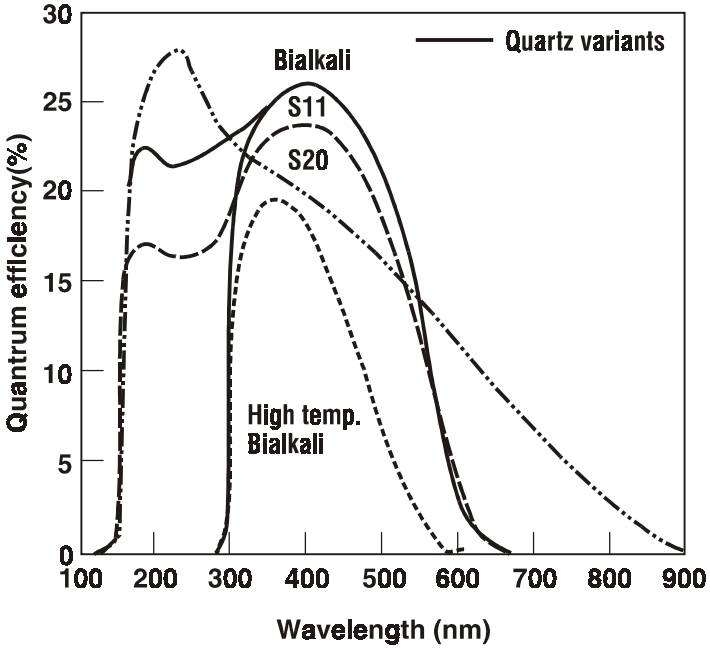

Figure 6-3. Spectral Response of Standard Photocathode Materials.
Taken from Electron Tubes LTD "Photomultipliers and Accessories" PMC/96

In contrast, the quantum efficiency of silicon detectors is high as shown in Figure 6-4. In the 400 nm region, silicon provides Q ≈ 70%. Also note that 400 nm is not the region of highest Q.

If a silicon detector could be used, a dye emitting at longer wavelengths could be used which would be advantageous from the standpoint of fiber transmission. The fiber loss increases rapidly with decreasing wavelength.

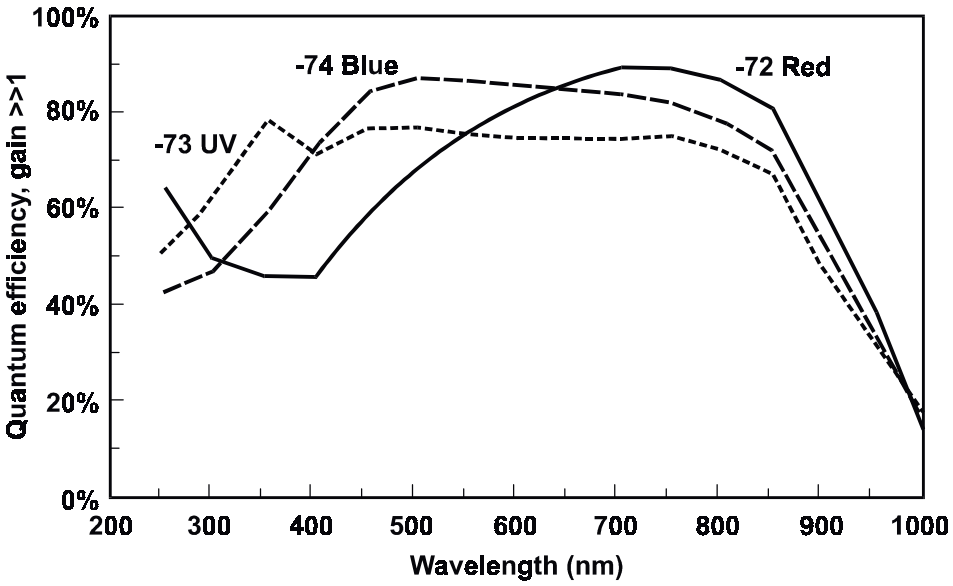

Figure 6-4. Spectral Response of Silicon APDs: From Product Brochure Supplied by Advanced Photonix, Inc.

6.2.4 Stability

For the test parameters assumed in the discussion of Section 6.2.1, the signal count rate is 3.5 counts/sec, which is small compared to a typical dark count rate of 100 c/sec. To deal with this situation, our measurement strategy is to collect data for two time periods. During the first period, the detector is exposed to the light from the fiber bundle and the bundle is immersed in tritiated water. For the second period, the bundle is immersed in non-tritiated water. Then we can express the total measured counts for the two periods as

$$C_1 = St + B_1t \tag{6.6}$$

and

$$C_2 = B_2t \tag{6.7}$$

where the counting time, t is assumed the same for both measurements.

Subtracting Equation (6.7) from Equation (6.6), we get

$$C = St + (B_1-B_2)t \tag{6.8}$$

Rearranging Equation (6.8), we can express S, which is the quantity of interest as

$$S = C/t - (B_1-B_2) \tag{6.9}$$

Since C and t are known quantities, it is clear from Equation (6.9) that the uncertainty in the

determination of S is expressed by the term

$$B_1\text{-}B_2 \equiv \Delta B \tag{6.10}$$

If the operating conditions of the photodetector are held constant so that there is no drift of the average background count rate, B, there is still a difference due to statistical fluctuations.

If the average count rate is B, the statistical fluctuations in the number of counts recorded during a period t is given by $\pm\sqrt{Bt}$. We can therefore write

$$B_1 = B \pm \sqrt{B/t} \tag{6.11}$$

and

$$B_2 = B \pm \sqrt{B/t} \tag{6.12}$$

Subtracting Equation (6.12) from Equation (6.11), we get

$$\Delta B = \pm \sqrt{B/t} \mp \sqrt{B/t} \tag{6.13}$$

Since the two error terms of equation (6.13) are uncorrelated, they combine as the RMS value so

$$\Delta B = \pm \sqrt{\frac{2B}{t}} \tag{6.14}$$

Combining Equations (6.9 and 6.14)

$$S = \frac{C}{t} \pm \sqrt{\frac{2B}{t}} = \bar{S} \pm \Delta S \tag{6.15}$$

Where ΔS is the uncertainty of the measurement
$\bar{S}$ is the true average value
and S is the value measured in a particular test.

From Equation (6.15), we can express the uncertainty (error) of the measurement as a fraction of the value as

$$\frac{\Delta S}{\bar{S}} = \sqrt{\frac{2B}{\bar{S}^2 t}} \tag{6.16}$$

From Equation (6.16) we see that regardless of how large B is with respect to $\bar{S}$, the measurement uncertainty can be made arbitrarily small by extending the measurement time, t.

Equation (6.16) is for the case where there is no drift and the error is due strictly to statistical fluctuations. If there is drift, the situation is quite different. Modifying Equation (6.9), we write

$$S = \frac{C}{t} - (B_1 - B_2) = \bar{S} + \Delta S \tag{6.17}$$

and

$$\frac{\Delta S}{\bar{S}} = \frac{B_1 - B_2}{\bar{S}} \tag{6.18}$$

Assuming that the experiment has been run over a time period that results in a negligible error due to statistical fluctuations, Equation (6-18) expresses the stability requirements for the detector. If we want a measurement error of less than 10%, then

$$0.1 \geq \frac{B_1 - B_2}{\bar{S}} \tag{6.19}$$

Dividing both sides by the nominal value of B and rearranging

$$\frac{B_1 - B_2}{B} \leq \frac{0.1\bar{S}}{B} \tag{6.20}$$

For the parameters assumed earlier, $\bar{S}$ = 3.5 and B = 100, so

$$\frac{B_1 - B_2}{B} \leq 0.0035 \tag{6.21}$$

The detector must therefore drift less than a fraction of a percent during the total experimental time period, 2t.

The primary cause of background count drift is tube temperature. The background rate dependence on temperature, T, can be expressed as

$$B(T) = B(T_o)e^{.07(T - T_o)} \tag{6.22}$$

where the temperatures are in degrees C. Combining Equations (6.22) and (6.20)

$$\frac{B(T) - B(T_o)}{B(T)} = 1 - e^{-.07\Delta T} \leq 0.0035 \tag{6.23}$$

Equation (6.23) can be solved to determine the temperature stability required to provide a measurement with 10% uncertainty when the nominal dark count is 100 c/sec. The calculated temperature stability is

$$\Delta T = \frac{\ln(1-.0035)}{0.07} = 0.05 \deg C \qquad (6.24)$$

It is quite difficult to maintain temperature control this precisely. A tube with a dark count of 25 counts/sec. would relax this requirement to ± 0.2 deg C. At the same time, the required counting time would be reduced by a factor of 4, which would also make the stability control easier.

6.3 AVAILABLE OPTIONS

6.3.1 HPMT

DEP Delft Instruments offers a hybrid photomultiplier with a built-in charge preamp that provides the following performance.

- S-20 photocathode with Q(400) ≈ 0.25
- 18 mm diameter active area photocathode
- 25 counts/sec dark count @ $20\,^{\circ}C$
- pulse height resolution similar to that shown in Figure 6-2
- pulse height due to a single photoelectron = 1.1 mV.

6.3.2 Photomultiplier Tubes

We obtained technical literature from all major PMT manufacturers and reviewed the specifications to identify tubes with potential for our application. The primary consideration was low dark count in the photon counting mode. Table 6-1 summarizes the characteristics of tubes with dark counts less than 50 c/sec.

The first five entries in the table have relatively small photocathode areas. They also have a side-on design that places the photocathode several mm behind the tube envelope which makes interfacing to an expanding beam from a fiber difficult. The tube from Burle, although an end-on design, also has a marginally sized photocathode.

Table 6.1. Potential PMTs

MANUFACTURER	TUBE #	PHOTOCATHODE AREA (mm)	Q (400 nm)	TYP. DARK COUNT (c/sec) @ 20°C
Hamamatsu	R1414P	4x13	.12	10
Hamamatsu	R2371P	4x13	.19	10
Hamamatsu	R4457P	4x13		20
Hamamatsu	R1527P	8x24	.19	10
Hamamatsu	R4220P	8x24	.19	10
Hamamatsu	R2560	25ϕ	.16	40
Hamamatsu	R2693P	18x16		15
Hamamatsu	R2557	10ϕ	.16	10
Hamamatsu	R3550	20ϕ	.16	20
Burle	C31304A-02	4x10	.27	12@-30°C
ETI	9078	15ϕ	.22	50
ETI	9131B/350	9ϕ	.20	30
ETI	9893B/350	9ϕ	.20	40

6.3.3 APD

Avalanche photodiodes (APDs) are the solid-state (silicon) version of a photomultiplier. Whereas a typical PMT operates at an internal gain of 10^6 the corresponding value for an APD is 200. The principle is the same in both cases, i.e., the internal electron multiplication provides gain with much less noise than can be obtained from external amplifiers.

The primary advantage (for our application) of an APD is high quantum efficiency. Figure 6-4 shows the spectral response of APDs available from Advanced Photonix, Inc. Not only is the Q at 400 nm more than 3X that of the best PMT, but also the high Q is available over an extended wavelength range. This means that dyes other than blue might be considered for the fiber dopant. As long as PMTs are the detector of choice, any potential efficiency increases achieved in the fiber by going to longer wavelength dyes would likely be offset by the drop in Q of the detector.

For many applications, the APDs internal gain of 200 is enough to put the signal above the input noise of subsequent amplification stages. Unfortunately, single photon detection is not one of those applications.

Single photon detection using a commercially available APD has been reported. (Applied Phys. Letters 64 (1994) No. 10, pp 1177-1179). The experimental parameters were, however, far from those that we could use. Table 6-2 compares the parameters used in the reported work with typical parameters for our application.

Table 6.2 APD Requirements

	Reported Work	Our Requirement
Internal Gain	4000	200
Detector Temperature	100K	300K
Detector Area	0.2 cm^2	2cm^2

The primary problem is the need to operate with liquid nitrogen cooling in order to raise the gain to the required level without initiating a self-sustaining discharge.

6.4 SUMMARY

The HPMT tube is superior to all alternatives in terms of virtually all significant parameters.

The one (significant) advantage of the listed PMTs is cost. For the fiber evaluation, this is secondary to the requirements to maximize the information obtained from the tests. For use in the final target instrument, however, cost becomes a more important parameter. We obtained and evaluated PMTs as part of the test program. The availability of a second detector provides the added advantage of allowing evaluation of the effects (possible enhancements) of adding coincidence counting to the signal processing.

We procured and tested the tubes from Table 6-1 that offer the best combination of properties, which are the R3350 and R2693P.

Based on the assumption that liquid nitrogen cooling is unacceptable in the target instrument, we have not included any APDs in the test plan.

7.0 RESPONSE MODEL FOR TRITIUM BETA DETECTOR

7.1 MODEL DEVELOPMENT

In this section, we present a model of the tritium beta detector response that can be used to plan and interpret the results of the component evaluation tests, and eventually to provide insight for prototype design. This model was used to guide test plan definition, but it ignores energy loss of β in water. See Appendix I for analysis that includes β energy loss in water.

When a β particle enters one of the sensing fibers, it excites fluorescence from the benzene rings of the polystyrene fiber material. The nominal wavelength of the benzene emission is 320 nm which is a wavelength for which the absorption coefficient of polystyrene is very high. The fiber material is therefore doped with a dye that absorbs the 320 nm photons and re-emits at longer wavelengths that can be more efficiently transmitted through the polystyrene.

If the energy of the β were all converted to 320 nm photons, the average number of 320 nm photons generated per incident β would be

$$n = \frac{\overline{E}}{E_{320}} \tag{7.1}$$

where $\overline{E}$ is the average energy of the incident β
and E_{320} is the energy of a 320 nm photon

In fact, of course, only a fraction of the energy is converted to 320 nm photons. Furthermore, not all of the 320 nm photons are converted by the dye to longer wavelength photons. We can therefore express the average number of longer wavelength photons generated per incident β as

$$\eta = \frac{\overline{E}}{E_{320}} \cdot q \cdot \delta \tag{7.2}$$

where q is the energy conversion efficiency of β electrons to 320 nm photons
and δ is the effective quantum efficiency of the dye.

The η photons are emitted isotropically through a 4π steradian solid angle. Some, therefore, encounter the fiber/water interface at angles close to normal, pass through the interface, and are lost. The fraction captured within transmission (guided) modes of the fiber in each direction is approximately given by

$$f = \frac{(NA)^2}{4} \tag{7.3}$$

where NA is the numerical aperture of the fiber.

As the trapped photons travel along the fiber toward the detector, some are lost due to absorption in the fiber material. The loss is exponential so we can express the fraction that are transmitted as

$$T(\chi) = e^{-k\chi} \tag{7.4}$$

where χ is the distance from the detector end of the fiber to the point of the beta absorption
and k is the attenuation coefficient.

We can determine the average transmission efficiency for a fiber exposed over its entire length, ℓ, as

$$T[avg] = \frac{\int_0^{\ell} e^{-k\chi}\, d\chi}{\int_0^{\ell} d\chi} \tag{7.5}$$

which carrying out the integration yields

$$T[avg] = \frac{1}{k\ell}\left[1 - e^{k\ell}\right] \tag{7.6}$$

Combining Equations (7.2), (7.3), and (7.6), we can express the average number of photons delivered to the detector per incident β as

$$\rho = \frac{\bar{E}}{E_{320}} \frac{q\delta f}{k\ell}\left[1 - e^{-k\ell}\right] \quad \left(\frac{\text{photons}}{\beta}\right) \tag{7.7}$$

Not every photon reaching the photodetector succeeds in liberating a photoelectron. The detector quantum efficiency, Q, is the fraction of incident photons that release an electron. We can therefore express the average number of photoelectrons released per incident β as

$$\xi = \rho Q \qquad \left(\frac{\text{photoelectrons}}{\beta}\right) \tag{7.8}$$

The number of incident β depends upon the activity, a, and the area of fiber exposed to that activity.

By definition there are 3.7×10^{-2} β/sec/pCi. If the activity of the water is expressed in the units of pCi/liter, the β flux will therefore be

$$F_{\beta} = a\left(\frac{\text{pCi}}{\chi}\right) \times 10^{-3}\left(\frac{\chi}{\text{cm}^3}\right) \times 3.7 \times 10^{-2}\left(\frac{\beta}{\text{sec pCi}}\right) \tag{7.9}$$

$$F_\beta = 3.7x10^{-5}\, a \left(\frac{\beta}{\sec\ cm^3} \right) \tag{7.10}$$

Consider a fiber with diameter d and length ℓ immersed in tritiated water with a volumetric β flux of F_β. The area of fiber exposed to the source is $\pi d\ell$. Consider an annular cylinder, concentric with the fiber, located a distance b from the fiber surface, and having a thickness *d*b. One half of the β emitted from the annular cylinder, *d*b, travel in a direction toward the fiber surface; the other half travels outward, away from the fiber. But, as they travel through the water, the β energy is exponentially attenuated so the β flux incident on the fiber from the annular cylinder is

$$d\beta_i = \frac{\pi d\ell F_\beta}{2} e^{-\frac{b}{\tau}}\, db \tag{7.11}$$

where τ is the characteristic absorption length.

Integrating Equation (7.11) over all b gives the total flux on the fiber as

$$\beta_i = \int d\beta_i = \frac{\pi}{2} F_\beta\, d\ell \int_o^\infty e^{-\frac{b}{\tau}}\, db \tag{7.12}$$

but

$$\int_o^\infty e^{-\frac{b}{\tau}}\, db = \tau \tag{7.13}$$

so

$$\beta_i = \frac{\pi}{2} F_\beta d\ell\tau \qquad \left(\frac{\beta}{\sec} \right) \tag{7.14}$$

Combining Equations (7.14) and (7.8), we can express the average number of photoelectrons per second generated when a fiber is immersed in water of activity a as

$$c = \xi\beta_i = \rho Q \frac{\pi}{2} F_\beta d\ell\tau \qquad \left(\frac{\text{photoelectrons}}{\sec} \right) \tag{7.15}$$

Equation (7.15) is the photoelectron rate for a single fiber. For a bundle of N fibers, the rate is

$$C = cN \tag{7.16}$$

If we assume loose packaging such that each fiber occupies a cross sectional area of d^2, and we assume a circular bundle of N fibers with a bundle diameter of Δ, we equate the areas as

$$Nd^2 = \frac{\pi\Delta^2}{4} \tag{7.17}$$

Combining Equations (7.16) and (7.17)

$$C = c\frac{\pi\Delta^2}{4d^2} \tag{7.18}$$

Substituting Equation (7.15) into (7.18)

$$C = \rho Q\frac{\pi}{2}F_\beta d\ell\tau\frac{\pi\Delta^2}{4d^2} \tag{7.19}$$

Substituting Equation (7.7) and (7.10) into (7.19), we get

$$C = \frac{\overline{E}}{E_{320}}\frac{q\delta f}{k\ell}\left[1-e^{-k\ell}\right]Q\frac{\pi}{2}3.7x10^{-5}\,ad\ell\tau\frac{\pi\Delta^2}{4d^2} \tag{7.20}$$

Simplifying the rearranging Equation (7.20) gives

$$C = 4.56x10^{-5}\,a\frac{\overline{E}}{E_{320}}\tau\Delta^2\frac{q\delta f}{kd}\left[1-e^{-k\ell}\right]Q \tag{7.19}$$

For tritium, the average β energy is

$$\overline{E} \approx 6000eV \tag{7.22}$$

and the energy of a 320 nm photon is

$$E_{320} = 3.9eV \tag{7.23}$$

So, we could get at most

$$\frac{\overline{E}}{E_{320}} = 1540 \text{ photon} \tag{7.24}$$

if the conversion were 100% efficient.

Each of the terms, q, δ, and f, represent less than 100% generation/capture of the 1540 potential photons.

The product

$$p = q\delta f \tag{7.25}$$

represents the fraction of the 1540 photons that are actually generated/captured in fiber guided modes. We define the term p as the fiber efficiency. Although the three terms whose product is p represent different physical mechanisms, our experiments do not separate the effects. It is the product of the three that can be measured. Accordingly, we rewrite Equation (7.21) in terms of p as

$$C = 4.56 \times 10^{-5}\, a \frac{\bar{E}}{E_{320}} \tau \Delta^2 \frac{p}{kd}\left[1 - e^{-k\ell}\right] Q \tag{7.26}$$

Substituting the numerical value from Equation (7.24) for the energy ratio, we get

$$C = .07\, a\, \tau \Delta^2 \frac{p}{kd}\left[1 - e^{-k\ell}\right] Q \tag{7.27}$$

The term τ is the range of β in water and is a constant. Extrapolating data from higher energies to the 6 KeV range, we estimate that $\tau \approx 10^{-4}$ cm. Substituting this into Equation (7.27) gives

$$C = 7 \times 10^{-6}\, a \Delta^2 \frac{p}{kd}\left[1 - e^{-k\ell}\right] Q \quad \left[\frac{\text{photoelectrons}}{\text{sec}}\right] \tag{7.28}$$

Equation (7.28) shows that the response depends respectively on:

exposed fiber area through the term Δ^2

the fiber characteristics through the term $\frac{p}{kd}\left[1 - e^{-k\ell}\right]$

and the detector through the term Q.

To summarize again,

- C is the average number of photoelectrons generated per second when the bundle of fibers is immersed in a tritiated water sample
- a is the activity of the sample in pCi/liter
- Δ is the diameter of the fiber bundle in cm
- p is the fiber efficiency
- k is the fiber absorption coefficient in cm^{-1}, averaged over the wavelength spectrum of the scintillating dye
- d is the fiber diameter in cm
- ℓ is the fiber length in cm
- Q is the quantum efficiency of the photodetector.

The photoelectrons, C, in Equation (7.28) are present with electrons generated by various noise sources. The performance of the tritium detector therefore depends upon not only the signal

level but also the noise level and the extent to which various signal processing techniques can suppress the noise.

If we accumulate counts for a period t, the total signal is

$$S = Ct \tag{7.29}$$

While the total number of noise counts is

$$N' = Dt \pm \sqrt{Dt} + N_{DRIFT} + N_{INT} \tag{7.30}$$

where D is the average count rate of the photodetector in the absence of any light inputs
N_{DRIFT} is due to drift of the photodetector dark count rate from the average value caused by factors such as temperature, magnetic field, and power supply voltage.
N_{INT} is due to response of the fiber bundle to radioactive species other than ^3H in the sample.

The first term in equation (7.30) represents a constant offset term which can be determined independently and subtracted from the noise while the second term represents statistical fluctuations of the dark-count noise that cannot be compensated.

7.2 ISSUES TO BE ADDRESSED

The ultimate performance of the prototype tritium beta detector depends upon the fiber, the photodetector, and the signal processing.

7.2.1 Fiber

As can be seen in Equation (7.28), the fiber parameters that affect the performance are d, ℓ, p, and k.

Equation (7.28) indicates that the signal increases with decreasing fiber diameter, d. Fabrication and handling considerations place a limit on how small the diameter can be. The fiber manufacturer determines in the course of the fiber development program how small d can be.

The parameter ℓ is the length of the individual fibers in the bundle. The signal increases in a non-linear fashion with increasing ℓ. At longer lengths, the increase per unit length tends to saturate due to transmission losses in the fiber. The optimum practical fiber length depends upon the magnitude of the absorption coefficient, k.

The two remaining parameters, p and k, depend upon fundamental material properties of the fiber and scintillating dye. Several different fiber designs were reduced to experimental fibers for evaluation in the test program. The parameters p and k are the primary performance criteria that are used to determine which fiber design is best for the prototype monitor.

An additional issue relating to the choice of the fiber is stability. This, of course, does not

appear as any parameter in Equation (7.28) but rather relates to the repeatability of C over extended periods of time. Since the sensing/interactive portion of the fibers is a very thin layer at the fiber surface, there is a question about long-term stability of the factor p when continuously exposed to water. There is a potential for leaching of the dye and/or changes in p due to water absorption by the fiber material.

7.2.2 Photodetectors

Four important parameters characterize the performance of the photodetector. They are:

- the quantum efficiency, Q, that appears in Equation (7.28)
- the dark count, D, from Equation (7.30)
- the dark drift sensitivity expressed as N_{DRIFT} in Equation (7.30)
- the energy resolution which does not appear in the discussion above, but which relates to the effectiveness of various signal-processing techniques as will be discussed later.

We procured three detectors for evaluation in the test program. They were chosen based on their published specifications for high Q and low D. Additionally, one of them was chosen based on its superior energy resolution characteristics.

7.3 SIGNAL PROCESSING

7.3.1 Threshold Discrimination

When a single photoelectron is released from the photosensing cathode of a photo-multiplier tube, it is internally multiplied to produce a detectable pulse of a million or more electrons at the anode (output). Because of statistical fluctuations inherent in the multiplication process, the number of output electrons (and hence the pulse height) varies from one event to the next.

Figure 7-1 shows the distribution of output pulse heights due to single photoelectron events for a typical photomultiplier tube (PMT). Also shown is the distribution of heights for dark noise counts. In a simple counting experiment, one merely determines the total number of counts which is the integral (area under the curves) of Figure 7-1. In such an experiment, it is

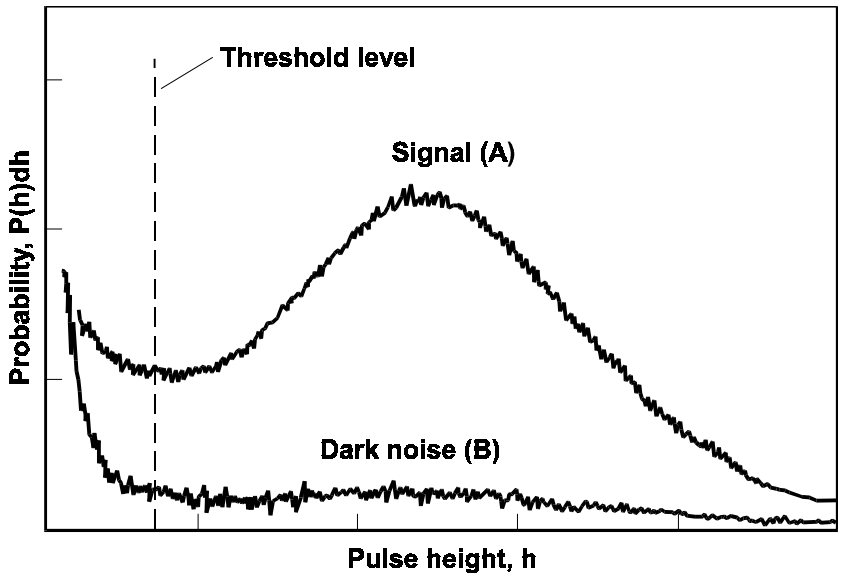

Figure 7-1. Probability Distribution of Pulse Heights For Typical PMT

common to use thresholding to discriminate against the dark noise counts. Electronically, all counts, both signal and dark, below some threshold level are rejected. The total counts can then be expressed as

$$\text{SIGNAL COUNTS} = \int_{\text{threshold}}^{\infty} P_s(h)dh \tag{7.31}$$

and

$$\text{DARK COUNTS} = \int_{\text{threshold}}^{\infty} P_D(h)dh \tag{7.32}$$

With the threshold set as indicated in Figure 7-1, it can be seen that, although some signal counts are lost, the fraction of total dark counts rejected is higher than the fraction of signal counts lost. The result is an overall improvement in the signal-to-noise ratio over the non-thresholding case.

There is a setting for the threshold that will optimize the signal-to-noise ratio. While its location is not obvious by inspection of Figure 7-1, the optimum threshold can be determined experimentally.

Two of the detectors chosen for our program are PMTs for which Figure 7-1 is typical. The third detector is a hybrid photomultiplier tube (HPMT). Figure 7-2 adds the single photoelectron pulse-height spectrum for the HPMT to that of Figure 7-1. The high-resolution feature of the HPMT means that the threshold can be moved higher to reject a larger fraction of the noise counts without affecting the number of signal counts. Furthermore, an upper threshold could be added to reject high-level noise counts.

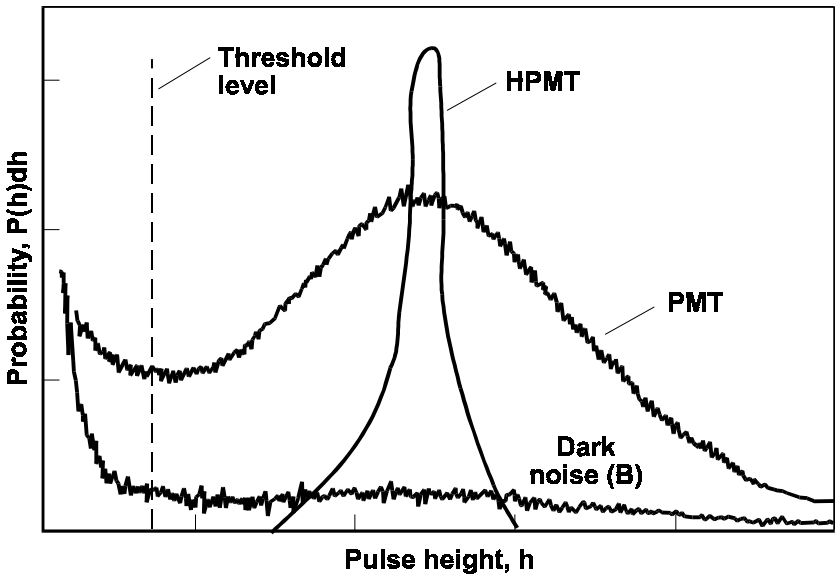

Figure 7-2. Probability Distribution of Pulse Heights for HPMT Compared to Distribution from Figure 7-1

7.3.2 Coincidence Counting

A high percentage of the dark counts can be rejected by employing a coincidence requirement. If the detector dark count is D, the probability that two independent detectors will "simultaneously" have at least one dark count within a time period τ is given from Poisson statistics as

$$P(\tau) = 1 - e^{-D\tau} \tag{7.33}$$

If the dark count is 20 sec^{-1} (typical of the level for the three photomultiplier detectors) and $\tau = 10^{-4}$ sec, Equation (7.33) can be solved to give $P(\tau) = .002$. By placing a detector at each end of the fiber bundle and requiring (electronically) that only counts that occur "simultaneously" (within a 10^{-4} sec widow) are recorded, the dark count noise will be reduced to .002D.

In order to determine the viability of the coincidence approach, we must experimentally determine by what factor the coincidence requirement reduces the true signal count.

8.0 PLAN FOR COMPONENT TESTING

8.1 INTRODUCTION

The conceptual design of the tritium beta detector consists of a bundle of scintillating fibers that is immersed in the water to be monitored. Light generated by the interaction between the fibers and the incident tritium β particles is guided to photodetector(s) at one or both ends of the bundle. The output of the detectors is a series of fast pulses whose number is proportional to the number of incident β particles.

The ultimate performance of the tritium beta detector depends on:

- the fiber
- the detector
- the signal processing used to discriminate the signal from the background noise.

In this section, an experimental program is outlined to evaluate the three performance factors to provide background information required for optimizing the design of a prototype tritium beta detector. A more detailed description of the tests, including drawings, is provided in Appendix G.

8.2 FIBER EFFICIENCY - TEST SERIES A

Objective - The objective of Series A is to experimentally determine overall conversion efficiency for each of the experimental fiber types so that the relative performance of the fibers may be compared and the best type selected for use in the prototype. Four bundles of four different fibers are to be tested -- three polystyrene, two doped with a blue fluor and one with a green fluor. The fourth fiber is PMMA doped with a blue fluor.

Approach

A bundle of fibers is encased in a Teflon tube and interfaced at one end with a hybrid photomultiplier tube (HPMT). Each bundle is held in a vertical test assembly and flooded to various levels with tritiated water of known activity. The output pulses from the HPMT are input to pulse height analyzer (PHA).

The fiber bundles consist of fibers whose length is L = 50 cm. Bundles of this length are convenient to test and it is straightforward to extrapolate the results to longer lengths. A bundle of each type of fiber is prepared and tested. Pulse height spectra are recorded for various fiber immersion lengths. The "dark count" pulse height spectra is also recorded.

The integral of the pulse height spectrum over all heights gives the total number of counts.

8.3 TEST SERIES B - STABILITY

Objective - Evaluate the effect of extended water immersion on the repeatability of response of the fibers.

Approach

The fiber assemblies are the same as in Series A except that the bundle length is15 cm. Shorter test lengths were chosen for convenience and to conserve the limited amount of experimental fiber. Three assemblies of each fiber type are prepared. Using a photon counting photomultiplier as a detector, the response of the assemblies when exposed to a known tritium activity is recorded for each assembly when first fabricated and again after 10, 20, and 40 days. Between readings, the three assemblies for a given fiber type are stored as follows:

- one in water at 120 deg. F
- one in water at 60 deg. F
- one in air at room temperature

The assemblies stored in air act as a control, while the two water-soaked assemblies are subject to change due to the water.

8.4 TEST SERIES C - THRESHOLDING

Objective - Determine the improvement in signal-to-noise ratio possible by optimizing the counter threshold.

Approach

The same fiber assemblies used in Test Series A are used here. The detector is a photon counting photomultiplier tube. The mV level pulses from the detector are converted to 5V pulses and directly input to a counter. The pulse height converter provides a tunable threshold that allows rejection of all input pulses below the threshold level.

The procedure is to

- measure the dark-noise count rate as a function of threshold level.
- measure the count rate with the fibers exposed to tritiated water as a function of threshold level.
- calculate from the above measurements the signal-to-noise ratio as a function of threshold to determine the threshold level that optimizes the ratio.

Measurements are made for each of two photomultiplier detectors for each of the different fiber types. The results are used along with the results of Test Series A to help select fiber type as well as detector type and threshold setting.

8.5 TEST SERIES D - COINCIDENCE

Objective - Determine the signal-to-noise ratio that can be achieved by employing coincidence counting between detectors at each end of the fiber bundle.

Approach

The thresholds on two pulse height converters are set at the optimal levels determined in Series C. The 10 nsec pulses from the outputs of the converters are first extended in length to 1) make them compatible with input to an appropriate counter, and 2) to simplify the coincidence timing requirements. A delay coil is used to provide the proper phasing between the signals from the two detectors. A pulse stretcher for the HPMT signal is adjustable up to 100 µsec to provide a coincidence window.

The stretched pulses from the two detectors are input to counters as well as being sent together into an AND gate. The AND gate outputs a pulse only when both detectors output a pulse during the coincidence time-window.

The procedure is to record for each fiber assembly

- HPMT counts
- PMT counts
- coincidence counts

for both

- shutter closed (dark counts)
- shutter open to fiber

for coincidence windows of

- 1 µsec
- 10 µsec
- 100µsec

8.6 TEST SERIES E - ABSORPTION CONSTANT

Objective - Determine the effective absorption constant for each of the fiber types. The fiber absorption constant could be extracted from the results of Test Series A since the absorption constant is one of several factors that influence fiber efficiency. But more precise results are expected from a separate test to measure the fiber absorption constant only.

Approach

A pulsed nitrogen laser illuminates the fiber at a right angle to the fiber axis. The 337 nm nitrogen laser light is converted by the scintillating dye to photons (characteristic of the dye) that are trapped in the fiber and transmitted to the entrance of the monochromator. A Princeton Instruments analyzer (electronic spectrometer) uses a 700+ element intensified detector to measure and record the scintillation light spectra.

The procedure is to record spectra of the light delivered to the monochromator for monochromator-to-illumination-point distances

ℓ = 10, 20, 30, 40, and 50 cm.

For each type of fiber, spectra are recorded for two different fibers.

8.7 TEST SERIES F - INTERFERENCES

Objective - determine the extent to which the fibers respond to radiation from radionuclides other than β from tritium.

Approach

Rationale: These tests are performed after all previous tests are completed. We have not yet determined what other species at what activity levels are likely to be present in the water samples for which the target tritium monitor is intended. For these preliminary interference tests we have chosen a range of radiations for which we have sources on hand. The sources to be used in this test are Sr-90 (β), Am-241 (γ,α), and Cs-137 (γ,β).

9.0 TEST RESULTS

9.1 INTRODUCTION

The purpose of the tests was to characterize the performance of a series of experimental scintillating fibers in order to:

- select the most promising fiber design
- and to provide a quantitative basis for the design of a prototype incorporating the preferred fiber.

The overall fiber evaluation work plan is outlined and its rationale discussed in Section 8 and Appendix G. The first five test series form the work-scope reported here. Each of the five test series is discussed in turn. Interference tests (Test Series F) were postponed until a scintillating fiber with acceptable sensitivity to tritium is developed.

9.2 FIBER EFFICIENCY – TEST SERIES A

9.2.1 Objective

The objective of this series was to determine the efficiency with which incident tritium β energy is converted to detectable counts from a photodetector. The efficiency is a key performance parameter for first selecting the preferred fiber design and then predicting the performance of a monitor incorporating that fiber.

9.2.2 Definition of Fiber Efficiency

The desired tritium monitor consists of a bundle of doped plastic fibers coupled to a photon counting photodetector and immersed in the water to be monitored. The principle is that incident β energy is converted in the fiber to photons - some of which are trapped in the fiber and transmitted to the photodetector. The detector is a “photon-counting” type which generates a single pulse (or count) in response to the arrival of the photons from a given β event. To optimize performance we desire a fiber that maximizes the number of photons delivered to the detector and thereby maximize the probability that a given β event will result in a detector count.

In 1995, McDermott sponsored the development and evaluation of a scintillating fiber that was specifically designed to maximize the response to low energy β from tritium. Experimental evaluation of this “prototype” fiber was performed using a tritium β source consisting of an oxidized aluminum planchet with a known concentration of tritium bound within the surface oxide. For those tests, a number of the fibers were laid directly in contact with the active area of the planchet so that they intercepted virtually all of the β energy emitted from the surface. All of the fibers were simultaneously input to a single photon-counting photomultiplier.

In the planchet experiment the measured count rate, C, in counts/sec was given by the expression

$$C = RApQT[avg] \qquad (9.1)$$

where

$R = \tau F_\beta$ is the β activity in $(\beta/sec/cm^2)$

$A = N\pi d\ell$ is the exposed fiber area in (cm^2)

N is the number of fibers

p is the fiber efficiency in (photons/β)

Q is the dimensionless quantum efficiency of the detector

$T[avg] = \frac{1}{k\ell}(1-e^{-k\ell})$ is the average transmission of the fiber

and where Eq. (9.1) is a simplified version of Eq. (7.28).

The fiber transmission was measured in a separate experiment so the fiber efficiency could be calculated from the measured count rate and other known parameters using Equation 9.1.

The fibers were laid directly on the active surface with nothing but a thin layer of air between. Since the range of tritium β in the air is a few mm, it was assumed that virtually all of the emitted β reached the fiber surface. With this assumption the fiber efficiency was measured as

$$p = 0.33 \text{ photons}/\beta \tag{9.2}$$

The target monitor and the tests reported here are not made in air but rather in water. Since the range of tritium β in water is on the order of 1 μm, the situation is quite different. The flux incident on a surface immersed in water with a volumetric activity of, $F_\beta \left(\frac{\beta}{sec\,cm^3}\right)$ is

$$R\left(\frac{\beta}{sec\,cm^2}\right) = \tau F_\beta \tag{9.3}$$

where τ is the range in water.

Combining Equations 9.1 and 9.3 and rearranging, we get

$$p\tau = \frac{C}{F_\beta AQT[avg]} \tag{9.4}$$

Since we do not have an accurate value for the range we shall express the results in terms of the product $p\tau$. For convenience we recast Equation 9.4 in terms of the activity, a, in pCi/L rather than $\beta/sec/cm^3$ and get

$$p\tau w = \frac{C}{a\left(\frac{pCi}{L}\right) * A * Q * T[avg]} \tag{9.5}$$

where w is a conversion constant equal to 3.7×10^{-5} (see Equation (7.9)).

Equation (9.5) is the expression for the fiber performance efficiency

$$\varepsilon = p\tau w \tag{9.6}$$

in units of (photons/sec)/(pCi/L)/cm^2 of exposed fiber area

This definition of performance efficiency is directly measurable even though we do not know the range, τ.

9.2.3 Approach

We can determine the efficiency, ε as defined in Equation 9.6 by exposing a bundle of fibers with known geometry and transmission efficiency to a solution with known tritium activity and recording the count rate produced by a photon counting detector whose quantum - efficiency is known.

A standard photon counting photomultiplier tube can be used to make these measurements, which is the approach we used. Originally (as discussed in Appendix G) we intended to use a hybrid-photomultiplier tube (HPMT) for these measurements because it provides additional information. The HPMT has a very good energy resolution so that one can not only determine the number of counts, but also how many photoelectrons were emitted from the photocathode for any given count. This additional information would be helpful in setting both high and low thresholds to discriminate against background noise. It would also provide information regarding the benefits of double-ended coincidence detection.

We were unable to get stable operation from the HPMT tube which has been returned to the factory for evaluation and/or repair. Consequently we made the fiber efficiency measurements using a standard photon-counting photomultiplier tube (PMT).

9.2.4 Fibers

We made efficiency measurements on five different experimental fibers whose general characteristics are summarized in Table 9-1 (and Appendix D). Note that Fiber Type #1 is the original prototype tested in the 1995 project. All but Fiber Type #7 were manufactured for this project by Nanoptics Inc. of Gainesville, FL with clear cores and the scintillator dye in a thin outer cladding layer. Fiber #7 is a fiber commercially available from Bicron with the scintillator dye distributed throughout the core. The clad is undoped PMMA.

For the efficiency tests one bundle of each fiber type was prepared. Figure 9-1 (below) is a sketch showing the components of the bundle assemblies. Parameters for the different bundles are summarized in Table 9-2. Teflon was used as the material for the assembly housings because of its low index of refraction. The outer layers of the fibers are polystyrene. Unlike conventional optical fibers which have a low-index cladding material around the high index core, these fibers

depend on the medium (water) they are immersed in to provide the low index necessary for waveguiding. To prevent light loss, other materials that may contact the fibers must have a low refractive index.

Table 9.1 Summary of Fiber Characteristics

FIBER TYPE DESIGNATION	DESCRIPTION
#1	500 μm O.D., polystyrene core with coextruded clad layer of polystyrene doped with 2% concentration of PMP blue fluor. Clad layer 5-19 μm thick
#4	500 μm O.D., DOW 252 polystyrene core with coextruded clad layer of polystyrene doped with 3-HF green fluor. Clad layer 5-10 μm thick. Approx. ½% concentration.
#5	400 μm O.D. polystyrene rod, polymerized and surface doped with PMP blue fluor. Approx. ½% concentration.
#6	750 μm O.D., PMMA extruded core, stretched and solution clad with polystyrene doped with PMP blue fluor at 2% concentration
#7	1000 μm O.D., Green fluor doping throughout core, low index PMMA clad

Table 9.2 Fiber Assembly Parameters

FIBER TYPE	NUMBER OF FIBERS	ACTIVE LENGTH
#1	45	43cm
#4	33	43cm
#5	76	43cm
#6	25	43cm
#7	48	28cm

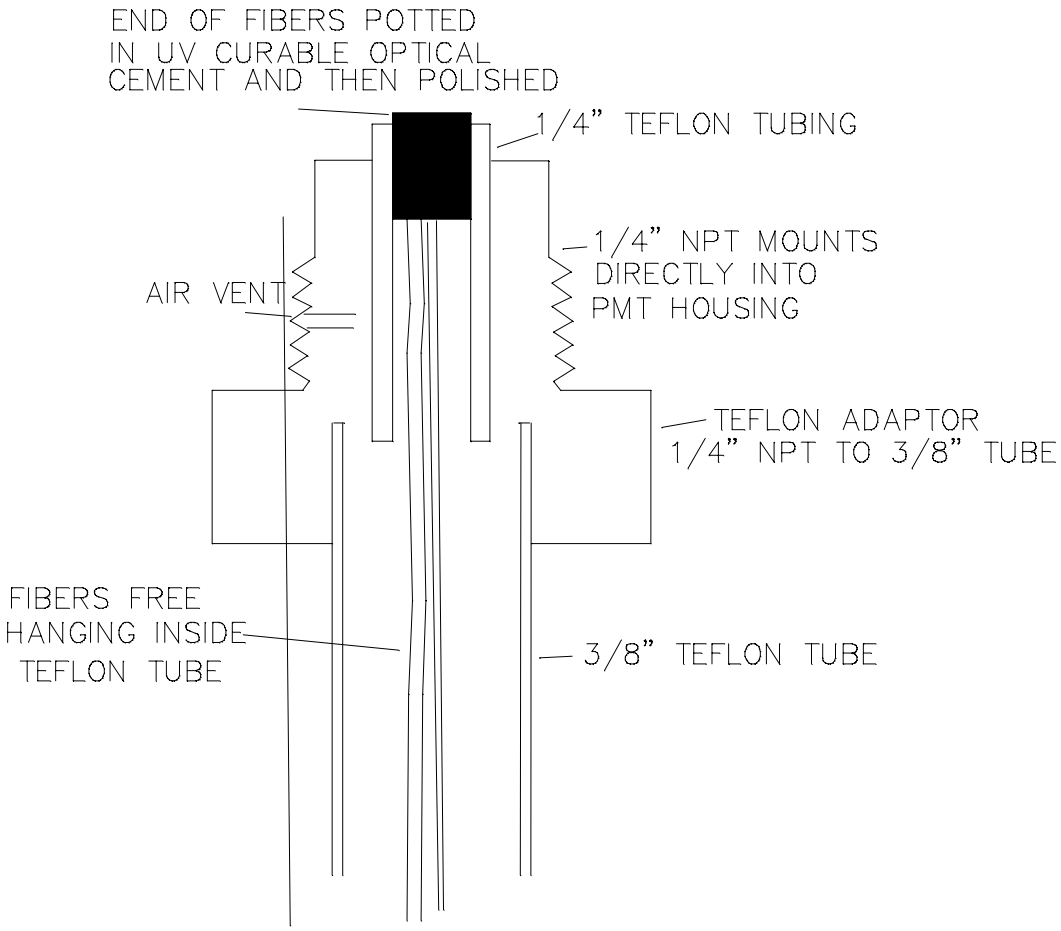

FIGURE 9-1. FIBER ASSEMBLY

Special care is required when handling these fibers to avoid potential contamination by finger oils, grease, etc. Most of the solvents used for cleaning normal glass fibers cannot be used because they attack the styrene.

Several approaches to terminating the fibers were tried (with varying degrees of success) before finally settling on a UV curable adhesive that provides:

- a relatively low refractive index
- non-attack of the styrene
- a rigid final state that allows end polishing

9.2.5 Apparatus/Procedures

9.2.5.1 Overview

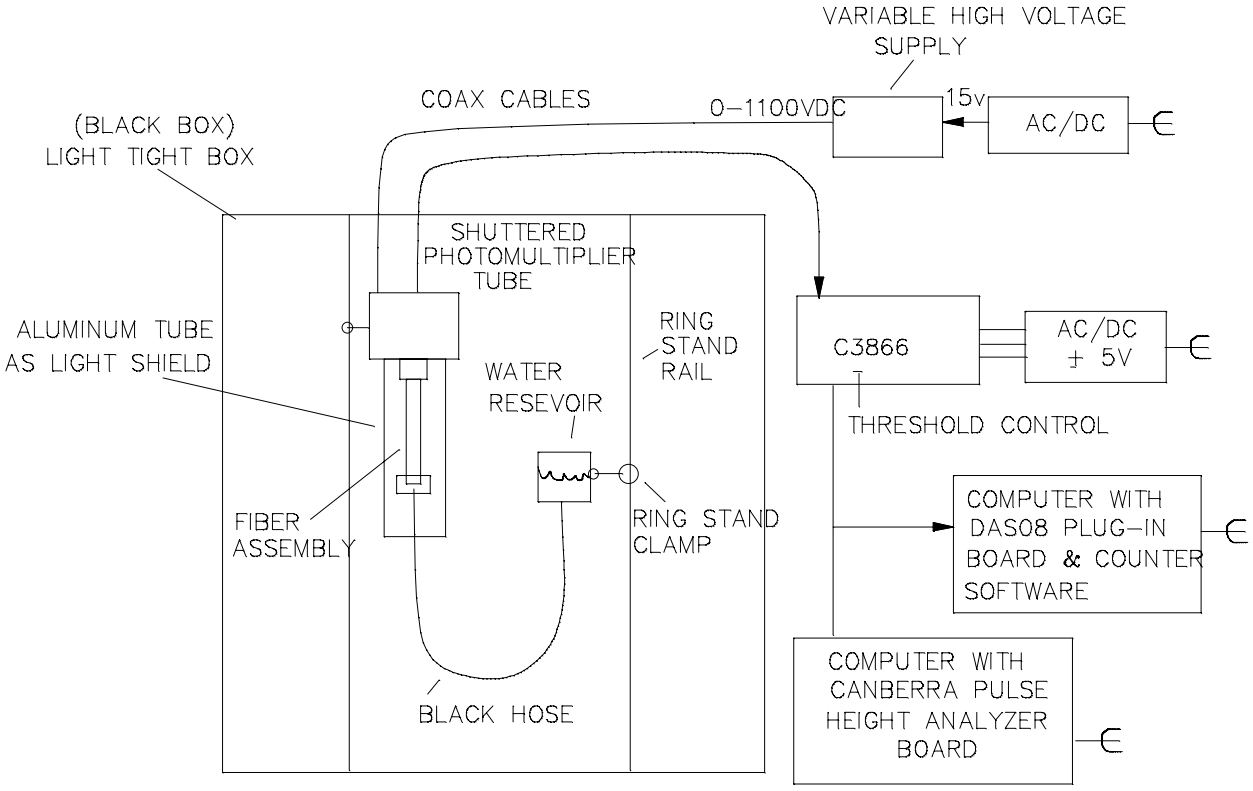

FIGURE 9-2. MAJOR COMPONENTS OF FIBER EFFICIENCY APPARATUS

Figure 9-2 (above) is a sketch showing the major components of the apparatus. The fiber assemblies and PMT (photomultiplier tube) were housed in a light tight box that was lined inside with black flocking paper (non-reflective). To further guard against the possibility of light leakage, an aluminum tube was put over the fiber assembly once the assembly was mounted to the PMT housing.

The PMT and water reservoir were mounted on a pair of ring stand rails that were built into the top and bottom of the “black box”. The level of submersion of the fibers was controlled simply by raising or lowering the water reservoir.

The high voltage supply to the PMT could be adjusted up to 1100V. In practice once the system had been optimized (see Section 9.4) the voltage was kept the same for all of the efficiency tests.

The output of the PMT was input to a Hamamatsu C3866 photon counting module that converted the short, low-level pulses from the PMT to logic level pulses. It further acted as a prescaler, outputting one logic level pulse for each 10 input pulses.

The output from the C3866 was simultaneously input to a counter chip on the DAS08 board and to the Canberra pulse height analyzer (PHA) board (Accuspec NaI). During initial shakedown of the apparatus both the counter and PHA were used to simultaneously record data. Since they were in agreement, and since data acquisition and reduction were simpler with the counter, the PHA was not used. It was however left attached as shown in Figure 9-2 because the system exhibited better stability with it attached.

9.2.5.2 Counter

A standard logic level counter chip (Intel 8254) included as part of a ComputerBoards Inc. data-acquisition board DAS08-PGA was used for the counter. A program was written in "C" language that:

- allows the user to specify a file name in which the data will be stored
- allows the user to specify the integration time
- upon keyboard command begins counting and saves a data point at the end of each integration period
- continues acquisition until the run is terminated by keyboard input
- saves the data as an ASCII file

For all of our efficiency tests the integration time was set for 60 seconds. The run duration varied anywhere from 10 minutes to several hours.

9.2.5.3 Test Procedures

To avoid warm-up problems, all of the electronics (the PMT, its power supplies, the C3866 and the computer/counter) were left on continuously throughout the test program. On the few rare occasions when they were powered down, they were allowed to warm up for a minimum of 1 hour before any data was taken.

Because PMT's exhibit hysteresis if exposed to even moderate light levels, care was taken to avoid exposing the tube to any light other than that from the fibers. The PMT housing included a hand-operated shutter that was always put in the closed position whenever a fiber assembly (with aluminum light shield) was not in place.

Early in the testing, we found that the fibers exhibit phosphorescence. To avoid problems from this effect the fiber assemblies were stored in a light tight box when not in use. During the transfer and mounting process the room was lighted by a single 60-watt bulb kept at a distance of more than 10 feet from the fiber assembly. The room in which the apparatus was set up had two exterior windows which were both blocked off with opaque covers so that the 60-watt lamp was the only illumination in the room. This was the situation not only during loading and setup but also during the actual data acquisition.

The light tight box in which the experiment was conducted had a sliding door that provided access to the set-up. After mounting a new assembly the door was shut and the system was left in the dark for a minimum of 10 minutes before any data was taken.

There were 4 different conditions involved in a typical test run. They were:

- with the shutter closed and the counter reading only the electronic “dark count” noise
- with the shutter open to expose the PMT to the fiber assembly which was dry i.e. no water
- with the shutter open and the fiber assembly filled with non-tritiated water.
- with the shutter open and the assembly filled with tritiated water.

The tritiated water was obtained from Isotope Products Laboratories of Burbank, CA and had an activity of .93mCi/liter as indicated in the certification sheet given in Appendix H.

To fill the fiber assembly with water the reservoir was filled and then alternately raised and lowered for a total of 3 cycles to insure that all of the air was forced out and the fibers were all wetted. During system shakedown this procedure was carried out with the aluminum light-shield tube removed so that the operator could view the fibers inside the assembly’s teflon tube. It was observed that the alternating up and down pumping action was very effective at wetting the fibers. No surface tension effects such as "wicking" were observed. After the second cycle, no residual air bubbles could be seen.

When changing between tritiated and “wash” water this up and down cycling also served to rinse away any residual droplets of the previous water type. A test run consisted of saving counter files at each of the conditions (shutter closed ≡ S, fibers in air ≡ D, fibers in “wash” water ≡ W, and fibers in tritiated water ≡ H). A separate file was saved for each change in condition. Typically several alternations between the W and H condition were recorded.

9.2.5.4 Stability

The fiber efficiency measurements were complicated by two forms of system noise, one a high-frequency instability and the other a low frequency drift.

High-frequency instability: Figure 9-3A plots the count rate as a function of time as measured during our system shakedown tests. It illustrates the short-term, high frequency instability. Note that except for a few short-lived incidents the count rate was low over the more than nine-hour period. Figure 9-3B shows the same data with the instability readings replaced with the average value of the stable readings.

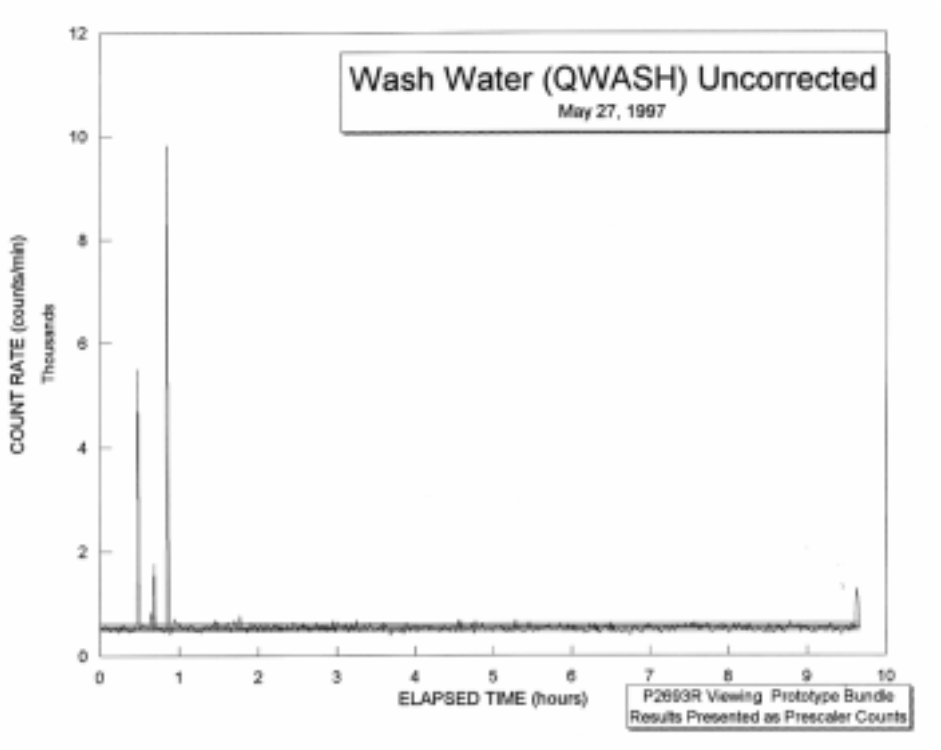

Figure 9-3A. Count Rate vs. Elapsed Time

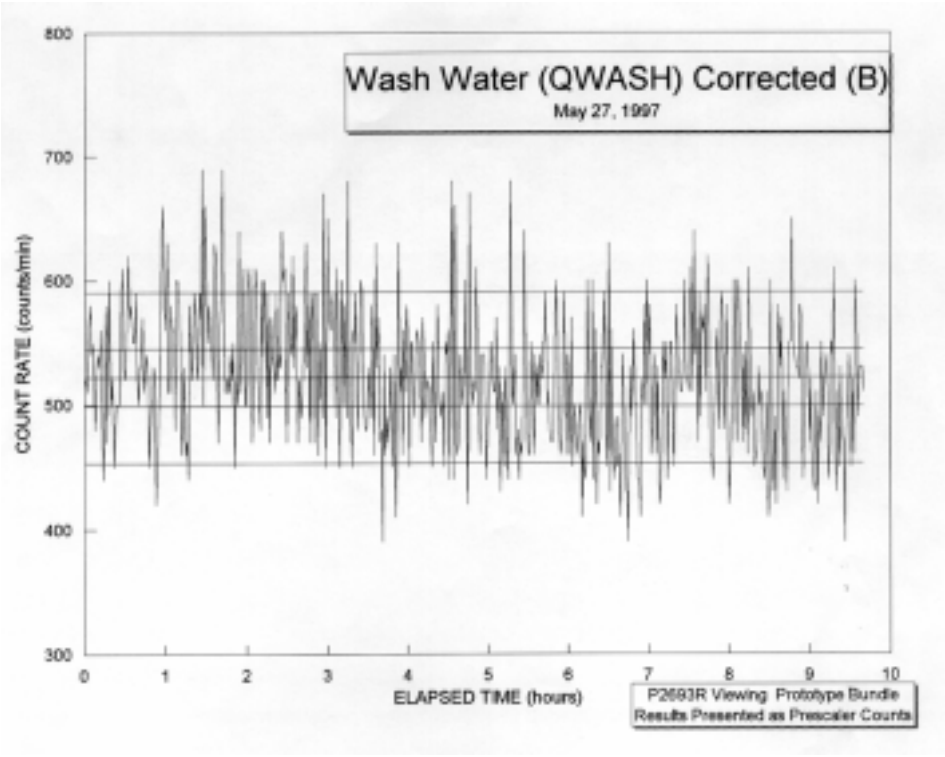

Figure 9-3B. Count Rate Vs. Elapsed Time

During system development we spent a great deal of time trying to eliminate this problem. It occurred whether we were using the counter or the PHA (pulse height analyzer) or both as the readout. Oscilloscope probing revealed that the high counts are due to the fact that the C3866 sometimes becomes unstable and breaks into a high frequency oscillation. We found that tendency toward instability could be reduced by changing the arrangement of the system grounding but that nothing we did was able to eliminate the problem altogether.

Similar instability was observed on another project in the past which employed a C3866 and a different PMT. The system operated properly during development and testing at our facility and during the first week of operation after shipment to the customer. At the end of the first week, the system suddenly became unstable for about 5 minutes and then returned to normal operation. Several more "incidents" occurred in the next week of operation. Working with Hamamatsu and the customer we eliminated light leakage and grounding as a problem, and concluded the problem must be due to some form of radiated interference. This hypothesis was confirmed during work on the present fiber-efficiency set-up. We noticed a correlation between the instability and the hum of a nearby lawnmower, and we deliberately recorded the data shown in Figure 9-4.

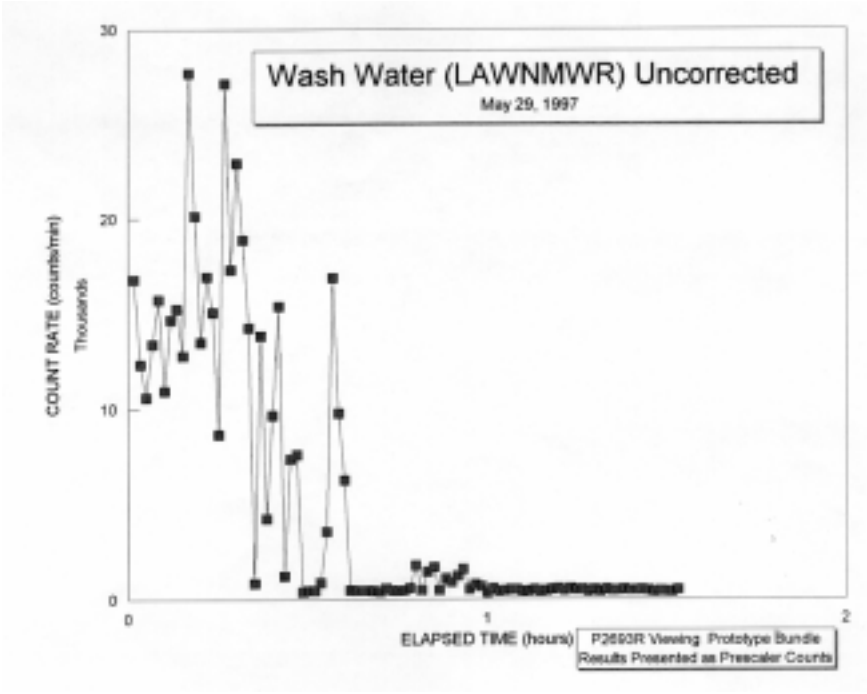

Figure 9-4. Count Rate vs. Elapsed Time

During the first 40 minutes of the file the mower was in an area that at its closest came within 50 feet of the C3866. During the last part of the first hour the mower moved to an area more than 100 feet away. The mower was shut off at the end of the first hour, after which the system recovered and showed no more instability. Neither the C3866 nor the PMT are provided with magnetic shielding. For any future testing they should be shielded.

Low Frequency Drift: The second "noise" problem is illustrated in Figure 9-5. The data was acquired at the usual 60-second integration time. For the plot however, a 30-minute rolling average was calculated. The reason for the longer averaging time is to reduce the random fluctuations in the number of counts. Although the 30-minute average does indeed reduce the minute to minute fluctuations, Figure 9-5, shows that significant variations remain with a period on the order of half and hour or so.

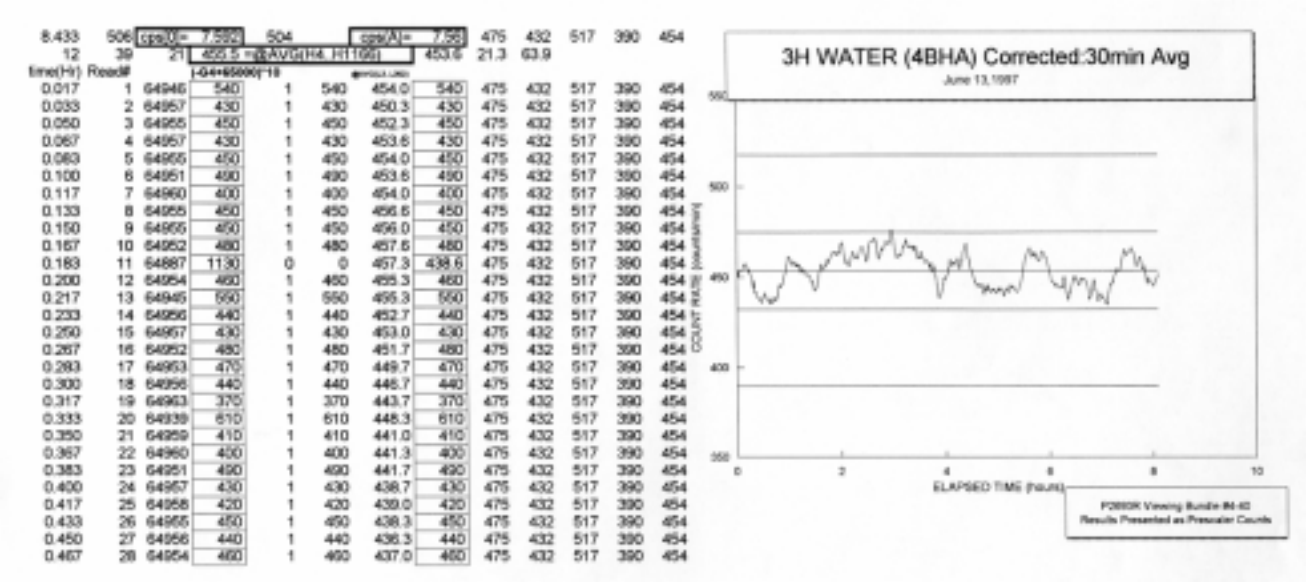

Figure 9-5. Count Rate vs. Elapsed Time

Clearly the accuracy of the measurements suffers if we make the transition from one test condition to another, e.g. H (tritiated) to W (wash) water, just when the detector is making one of its significant level shifts such as that at about 5.5 hours in Figure 9-5. This is why the test procedure involves several back and forth transitions between the H and W conditions.

9.2.5.5 Data Reduction

The data files saved by the counter program consist of a column of numbers, one for each 1-minute integration period of the test. At the beginning of the integration period the software loads the counter chip register with an initialization number (any number up to 65536 can be specified at the start of the program), which is then decremented by one each time a pulse is received. At the end of the integration time the software reads the current register value, saves it, and reinitializes. The numbers in the data files are therefore the initialization number minus counts received rather than just the counts received.

A Lotus-123 spreadsheet template was prepared for reduction of the data files. The template:

- converts the file values to counts
- rejects readings that are “out of bounds”
- calculates a rolling average over a selectable time period
- calculates the average count rate over the file run time
- and plots the count rate as a function of time

Figure 9-6 shows the structure of the worksheet template. Since the C3866 outputs one count for every 10 pulses from the PMT, the count data must be multiplied by 10 to convert to actual counts from the PMT. This is done in column D along with removing the counter initialization offset. The “out of bounds” filter is based on a logic command that rejects any reading >1.15 times the average reading.

The equation used to calculate column H gives the same values as in column D for points that pass the filter. For those points that the filter rejects, the column H numbers are the average of all points that pass the filter.

9.2.6 Results

Measurements were made on the first four fiber types in June of 1997. In October, the Bicron fiber was added to the test program. While the system was set up to test the Bicron fiber assembly the original 4 bundles were re-tested.

Table 9.3 summarizes the results of both sets of tests. The response values given in Table 9.3 are those calculated as the average rate over the duration of the file time using the template described in the previous section. The columns designated "Condition" in Table 9.3 indicate whether the data was taken in wash (W) or tritiated (H) water. The results are presented in the sequence in which the data was taken. The column designated as DIFF gives the increase in count rate caused by going from wash to tritiated water. Note that frequently this is a negative number indicating that the tritium effect is smaller or on the same order of magnitude as the stability of the test apparatus.

The June data indicates that fiber Type #1 is unquestionably the best. The October data confirms this but indicates a significantly lower sensitivity than that determined in June.

One significant difference between the June and October tests was time. In October each condition was maintained for about 45 to 60 minutes while in June the duration was frequently much longer. Figure 9-7A shows a plot of the raw data for the entire test sequence on the Type #1 fiber assembly. There were periods when the instability was severe. Use of a mu metal shield around the photomultiplier tube and/or a Faraday cage around the signal processing electronics could reduce the instabilities caused by stray electromagnetic fields.

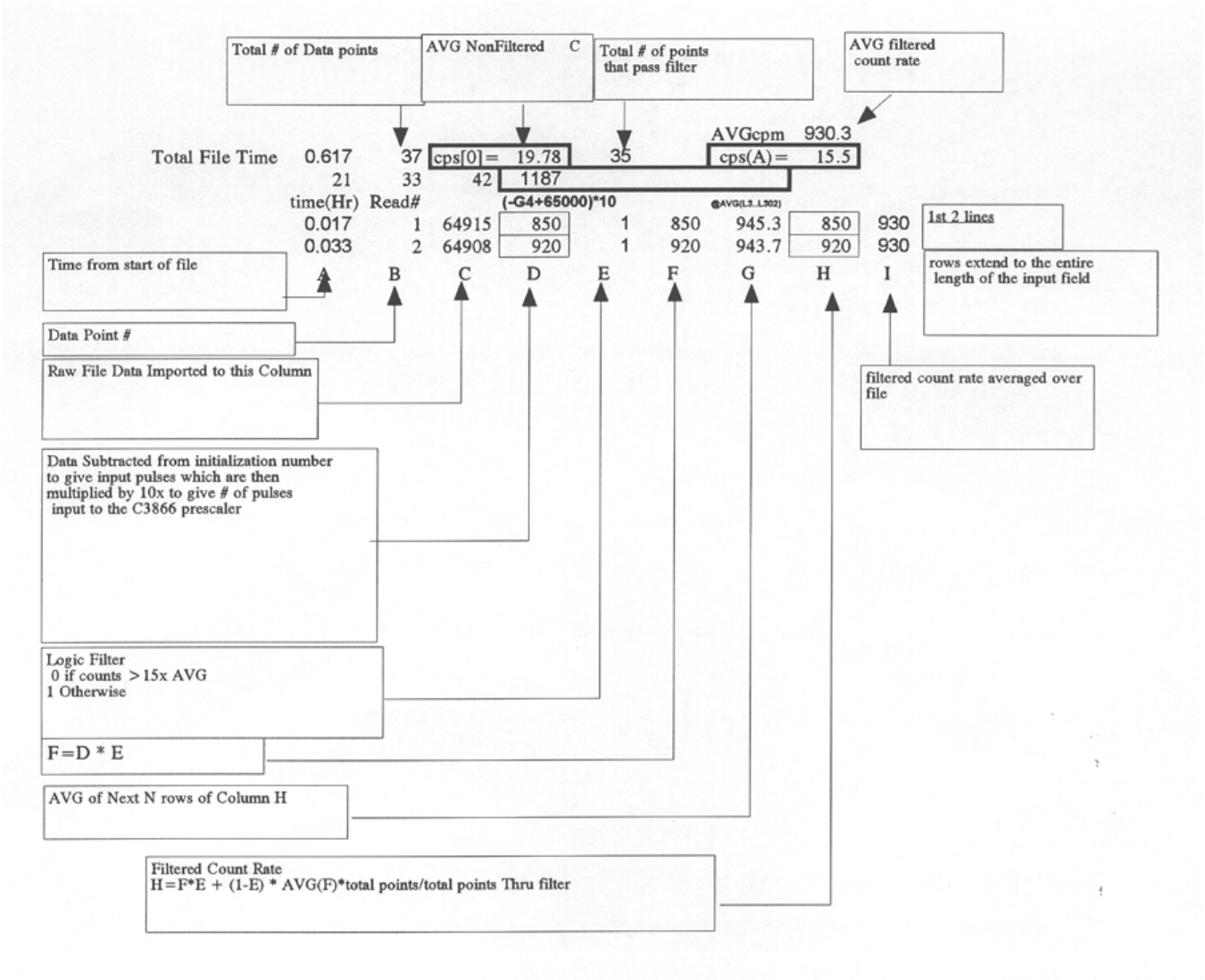

Figure 9-6. Counter Data Reduction Template

Table 9.3 Test Summary

June 1997

CONDITION			CONDITION			CONDITION			CONDITION			CONDITION	
	TYPE#1	DIFF		TYPE#4	DIFF		TYPE#5	DIFF		TYPE#6	DIFF		TYPE#7	DIFF
W	14.51		W	16.07		W	13.77		W	8.12				
H	15.94	1.43	H	15.97	-0.1	H	12.82	-0.95	H	7.86	-0.26			
W	14.13	1.81	H	15.28		W	11.89	0.93	W	8.16	-0.3			
H	16.11	1.98	W	14.14	1.14				W	8.37				
H	14.74		H	12.81	-1.33				H	7.72	-0.65			
W	13.35	1.39							W	7.29	0.43			
	AVGDIF	1.65		AVGDIF	-0.10		AVGDIF	-0.01		AVGDIF	-0.20			

October 1997

W	6.97		W	5.504		W	5.274		W	5.129		W	34.53	
H	7.49	0.52	H	5.217	-0.29	H	5.336	0.062	H	5.466	0.337	H	35.62	1.09
W	6.72	0.77	W	4.968	0.249	W	5.667	-0.33	W	5.322	0.144	W	35.67	-0.05
W	6.89		H	5.347	0.379	W	5.679		H	5.052	-0.27	W	35.86	
H	7.29	0.4	W	5.337	0.01	H	5.192	-0.49	W	4.729	0.323	H	36.07	0.21
W	6.41	0.88				W	5.106	0.086						
												W	21.72	
												H	21.28	-0.44
	AVGDIF	0.643		AVGDIF	0.088		AVGDIF	-0.17		AVGDIF	0.134		AVGDIF	0.203

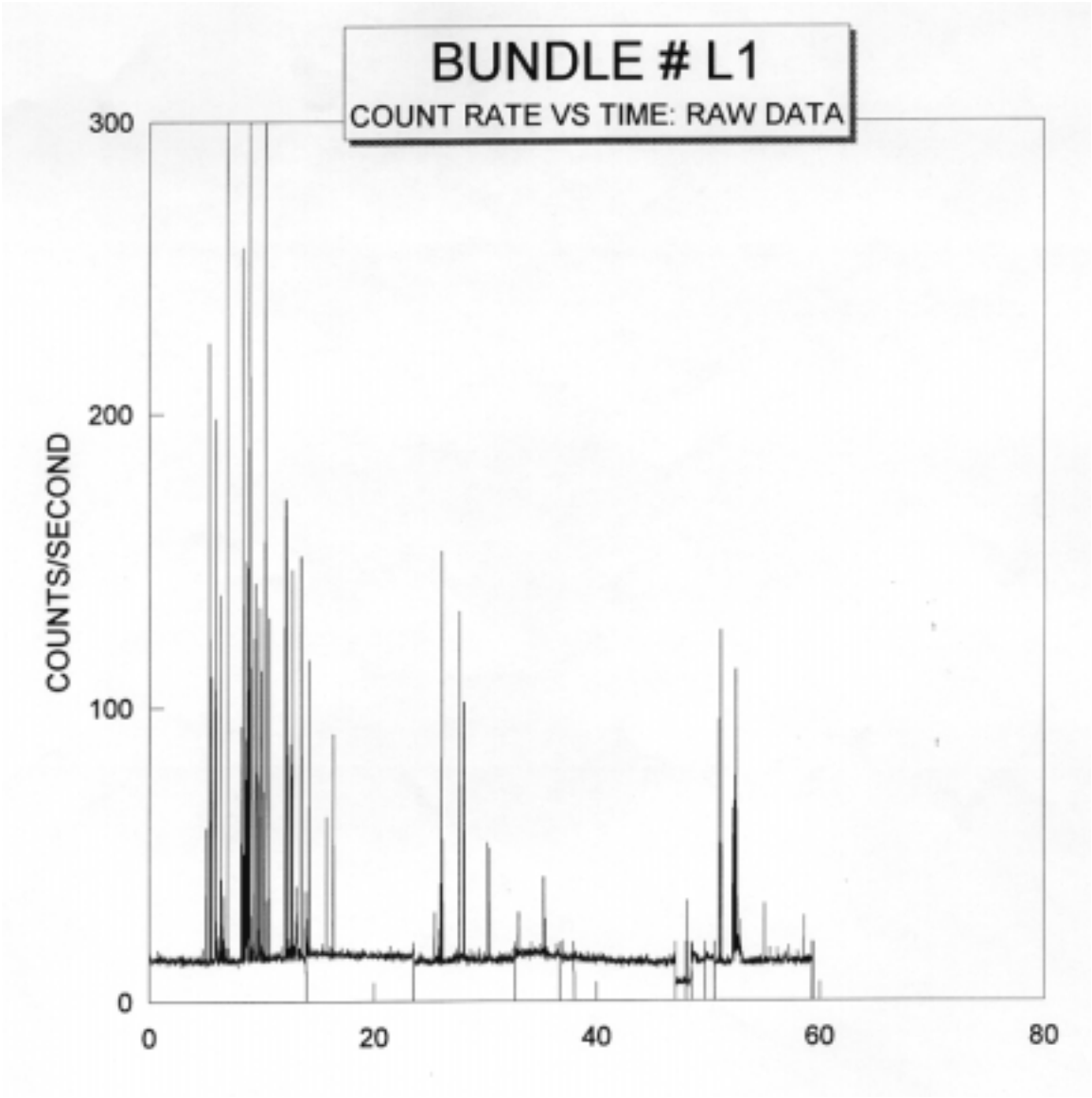

Figure 9-7A. Count Rate vs. Time

Figure 9-7B shows the same data after filtering of the instability and averaging the data over 10-minute periods.

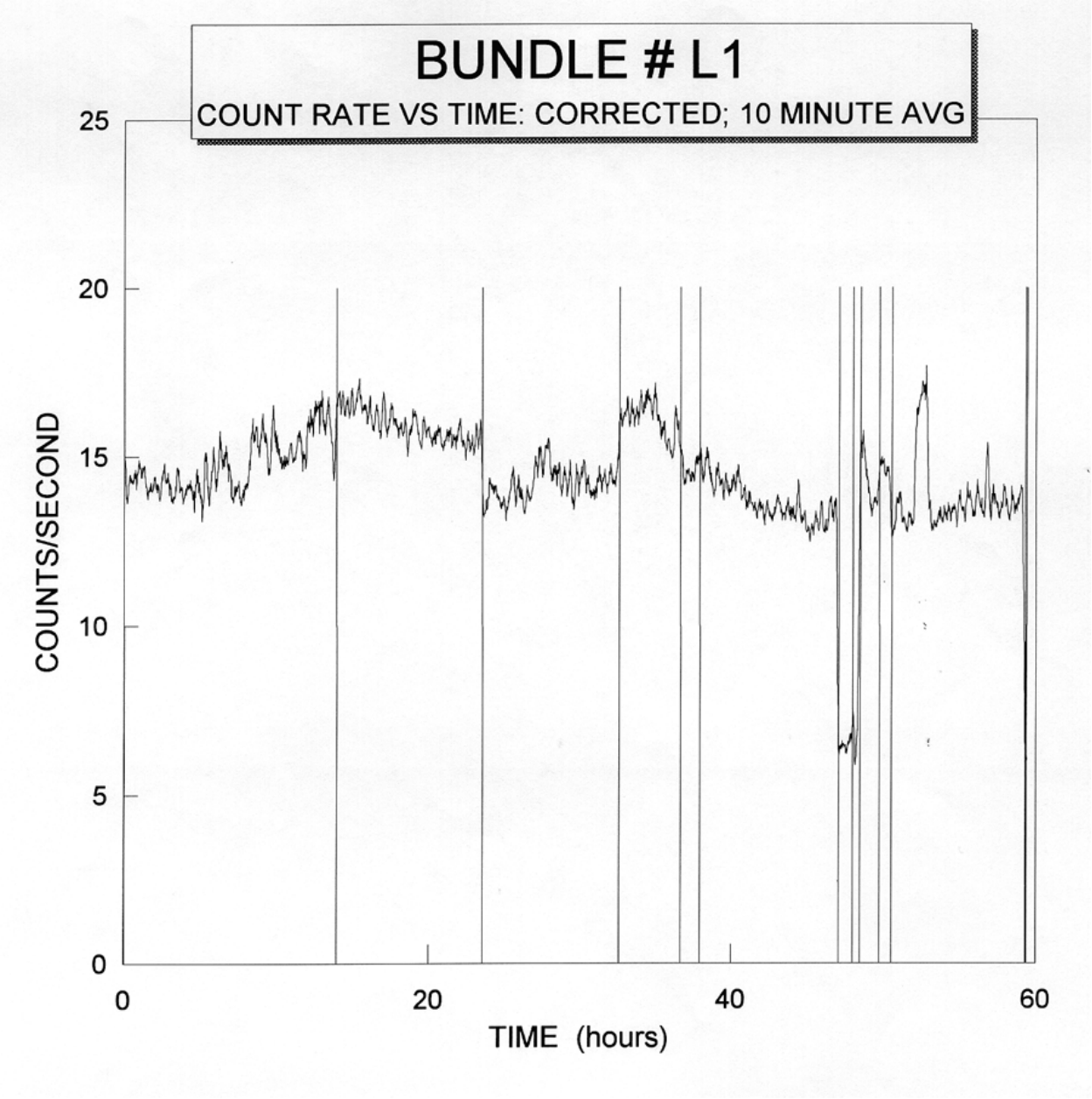

Figure 9-7B. Count Rate Vs Time

The drift from beginning to end of each condition period (indicated by the vertical lines) is significant and brings into question the approach of using the value averaged over the entire condition period. What if we looked instead only at the data near the transition points between the W and H conditions?

The template was modified to determine the average count rate over the 40 data points (1minute/point) adjacent to the condition transition. Figure 9-8 is a typical plot of the data from one such truncated data file. It can be seen that the data points are scattered evenly about the average rather than showing any significant drift trend.

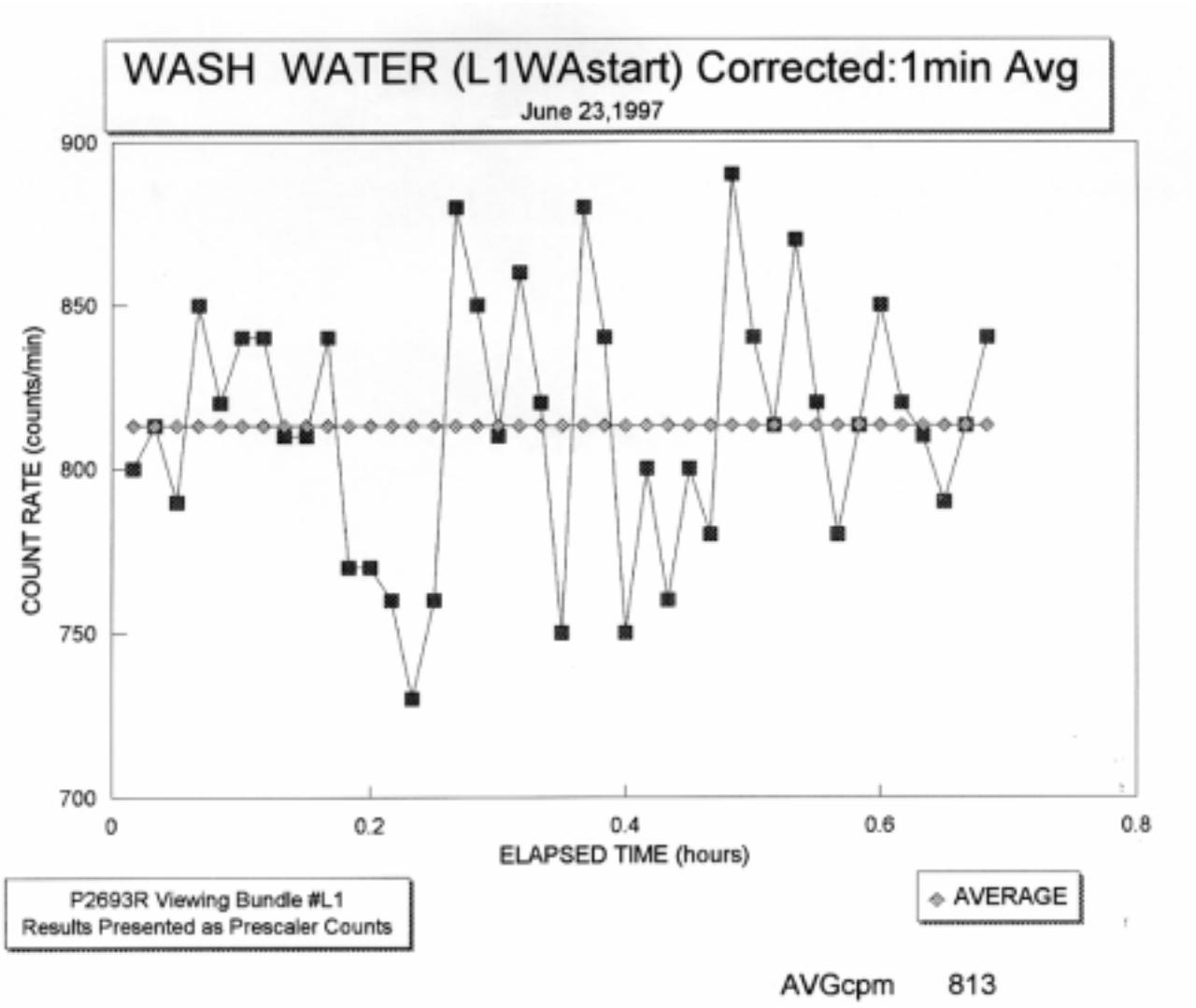

Figure 9-8. Count Rate vs. Elapsed Time

Table 9.4 summarizes the data from the truncated reduction. The earlier data from Table 9.3 is repeated for comparison. Surprisingly the end result average for the two approaches turns out to be the same.

Table 9.4 Data From Truncated Reduction

DATA FROM BUNDLE OF TYPE #1 FIBERS				
	TRUNCATED DATA		**ENTIRE RUN AVG**	
CONDITION	CPS	H-W	CPS	H-W
W	15.60		14.51	
H	16.63	1.03		1.43
H	15.54		15.94	
W	13.55	1.99		1.81
W	14.22		14.13	
H	16.20	1.98		1.98
H	15.41		16.11	
H/2	14.52		14.55	
H/2	16.52		14.31	
H	14.61		14.74	
H	14.60			
W	13.01	1.59	13.35	1.39
	AVERAGE = 1.65		AVERAGE = 1.65	

The loss of sensitivity between the June and October readings seems then, to be real rather than an artifact. At the end of the June tests the Type #1 fiber bundle was not removed from the setup. It remained in place, filled with “wash” water for the next 39 days. Perhaps a surface contamination or leaching occurred.

9.2.7 Efficiency

Let us convert the 1.65 count/sec value for the Type #1 fibers to fiber efficiency. The bundle assembly consisted of 45 fibers each with a diameter of 0.05cm and an immersed length of 43cm. The fiber area is

$$A = 304\text{cm}^2$$

Based on the measured value of $0.034cm^{-1}$ for the fibers absorption coefficient (see Section 9.6) and a total fiber length of 45cm the average transmission efficiency is T[AVG] = 0.51. The quantum efficiency of the R2693P PMT is Q = 0.2 and the activity of the test solution is a = 0.93 mCi/L.

Combining the above values in Equation 9.5, we can calculate the fiber efficiency as

$$\varepsilon = \frac{1.65}{0.93\text{x}10^{9}\,\text{x}304\text{x}0.2\text{x}0.51}$$

$$\boxed{\varepsilon = 5.7\text{x}10^{-11}\,\frac{\text{photons/sec}}{(\text{pCi/liter})\text{cm}^2}}$$

If we assume the range of tritium betas in water to be 10^{-4} cm and use the value above in Equation 9.6, we can calculate the value of *p*

$$p = \frac{\varepsilon}{\tau w} = \frac{5.7\text{x}10^{-11}}{10^{-4}\,\text{x}3.7\text{x}10^{-5}} = .015\,\frac{\text{photons}}{\beta}$$

The value of p expresses the average number of photons generated and trapped in fiber transmission modes for each incident beta particle. The value of p measured in our earlier planchet tests was 20 times as large as the value determined here. The difference is due to the fact that the betas incident on the fibers in the planchet test arrived with an average energy of 6keV while the average energy of those reaching the fiber through water is much less. (See Appendix I.)

9.3 STABILITY - TEST SERIES B

9.3.1 Objective

The objective of this series is to assess the effect of long-term water immersion on the response repeatability of the fibers.

9.3.2 Approach

Two fiber bundles of each of the four types (1,4,5,6) were prepared for this test series. These bundles were of the same design as those used for the fiber efficiency tests, but they were shorter.

The response (count rate) produced by these bundles when exposed to the tritiated water was measured before and after an extended (22 day) soak in hot water. The water temperature was maintained at 120 deg F which was chosen to accelerate any change without danger of causing irreversible thermal damage to the fibers.

9.3.3 Apparatus

Figure 9-9 is a diagram showing the components of the thermal bath. The fiber bundles were placed inside a glass container filled with water obtained from Aquabar. This is the same water source used for the “wash” water in the fiber efficiency tests. It is processed to remove both particulate and organic contaminants. Independent background radiation tests on this water are

provided in Section 9.7. The temperature of the bath was monitored throughout the 22 day soak period and found to remain at 119 ± 3 deg F.

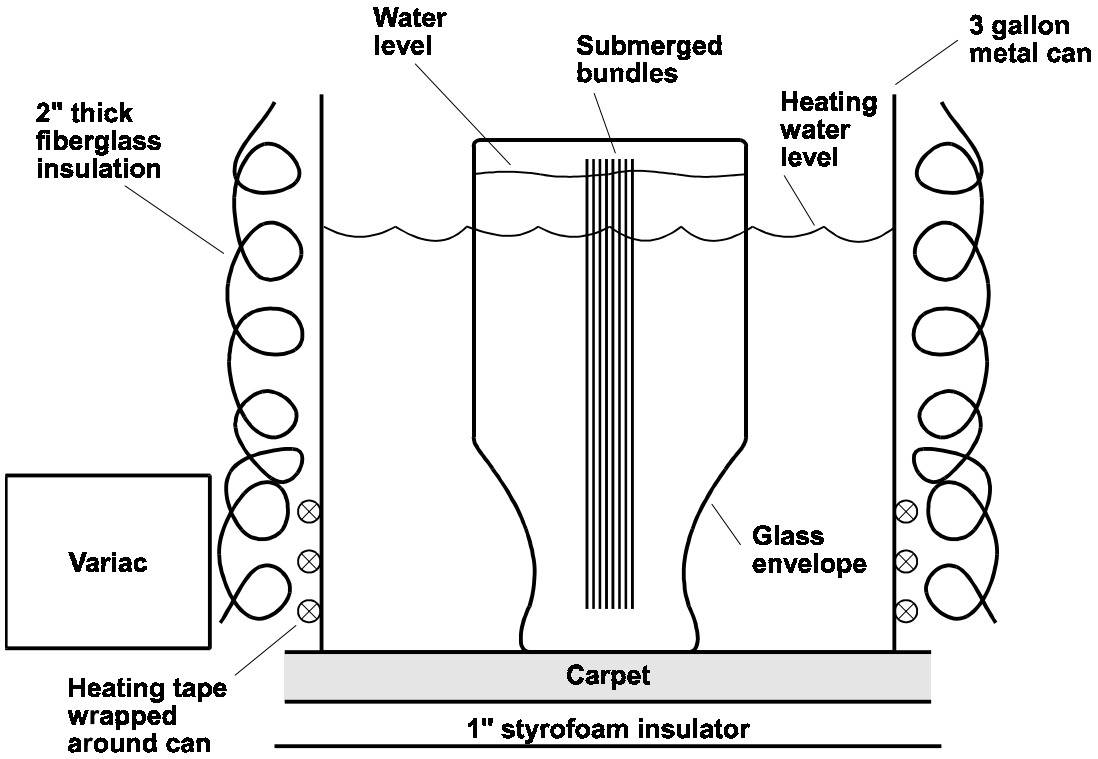

Figure 9-9. Diagram of Thermal Bath

9.3.4 Results

Table 9-5 summarizes the results of the measurements made on the two Type #1 fiber bundles. Measurements after soak of the other fiber types were not made because the presoak performance was so poor. Table 9-5 indicates a significantly lower response after the soak.

Table 9.5 Summary of Short Bundle Measurements

PRESOAK MEASUREMENTS					
BUNDLE # 1 – 40			**BUNDLE # 1 - 41**		
CONDITION	**COUNTRATE (CPS)**	**$C_H - C_N$**	**CONDITION**	**COUNTRATE (CPS)**	**$C_H - C_N$**
W	8.038		W	8.359	
H	9.116	1.08	H	9.694	1.34
W	7.898	1.22	W	8.675	1.02
H	9.528	1.63	W	8.300	
H	9.062		H	9.656	1.36
W	7.968	1.09	W	8.191	1.465
	AVG DIFF 1.25			AVG DIFF	1.29
POSTSOAK MEASUREMENTS					
BUNDLE #1 - 40			BUNDLE #1 - 41		
CONDITION	**COUNTRATE (CPS)**	**$C_H - C_N$**	**CONDITION**	**COUNTRATE (CPS)**	**$C_H - C_N$**
W	6.427		W	9.698	-.241
H	6.778	.351	H	9.457	1.335
W	8.776		W	8.122	.327
H	10.140	1.364	H	8.449	-2.561
H	7.182		W	11.01	.590
W	8.909	-1.727	H	11.60	.730
W	7.342		W	10.87	-1.062
H	7.942	.600	H	9.808	1.735
W	8.233	.291	W	8.073	
H	8.247	.014			
W	8.060	.187			
	AVG DIFF 0.071			AVG DIFF	0.107

9.4 THRESHOLDING - TEST SERIES C

9.4.1 Objective

Two low dark-count PMTs were purchased for evaluation for potential use in the tritium monitor prototype. The objective of this test series was to determine the threshold settings that optimize the PMT performance and to determine which of the two PMTs is preferred.

9.4.2 Apparatus

Figure 9-10 shows the relevant components of the setup used to determine the optimum threshold. The tests were run in the light tight box described in Section 9.2. The aluminum tube was the same as used as a light shield around the fiber assemblies in the Section 9.2 tests. In this case it served to restrict the amount of light from the LED that could reach the PMT. The LED provided a stable repeatable low level light source for making comparative response measurements.

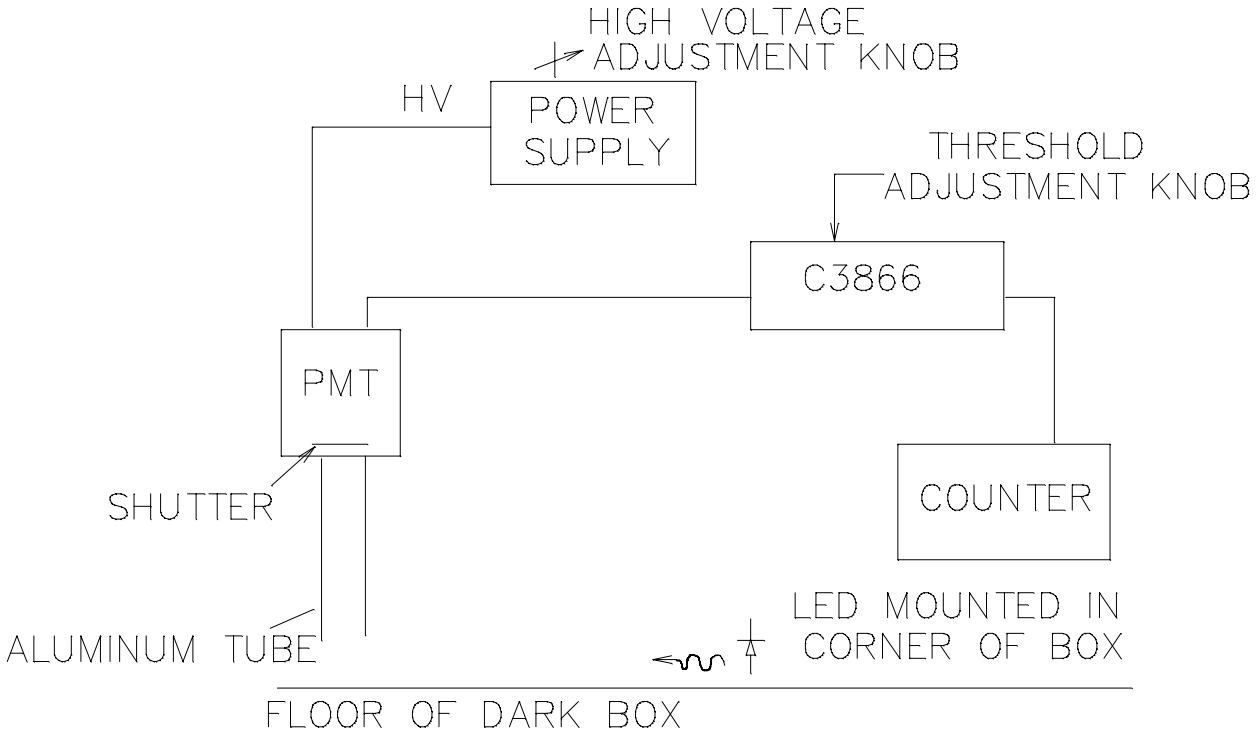

Figure 9-10. Diagram of Apparatus for Test Series C

Figure 9-11 is a conceptual sketch of the thresholding process.

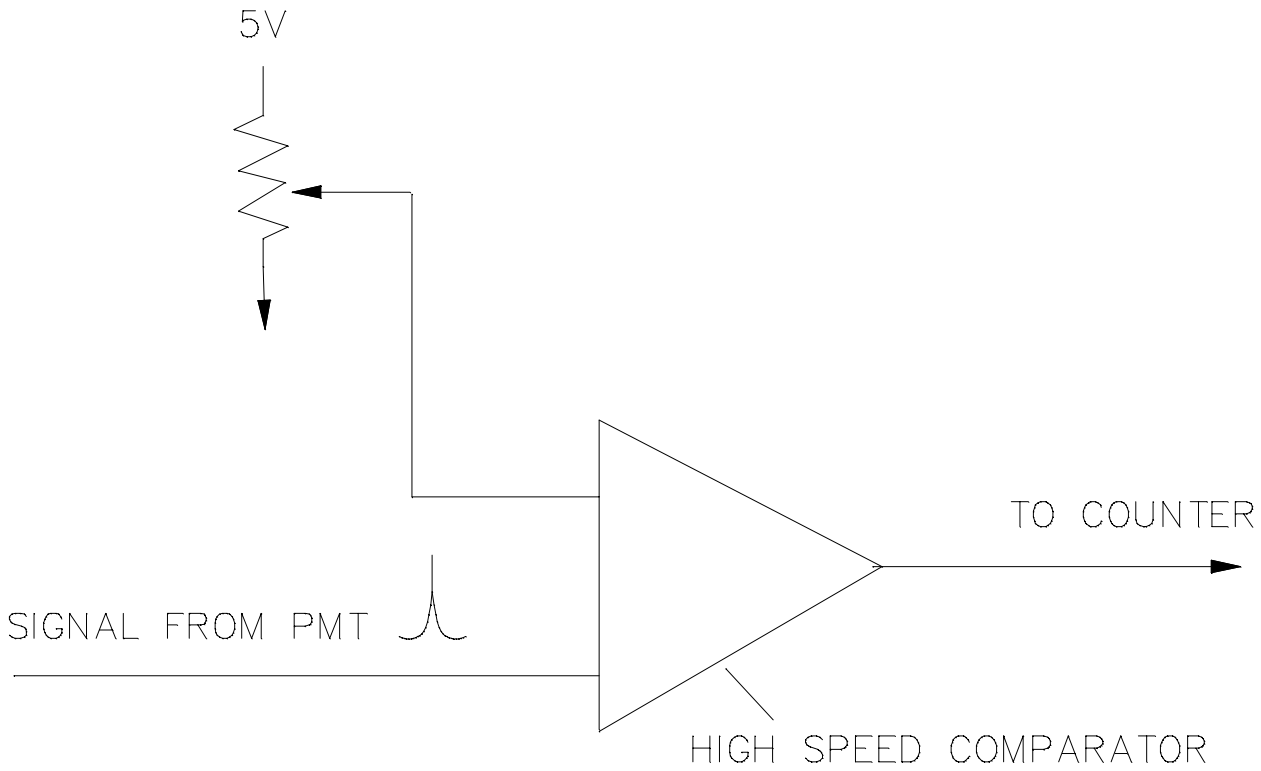

Figure 9-11. Thresholding Concept Sketch

The PMT signal is connected to one input of a comparator and a threshold voltage is connected to the other input. When the threshold voltage is higher than the peak height of the input pulse the output state of the comparator does not change and no count is recorded. If the peak height of the input pulse is higher than the threshold value the comparator will output a pulse. Setting the threshold level high will therefor reject low level “dark-noise” pulses. Unfortunately it also rejects a certain fraction of the signal pulses as well. The purpose of our tests was to determine at what threshold level the signal to noise ratio is an optimum.

There is a second parameter (the high voltage supply voltage) that also effects the signal to noise ratio. The signal to noise ratio as a function of threshold voltage was measured for several different supply voltages.

9.4.3 Results

Figure 9-12 summarizes the results of the measurements made on the R2693P PMT. Note that although the relative signal level continues to increase with applied voltage (middle plot), the noise increases even faster so that the ratio S/N begins to decrease. Based on the data in Figure 9-12 we chose an applied voltage of 950V with a threshold of 320mV as the optimum operating point.

We chose the R2693P PMT over the R3550 whose performance is summarized in Figure 9-13 on the basis of its lower dark-count. The data in Figure 9-12 was taken with an integration time of 150 seconds. The nominal dark count rate at 950V, 320mV threshold was 7.7 PMT counts/second. The R3550 data of Figure 9-13 was taken with an integration time of 120 seconds and a nominal dark count at 975V and 250mV threshold of 10.8 PMT counts/sec

Threshold (mV)	800V S	800V N	800V S/N	900v S	900v N	900v S/N	950v S	950v N	950v S/N	1000v S	1000v N	1000v S/N	1050v S	1050v N	1050v S/N
260	929	101	9.20												
280	352	17	20.71	2844	139	20.46				5155	181	28.48	6159	415	14.84
300	165	13	12.69	2297	73	31.47	3669	114	32.32	4794	179	26.78	5266	231	22.80
320	77	10	7.70	1679	52	36.13	3391	115	29.48	4390	152	28.88	5047	204	24.74
340	41	7	5.86	1691	57	29.67	3144	101	31.28	3976	132	30.12	4642	198	23.44
360				1552	50	31.04				3598	131	27.47	4157	185	22.47

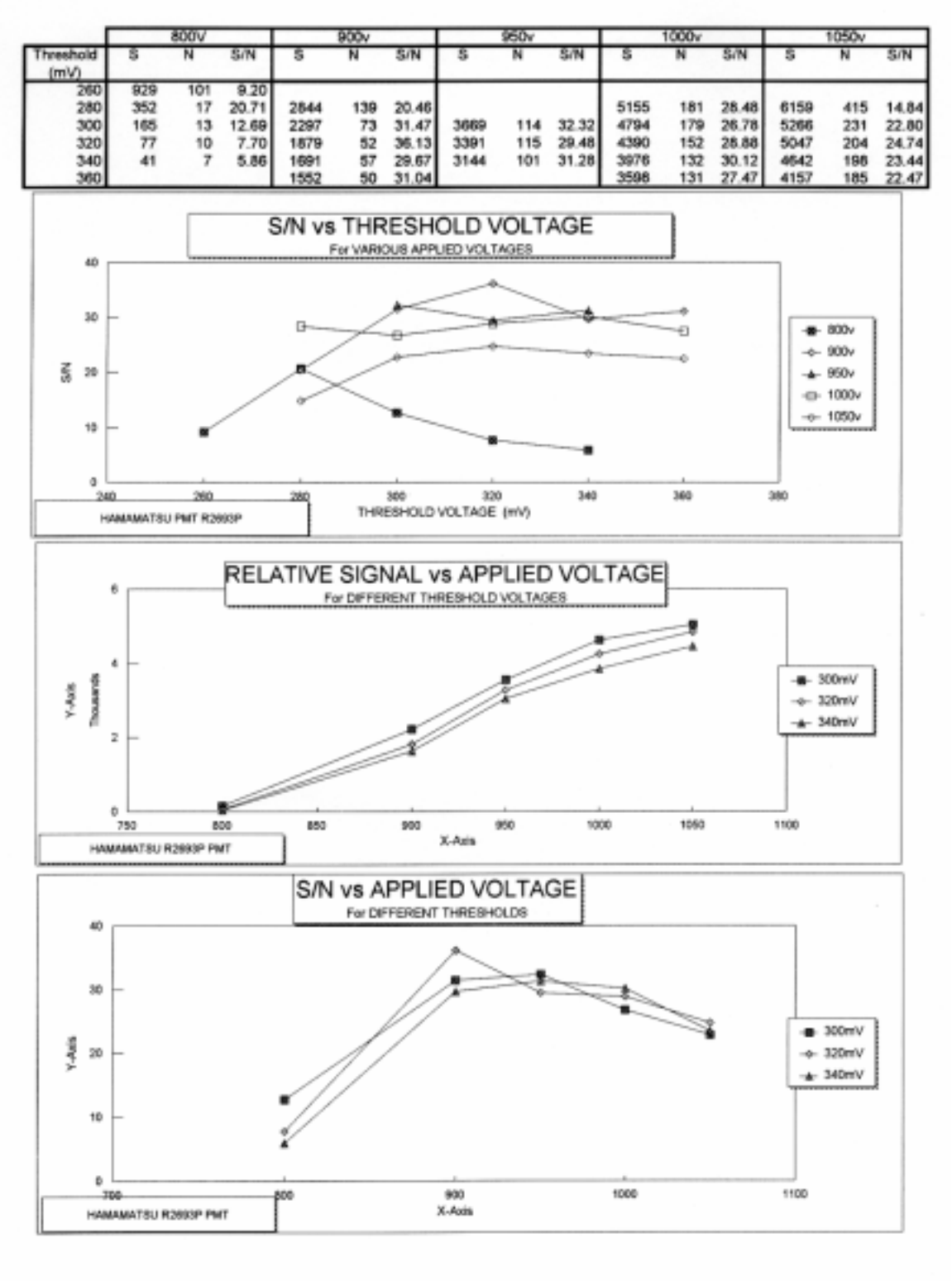

Figure 9-12. Characterization Data Plots for PMT R2693P

Threshold (mV)	950V S	950V N	950V S/N	975v S	975v N	975v S/N	1000v S	1000v N	1000v S/N	1050v S	1050v N	1050v S/N
125	2642	156	16.94	2865	185	15.49						
150	2514	150	16.76	2698	155	17.41	2846	180	15.81			
175	2416	145	16.66	2676	162	16.52	2812	184	15.28	3848	268	14.36
200	2295	135	17.00	2468	155	15.92	2716	148	18.35	3722	258	14.43
225	2108	133	15.85	2439	144	16.94	2622	158	16.59			
250	1899	119	15.96	2299	129	17.82	2560	158	16.20	3622	224	16.17
275	1783	116	15.37	2266	124	18.27	2472	140	17.66	3452	238	14.50
300	1593	115	13.85	2031	128	15.87	2370	136	17.43	3487	224	15.57
325	1413	100	14.13	1968	115	17.11	2326	142	16.38	3391	206	16.46
350	1233	86	14.34	1844	114	16.18				3411	196	17.40
375	1022	80	12.78							3286	200	16.43

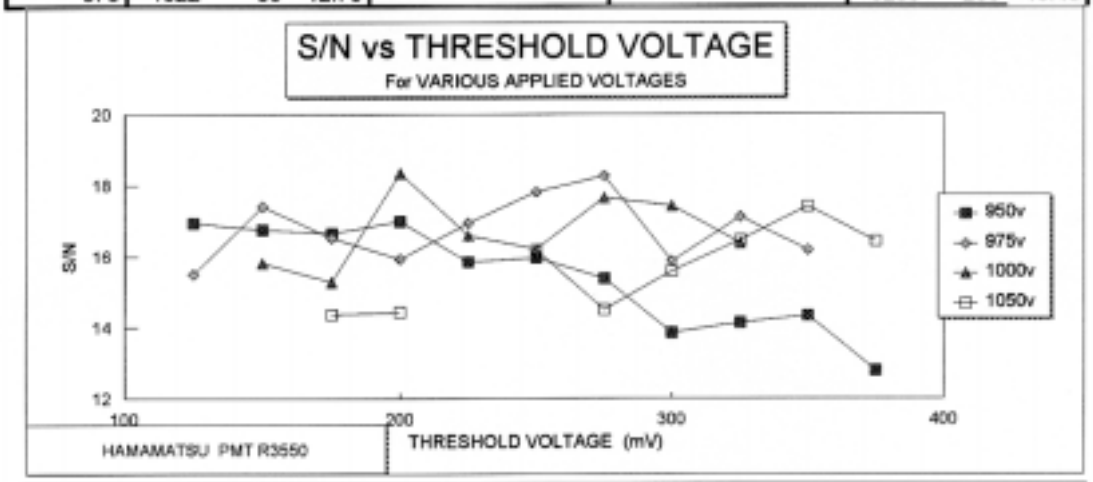

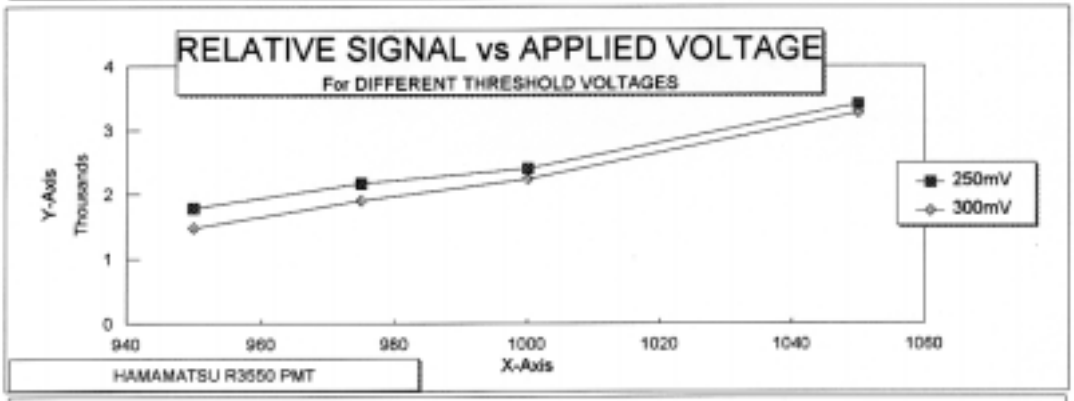

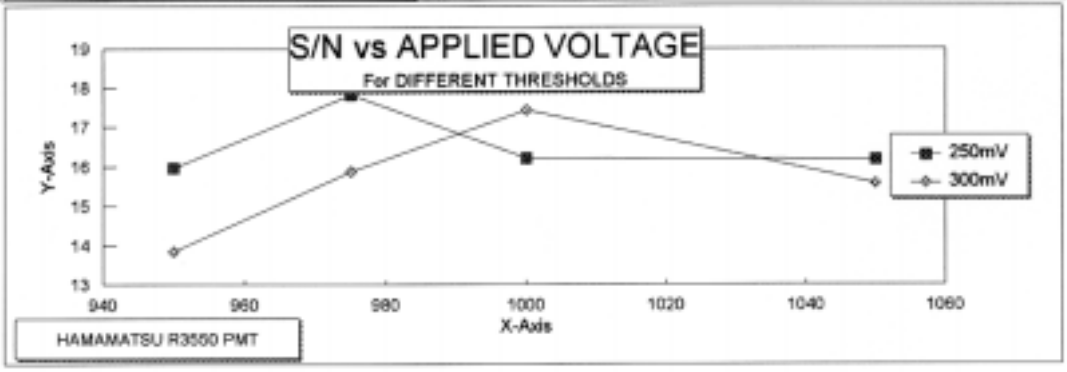

Figure 9-13. Characterization Plots For PMT R3550

9.5 TEST SERIES D - COINCIDENCE

9.5.1 Objective

The purpose of this test series was to determine the improvement in signal to noise that could be achieved by employing a detector at each end of the fiber bundle and requiring coincidence between the counts received in order to reject dark counts.

9.5.2 Approach

The original plan was to build fiber bundles that were terminated at each end, attach a separate PMT to each end, record the dark counts of each PMT separately and record the counts that occurred simultaneously (within set time windows).

9.5.3 Denouement

The coincidence circuit was designed and built, counter software was written and fiber bundles were prepared. However, the test series was aborted when results of the fiber efficiency tests became available. The probability of registering a count at one detector when a β hits the fiber is given by $p * Q * T$ and the probability of simultaneous registry at both ends is $(pQT)^2$. The efficiency tests showed that

$$(pQT)^2 \approx (.015*.2*.5)^2 = 2x10^{-6}$$

Until a better fiber is available there is no reason to pursue coincidence detection to improve performance.

9.6 ABSORPTION COEFFICIENT TEST – SERIES E

9.6.1 Objective – Determine the "effective absorption coefficient", k, for each of the fiber types.

9.6.2 Approach

Figure 9-14 shows the major components of the set-up. The pulsed N_2 laser illuminates the fiber at a right angle to the fiber axis. The 337 nm N_2 light is converted by the scintillating dye to photons (characteristic of the dye) that are trapped in the fiber and transmitted to the entrance of the monochromator. The Princeton Instruments analyzer is an electronic spectrometer employing a 700+ element intensified detector.

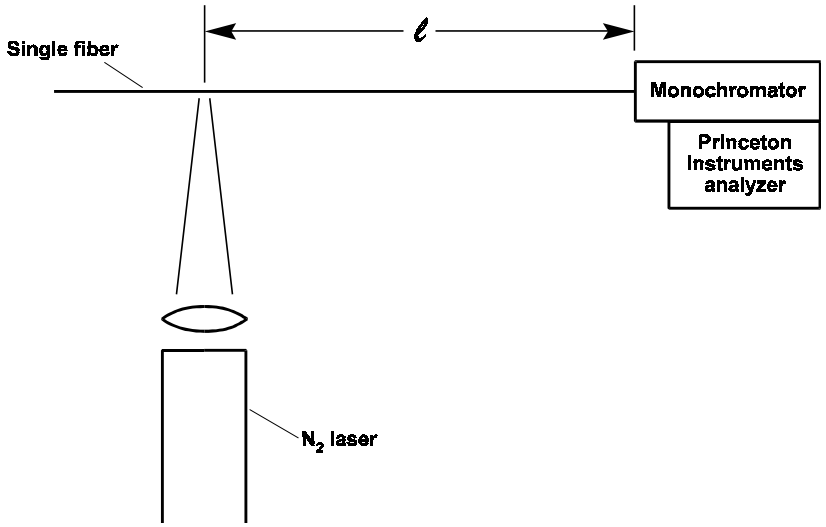

Figure 9-14. Diagram of Setup for Absorption Test

Because fiber Type 1 was the preferred fiber from the efficiency standpoint, absorption measurements were made over an extended length up to 150 cm. The planned procedure was to record light intensity delivered to the monochromator and plotted for monochromator-to-illumination point distances, ℓ, out to 50 cm. Also, for each type of fiber, transmission spectra were recorded.

Each recorded spectrum is a plot of intensity as a function of wavelength. Since the losses are exponential, we can write

$$I(\lambda)d\lambda = I_o(\lambda)e^{-k(\lambda)\ell}\, d\lambda \tag{9.7}$$

And the transmission between ℓ and a point 10 cm from the monochromator is

$$T(\lambda) = \frac{I_o(\lambda)e^{-k(\lambda)\ell}}{I_o(\lambda)e^{-k(\lambda)10}} = e^{-k(\lambda)[\ell-10]} \tag{9.8}$$

The effective transmission, i.e., the transmission averaged over all wavelengths, is

$$T = \frac{\int T(\lambda)d\lambda}{\int d\lambda} \equiv e^{-k[\ell-10]} \tag{9.9}$$

where k is the effective (averaged over all λ) absorption coefficient.

Note that k is a constant for small values of ℓ, but decreases as ℓ increases. The effective absorption coefficient was calculated from Equation (9.9) using values of $T(\lambda)$ calculated from Equation (9.8) using the recorded spectral data.

9.6.3 Results

The results for the integrated spectral intensity measurements are plotted in Figures 9-15 through 9-18. The transmission spectrum for each fiber is plotted in Figures 9-19 through 9-22. The absorption coefficients and fiber transmission are calculated from Equations (9.8) and (9.9). The results are tabulated in Table 9.6.

Table 9.6 Summary of Fiber Absorption Coefficients Calculated From Measured Data

Fiber Type	k (cm^{-1})
#1	.034
#4	0.02
#5	0.014
#6	0.093

SCINTILLATING FIBER ATTENUATION MEASUREMENT
USING EXCITATION BY NITROGEN LASER

FILE	PEAK (nm)	L	I	Ln(I)
F1 15	430.9	11	12996741	16.38
F1 20	433	15	12921085	16.37
F2 00	429.8	20	11064767	16.22
F2 50	435.2	25	9685651	16.09
F3 00	439.6	30	8358395	15.94
F3 50	440.7	35	6727108	15.72
F4 00	439.6	40	6127633	15.63
F4 50	440.7	45	4806748	15.39
F5 00	440.7	50	4264384	15.27
F5 50	440.7	55	3610191	15.10
F6 00	440.7	60	2657447	14.79
F6 50	454.9	65	2062653	14.54
F7 00	452.8	70	1879298	14.45
F7 50	452.8	75	1597230	14.28
F8 00	453.8	80	1323461	14.10
F9 00	454.9	90	990018	13.81
F1 000	453.8	100	714303	13.48
F1 10	461	110	543827	13.21
F1 200	462.6	120	360400	12.79
F1 300	464.2	130	261765	12.48
F1 400	461.5	140	202893	12.22
F1 500	462.6	150	152900	11.94
F1 600	461.5	160	120633	11.70

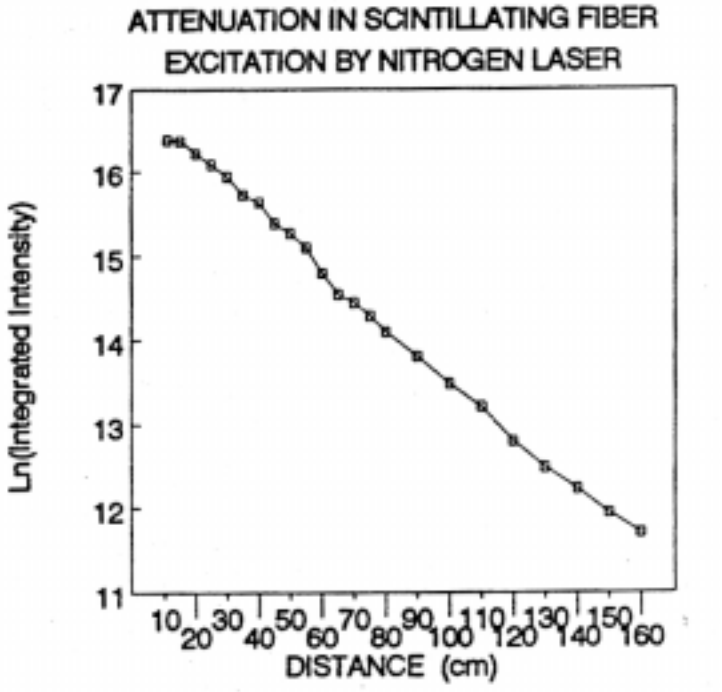

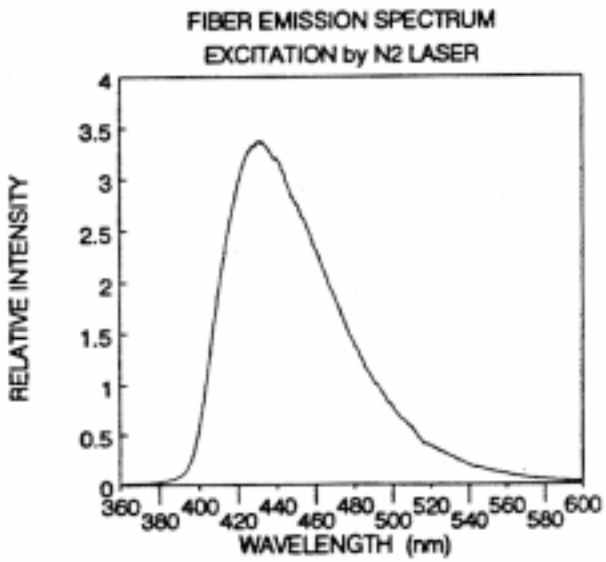

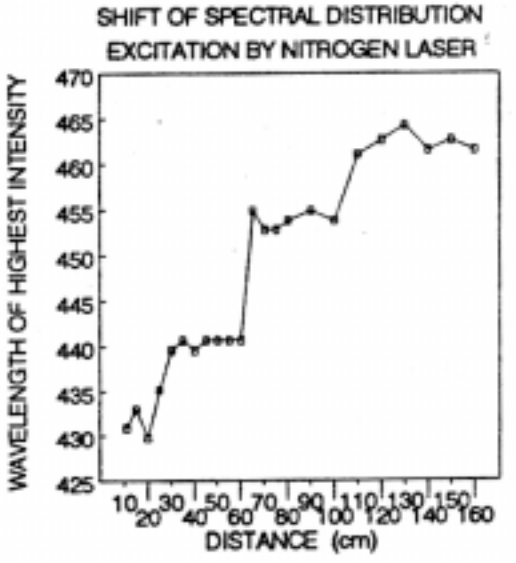

Figure 9-15. Characterization Data for Fiber Type 1
Includes: - Integrated Spectral Intensity vs. length
- Spectral intensity vs. wavelength
- Wavelength of highest intensity vs. length

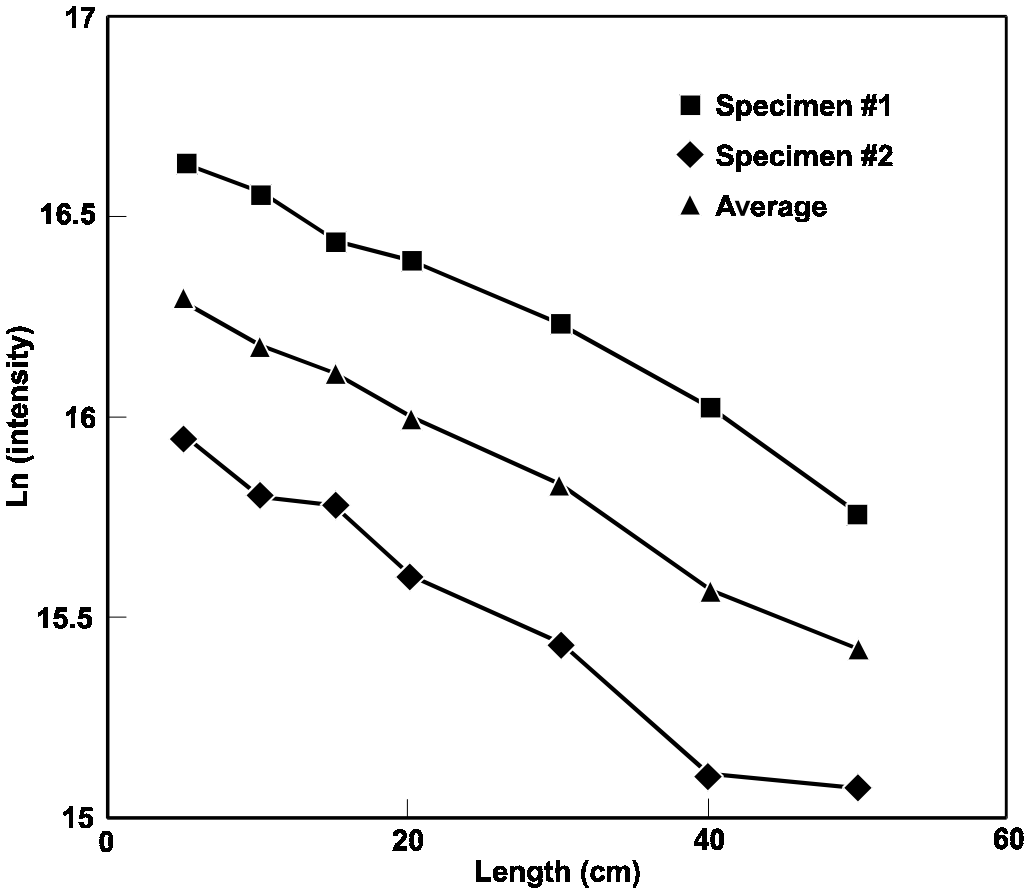

Figure 9-16. Integrated Spectral Intensity vs. Length for Fiber Type 4

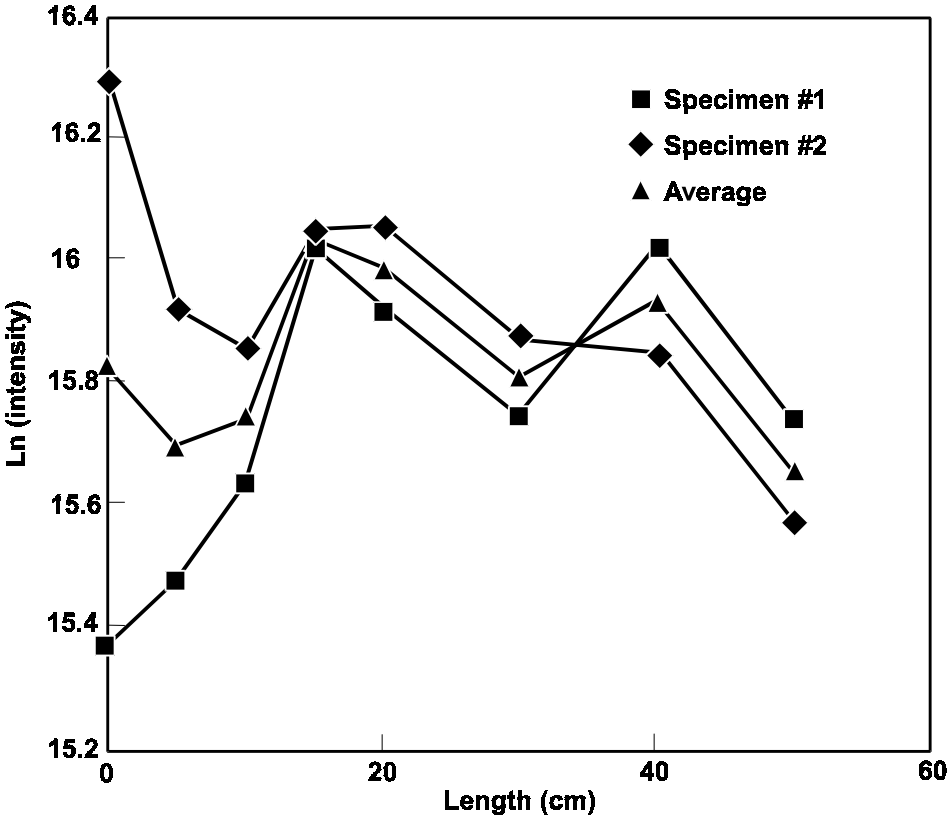

Figure 9-17. Integrated Spectral Intensity vs. Length for Fiber Type 5

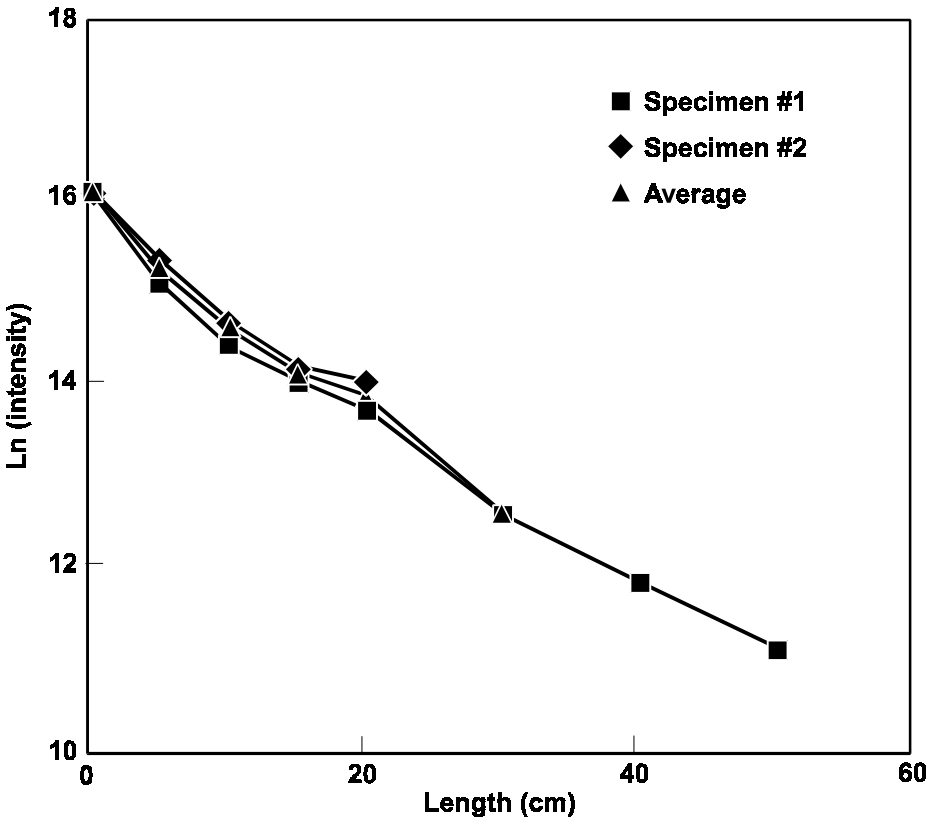

Figure 9-18. Integrated Spectral Intensity vs. Length for Fiber Type 6

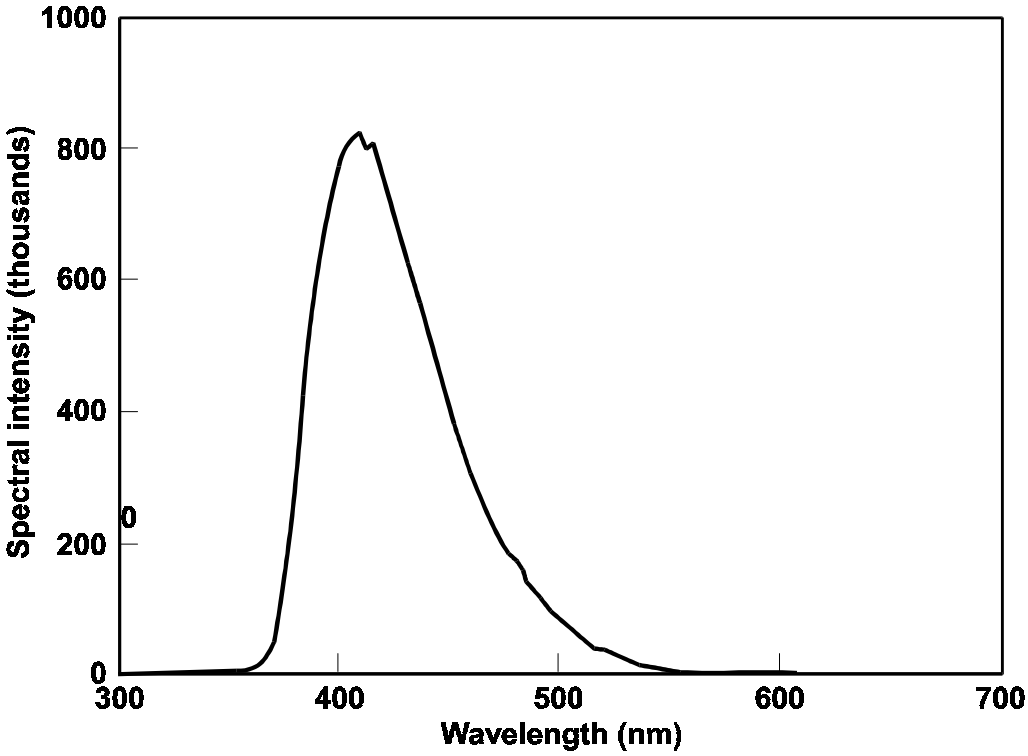

Figure 9-19. Spectral Intensity vs. Wavelength for Fiber Type 1

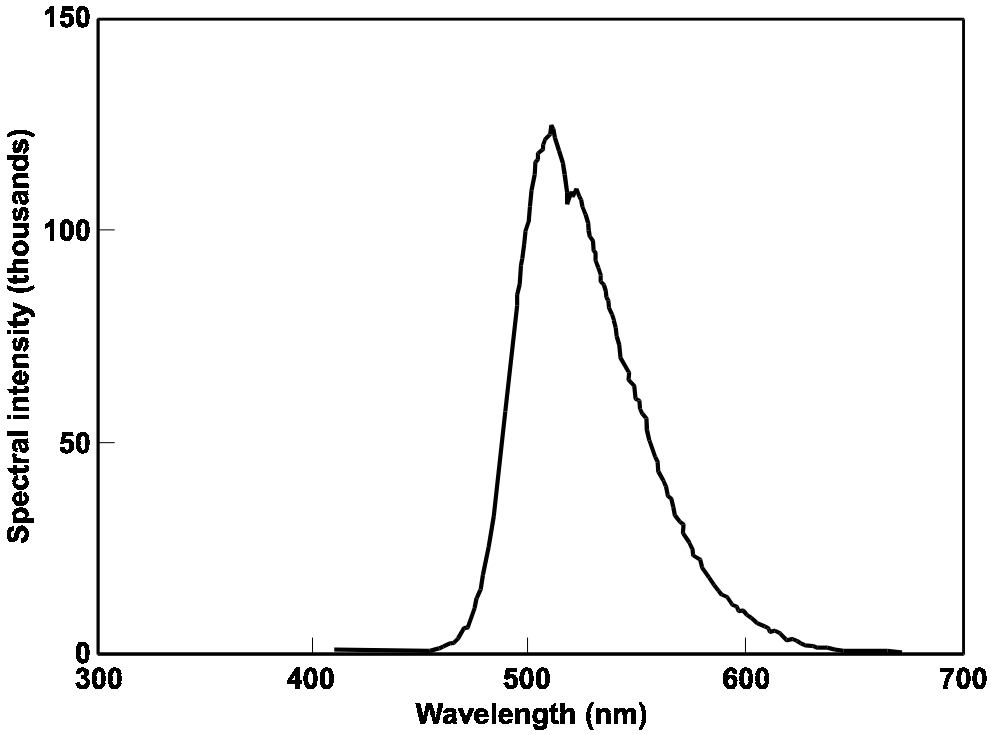

Figure 9-20. Spectral Intensity vs. Wavelength for Fiber Type 4

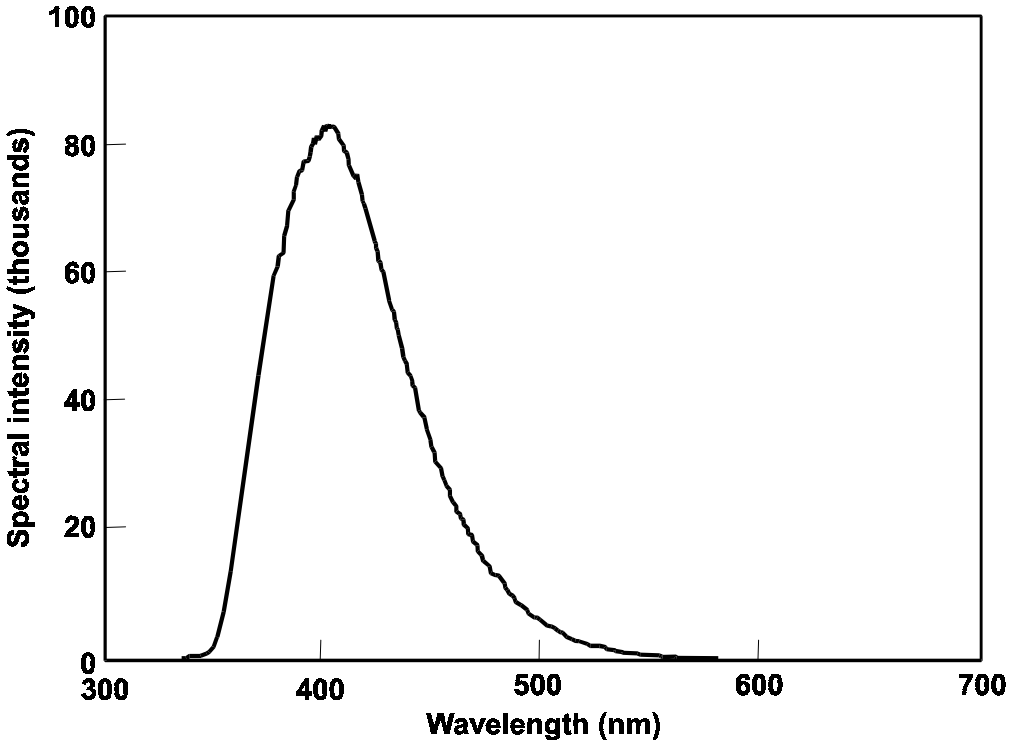

Figure 9-21. Spectral Intensity vs. Wavelength for Fiber Type 5

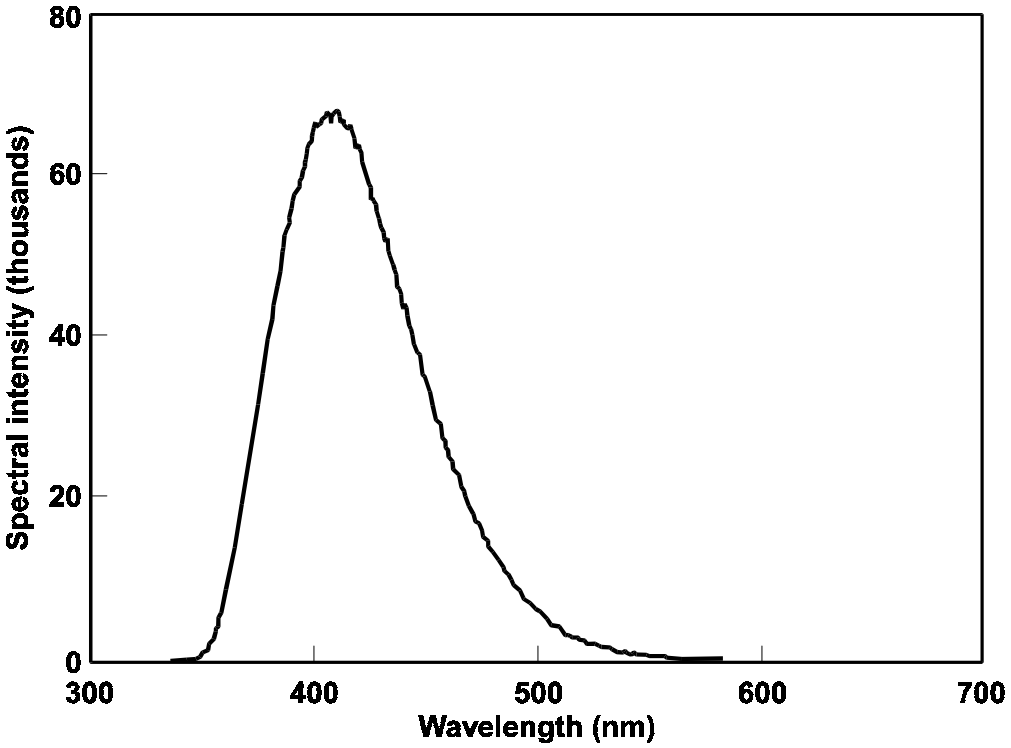

Figure 9-22. Spectral Intensity vs. Wavelength for Fiber Type 6

9.7 WASH WATER ANALYSIS

Provided in Table 9.7 is a report on analysis of samples of wash water used to provide a zero calibration check on the fluor-doped fibers tested. The analysis was performed to verify that the wash water was not contaminated with β emitters. The only radionuclide detected was ^{212}Pb which was slightly above its detection limit of 4.98 pCi/L. None of the other gamma-emitting nuclides in the uranium or thorium decay chains were detected. Gross alpha and gross beta analyses showed no contamination. It is possible that radon could be present. We do not have the capability of measuring radon. ^{222}Rn (uranium series) is the longest-lived of these nuclides with a half-life of 3.82 days.

Table 9.7 Radiochemistry Data Report

NUCLEAR ENVIRONMENTAL LABORATORY SERVICES P. O. BOX 11165 LYNCHBURG, VIRGINIA 24506-1165

LEVEL 1 RADIOCHEMISTRY DATA REPORT

MULTIPLE SAMPLES OR MULTIPLE ANALYTES

Report Date: September 26, 1997	Report No.: 9709060	NEL Contract No.: 43566-002	COC No.: 017219
Customer: MTI Research and Development Div.		Customer Site: Alliance OH	Customer SDG No.: NA
Customer Representative: John Berthold		Customer Authorization No.: NA	
Sample Description: Tap Water Sample			
No. of Samples: 1	Sample Receipt Date: September 18, 1997		Reference Date:September 18, 1997

Customer's Sample ID	NEL's Sample No.	Analytical Method	Analyte	Results	Units	1 Sigma Uncertainty	Unit
Water Sample	9709060-01	Gamma Spec	Pb-212	6.38	pCi/L	3.04	pCi/L
		Gamma Spec	Bi-212	< 27.8	pCi/L	---	pCi/L
		Gamma Spec	Pb-214	< 7.55	pCi/L	---	pCi/L
		Gamma Spec	Bi-214	< 8.06	pCi/L	---	pCi/L
		Gamma Spec	Tl-208	< 3.74	pCi/L	---	pCi/L
		Gamma Spec	K-40	< 71.2	pCi/L	---	pCi/L
		Gas Prop	Gross Alpha	< 1.12	pCi/L	---	pCi/L
		Gas Prop	Gross Beta	< 2.48	pCi/L	---	pCi/L
		Liq Scint	Gross Beta	< 175	pCi/L	---	pCi/L

Data Reviewed By: Date: 9/26/97

Data Approved By: Date: 26 Sept 1997

10.0 CONCLUSIONS

We have completed Phase 1 of a project to characterize the sensitivity of fluor-doped plastic optical fiber to tritium beta radiation. In parallel with this work, we have defined the functional requirements, target specifications, and system configuration for an in-situ tritium beta detector that would use the fluor-doped fibers as primary sensors of tritium concentration in water. The conclusions from the characterization work are summarized as follows:

- A polystyrene optical fiber with fluor dopant on the outside surface of the fiber performs better than a fiber that consists of a doped polystyrene core and undoped polymethylmethacrylate (PMMA) clad.
- A polystyrene optical fiber with fluor dopant concentration of 2% performs better than the same fiber with 0.5% dopant concentration.
- Blue fluor dopants perform better than green fluor dopants.
- Because of energy loss experienced in water, the average beta energy incident on fibers immersed in water is much less than the 6keV average energy characteristic of tritium beta. This results in a low photon yield that makes the coincidence counting approach impractical.
- Stability may be a problem. The fibers exposed to a 22-day soak in 120°F water experienced a 10x reduction in sensitivity. It is not known whether this was due to the build up of a deposit (a potentially reversible effect) or an irreversible process such as leaching of the scintillating dye.

The characterization test results in water for 2% doped fibers were used as input to the system design, and are tabulated in the accompanying table. We find that the immersible probe must contain approximately 34,000 optical fibers in order to achieve a detection sensitivity of 200,000 pCi/L tritium in water. Based on this predicted performance, possible applications can be identified which include:

- Real time, in-situ monitor of high levels of tritium in storage tanks at DOE sites.
- Real time, in-situ monitor to alarm near the lower detection limit for Canadian and World Health Organization drinking water standards.

Applications to verify compliance with the US EPA drinking water standard of 20,000 pCi/L cannot be performed with an in-situ tritium beta detector system of the present design, because the fiber bundle diameter is too large to interface with a single photomultiplier detector. Practical limits on individual fiber diameter and length are 100 μm and 60 cm, respectively.

Design Performance Summary

a (pCi/liter)	N (fibers)	Bundle Dia. (cm)
2000	3389002	24.9
20000	338900	7.9
200000	33890	2.49
1000000	6778	1.11

11.0 RECOMMENDATIONS

Based on the results achieved in Phase 1 of this project, B&W Services, Inc. (formerly NESI) and MTI believe it is premature to initiate Phase 2 and commit to a prototype design for construction and test. We believe it is more appropriate to perform further Phase 1 work first. MTI recommends further Phase 1 work and is willing to submit a detailed workscope and cost estimate, if requested by the DOE. However, if the need for monitoring higher levels of tritium in water at concentrations greater than 200,000 pCi/L is justified, then prototype development and testing could proceed either as a Phase 2 stand-alone effort, or in parallel with continued Phase 1 development work.

Based on the Phase 1 results obtained and information presently available, significant improvements must be made in fluor-doped fiber performance in order to use the method for in-situ monitoring to verify compliance with current EPA drinking water standards. Additional Phase 1 fiber development work should be performed to increase the fluor dopant concentration above 2% until the self-absorption limit is observed. Continued fiber optimization work is expected to improve the sensitivity limits.

List of Acronyms

Acronym	Definition
ALARA	As Low As Reasonably Achievable
ARC	Alliance Research Center
CCD	Charge Coupled Device
CRD	Contract Research Division
D&D	Decontamination and Decommissioning
DWS	Drinking Water Standard
EPA	U.S. Environmental Protection Agency
LDL	Lower Detection Limit
LRC	Lynchburg Research Center
LSC	Liquid Scintillation Counting
MTI	McDermott Technology, Inc.
NESI	Nuclear Environmental Services, Inc.
pCi/L	Pico Curies per Liter
NA	Numerical Aperture
PMMA	Polymethyl Methacrylate
PMT	Photomultipler Tube
R&DD	Research and Development Division
UV	Ultraviolet
WLS	Wavelength Shifter

APPENDIX A

DETAILS ON SEVERAL SITE NEEDS FOR TRITIUM MEASUREMENT

NEVADA
TECHNOLOGY NEEDS/OPPORTUNITIES
STATEMENT OUTLINE

Need Identifier: NV0013
Date: January 3 1, 1997

OPS **Office/Site: DOE/ NV**
Operable Unit (if applicable): Underground Test Areas and Offsites
Waste Stream: Not Applicable
Waste **Management Unit (if applicable):** Not Applicable
Facility: Nevada Test Site and Offsites

Need Title: Real Time Monitoring for Radiation (Mainly Tritium) in Monitoring Boreholes
Need Description: The need is for a durable, reliable, and accurate system that will monitor relatively low levels of radiation in deep monitoring wells. Tritium is the major radionuclide of interest, but other radionuclides associated with underground testing are also of interest. Also parameters such as water level, **temperature, pH,** and conductivity, would be of interest.

Functional Performance Requirements: The detection limit for Tritium should be approximately 1000 pCi/l or as low as reasonably achievable. The wells may be in excess of 1000 meters deep and the probes could be under several hundred meters of water. The probes also need to be able to be rapidly removed so water samples can be collected. The non-rad parameters should be measured in a manner consistent with the best available field techniques.

Schedule Requirements: The system should be able to be deployed in approximately five years.

Problem **Description:** The current system involves pumping considerable volumes of water from deep wells with either dedicated pumps or pumps set for each sampling. The pumps set for each sampling require a drill rig or similar equipment and are very expensive to operate and considerable decontamination of equipment is required. The pumping produces considerable volumes of contaminated water that also need to be disposed of in some manner. The monitoring is envisioned to last from 50 to 100 years.

ADS No. 225 WBS No. PBS No. NV212

Justification For Need:

Technical: There is need for more accurate, real-time data.
Regulatory: The monitoring system is required as part of an agreement with the state of Nevada (Federal Facility Agreement and Consent Order).
Environmental Safety and Health: In-situ monitoring reduces worker exposure. **Cost Savings Potential (Mortgage Reduction): The cost** savings would be on the order of $100 million. Assuming **a** savings **of** $50K per well, sampling 40 wells once per year and a 50-year monitoring duration.
Cultural/Stakeholder Concerns: The perceived risk is reduced.
Other: None

Consequences of Not Filling Need: Without this technology there would be higher costs and a greater potential to expose workers during sampling and decontamination.
Privatization Potential: The privatization potential is relatively low. The need is primarily at DOE sites with radionuclides in groundwater.
Current Baseline Technology: The current system involves pumping considerable volumes from deep wells with either dedicated pumps or pumps set for each sampling. The pumps set for each sampling require a drill rig or similar equipment and are very expensive to operate and considerable decontamination of equipment is required. The pumping produces considerable volumes of contaminated water that also need to be disposed of in some manner. The monitoring is envisioned to last from 50 to 100 years.
End-User: Nevada Operations Office - Environmental Restoration Division (ERD)

Site Technical Point(s) of Contact: Robert M. Bangerter (ERD) / Monica L. Sanchez (ERD)
DOE End-User/Representative Point of Contact: Clayton W. Barrow (ERD)

FOCUS AREA RESPONSE

Focus Area:
TTP(s):
TTP Task(s):
Total Funding:
Comment/Response:
Focus Area Contact:
Principal Investigator:

http://www.ead.anl.gov/~cnstog/CH-0005.HTM

TECHNOLOGY NEEDS/OPPORTUNITIES STATEMENT

Identification No: CH-0005

Date: November 1996

OPS Office/Site: Chicago Operations Office/Brookhaven National Laboratory

Operable Units: I, III, IV and VI

Waste Stream: Contaminated soil and groundwater

Waste Management: N/A

Facility: N/A

Site Priority Ranking: 5

Need Title: Long-Tam Groundwater Monitoring

Need **Description:**

Volatile Organic Compounds (VOCs) and radionuclides from past agricultural pesticide use, accidental solvent spills and leaching from landfills, have entered the groundwater at BNL. For example, plumes of groundwater contaminated with tetrachloroethene (PCE) and carbon tetrachloride (CCl_4) has been identified in Operable Unit III through a series of monitoring wells. These plumes have migrated off-site in concentrations above drinking water standards and into a residential area south of the laboratory. Two **pump-and-treat** systems designed to stop the migration of high levels of VOCs at the southern boundary are under construction and are scheduled to start operation during 1997. Natural attenuation and long term monitoring is planned for low levels of VOCs, i.e. less than 50 ppb total VOCs. Radiological groundwater contamination by strontium-90 and tritium on-site at BNL has been detected. Radiological decay and long term monitoring are the current solutions. These long term monitoring needs require enhanced or new monitoring techniques that allow reliable, quick and inexpensive groundwater analysis.

Functional Performance Requirements:

The VOC chemicals ofconcem at BNL include 1,1,1-trichloroethane (TCA), trichloroethylene (TCE), CCl_4, dichloroethylene, ethylene dibromide (EDB), tetrachloroethane, and PCE. Radiological contaminants of concern include strontium-90 and tritium. Systems for reliable and quick measurements of these chemicals and radionuclides and methods for accurate data integration and interpolation are needed. Such **systems must he** sensitive in the low concentrations (e.g., 1 &g/l for VOCs) required by groundwater standards.

In addition, enhanced data management and integration and interpretation with fate-and-transport models can improve the ability to monitor plume movement. It is essential to find more rigorous methods and software for integrating different types of data and interpolating between sampling points. Such methods include statistical methods? 3-dimensional visualization, and integration of fate-and-transport models with site contaminant and geophysical data.

Schedule Requirements:

Since groundwater monitoring is a long-term need for the BNL environmental restoration program, technology improvements are always needed.

Problem Description:

The traditional means for long term monitoring of groundwater contaminant plumes rely on **the** grab samples

http://www.ead.anl.gov/~cmstg/CH-0005.HTM

from apermanent monitoring well and subsequent analysis of samples at a laboratory. Also, even after an extensive site characterization effort, uncertainty may remain regarding the detailed distribution of contaminants due to collection by grab samples.

ADS No: CH 2321

RDS No: R96Z001, R96Z002, R96Z0005, R96Z0008, R96Z0010, R96Z0013

WBS No: N/A

Justification for Need:

Technical:

Groundwater plumes are traditionally characterized by extensive collection and chemical analysis of groundwater samples. Samples are subdivided by depth interval to obtain information on three-dimensional plume distribution. Sampling techniques for plume delineation in the saturated zone employ a variety of borehole sampling devices (e.g., standpipe piezometers, multilevel samplers). Additional techniques for vadose zone sampling include suction lysimeters and soil gas samplers. These techniques provide only point estimates of contamination and they are limited by their low spatial resolution.

The large number of processes that affect the subsurface transport and fate of contaminants make monitoring a formidable task. Only a finite amount of data can be collected, and, in addition, plume characterization requires a groundwater monitoring network based on site specific characteristics, contaminant properties and water usage patterns. Reliable integration and interpolation of data from existing wells can aid the placement of additional monitoring wells and the continuous and efficient monitoring of contaminants.

Monitoring a plume is necessary even when no active remediation action is required. The levels of VOCs and radionuclides in a plume should be analyzed periodically to verify that the extent of physical and chemical transformations in the plume occur as planned. Changes in the location of the plume require additional data and data interpretation. Application of fateand-transport models can also assist in data interpretation.

Technology needs in this area are: improved data management, integration and interpolation tools and improved sampling and anlytical tecnhiques include m-situ and rea time analysis. To improve the ability to monitor plume movement, it is essential to find more rigorous methods and software for integrating different types of data and interpolating between sampling points. Such methods include statistical methods, 3-dimensional visualization, and integration of fate-and-transport models with site contaminant and geophysical data.

Regulatory:

VOC and strontium-90 levels in the groundwater in some areas at BNL exceed regulatory limits, namely the New York State Groundwater Quality and Drinking Water Standards. Long-term monitoring of a contaminated site forms the basis for determining if the selected remedy is working as planned and is required by regulatory agencies. BNL is involved in groundwater monitoring programs and remediation activities to comply with a CERCLA Interagency Agreement as well as other state and federal regulations.

Environmental Safety & Health:

Off-site VOC groundwater contamination above State Drinking Water Standards exist and poses immediate concern for public health. The susceptibility of public water supply wells in the proximity of BNL to contamination from the site will need to be assessed over long periods of time.

Cost Savings Potential (Mortgage Reduction)

Cost savings will be realized in reducing the costs of the long term monitoring required for the next 20 to 40 years since pump-and-treat and natural attenuation remedies have been selected.

Cultural/Stakeholder Concerns:

Groundwater contamination from past practices is presently a key concern at BNL. Stakeholders concerns were exemplified by recent protests of local residents regarding the potential contamination of their drinking water wells. DOE has provided public water to almost 1000 nearby residents of BNL as a precautionary measure.

Consequences of Not Filling Need:

If groundwater monitoring is ineffective, groundwater contamination may spread and have a greater impact on the local communities than what is currently assessed. Also, an advanced, credible monitoring system may help to alleviate public fears and concerns about BNL contamination sources.

Privatization Potential:

Demonstration of the effectiveness of an advanced monitoring and data integration/interpolation system for VOCs, other organics, and radionuclides at BNL would be beneficial in developing similar systems for larger DOE sites. Such technology has also private sector marketing potential.

Current Baseline Technology:

Monitoring the movement of contaminant plumes currently rely on the **chemical** analysis of samples of the soil and groundwater. That is, it involves digging wells and boreholes, collecting soil and water samples, and performing laboratory analyses. The baseline technology for long term monitoring involves permanent monitoring wells which would be grab sampled on a regular basis, maybe quarterly.

Software packages **for data** analysis include PLUME, Smart Sampling, and SADA. PLUME is used at BNL, SmartSampling is used at Sandia and Fernald, SADA is **used** at Oak Ridge National Laboratory. These packages use geostatistical techniques to evaluate plume location, perform data worth analysis and recommend sampling location. They are, however, first generation tools and need to be benchmarked and demonstrated in the field.

End-User:

BNL will be responsible for implementing. all long-term groundwater monitoring programs.

Site Technical Point-of-Contact:

William Dorsch

Brookhaven National Laboratory

Office of Environmental Restoration

(516) 344-5186

DOE End-User/Representative Point-of-Contact

Mohammed Ali

DOE Brookhaven Group

(516) 344-4085

TECHNOLOGY **NEEDS/OPPORTUNITIES**

STATEMENT OUTLINE

Identification No.: CH-0013

Date: October 1996

Ops Office/Site: CH/Argonne National Laboratory

Operable Unit: TBD

Waste Stream: N/A

Waste **Management Unit:** Not Applicable

Facility: CP-5

Site Priority Ranking:

Need **Title:** Spent Fuel Pool **Water Processing**

Need Description:

The CP-5 Spent Fuel Pool currently contains **25,000** gallons of water contaminated with cesium, cobalt and trace amounts of tritium which requires processing for disposal.

Functional Performance Requirements:

Liquid processing technologies must be cost effective and minimize secondary waste.

Schedule Requirements:

The fuel pool water will be processed as the first step in the decommissioning of the CP-5 fuel pool. Currently the processing is scheduled for November 1996.

Problem **Description:**

The fuel pool water contains 0.60 _ 0.06 pCi/ml of Cs-137 and <0.2 pCi/ml of Co-60. Gross alpha analysis of the water resulted in <0.02 pCi/ml and gross beta analysis of 1.1 _ 0.1 pCi/ml. Tritium concentrations of **1850** _ 100 pCi/ml were also found.

There are various technologies available or in development for processing waste liquids for volume reduction such as clarifiers, filters, membranes, ion exchangers, evaporators, and liquid incinerators. In addition, there are absorption methods such as absorption pads and absorption powder with large ratios of absorption material to water absorbed for disposing of contaminated liquid.

The previously mentioned methods of liquid waste treatment oan be costly and some are still in the experimental stage. The clarifiers and filters are only applicable if the radioactive contaminants are isolated to the removed particles. After clarifying or filtering the liquid may still be above the release criteria Membranes can remove much smaller particles; however, the liquid may still be above the release criteria. This may be acceptable for reuse of the liquid by not for final disposition.

ADS: 1437/1441 **RDS:** R96A0007 **WBS:** 17.1.2.1.1 PBS No.: CH-ANLEDD

Justification For Need:

Technical

A cost effective method for disposing of radiologically contaminated liquid wastes is needed. Current technologies are costly and are not always effective.

Regulatory

There are no current regulatory requirements or drivers.

Environmental, Safety and Health

No concerns have been identified.

Cost Savings Potential (Mortgage Reduction)

There is significant cost savings potential through waste reduction.

Cultural/Stakeholder Concerns

No concern has been identified.

Other

None identified

Consequences of Not Filling Need:

A process needs to be developed to process the CP-5 fuel pool water to lower the amount of water which would require disposal at a great cost to the generator.

Privatization Potential:

Fuel pool water processing is an issue for both DOE and private industry facilities. A cost effective, efficient method of processing for disposal would be utilized by both parties.

Current Baseline Technology:

Sending water to evaporators is the current baseline technology; however, this is expensive and the evaporators cannot handle large volumes or liquid mixed waste.

End *User*:

TBD

(Optional): Site Technical Point of Contact

(Optional): DOE End User/Representative Point of Contact

TECHNOLOGY NEEDS/OPPORTUNITIES (AL-07-02-03-SC)
KIRTLAND AREA OFFICE (SNL)

Date: 15 Nov 1996
Ops Office/Site: Albuquerque/Sandia National Laboratories
Operable Unit: ADS 1289
Waste Stream: Low-level radioactive waste
Waste Management Unit: - NA-
Facility: Mixed Waste Landfill

Site Priority Ranking: 23/34

Need Title: Low-Level Radioactive Waste Landfill Cap Design, Tritium Treatment/Removal Technology, In-Situ Vitrification, Pressure Grouting, and Real-Time Tritium Monitor

Need **Description:** In -situ vitrification, pressure grouting, low-level radioactive waste real-time tritium monitor.

Functional Performance Requirements: Cap, grout, and vitrification would have to last for 100 yrs. Tritium treatment would have to lower levels in soil to within SNL background .004-.042 pCi/g.

Schedule Requirements: Duration of two years.

Problem **Description:** Tritium-contaminated soils, no treatment technology exists.

ADS No:	RDS No:	WBS No:	PBS No:
1289	NA	1.18	AL/SNL/ER

Justification For Need:

Technical: The Mixed Waste Landfill (MWL) is a 2.6 acre site located in the north-central portion of TA-III. The landfill was operated from March 1959 to December 1988 as the primary disposal site for SNL/NM technical and remote test areas involved in nuclear weapons research and development. The MWL accepted low-level radioactive waste and minor amounts of mixed waste during its years of operation. Approximately 100,000 ft3 of low-level radioactive waste containing approximately 6,300 curies of activity wore disposed of at the landfill. Wastes disposed of in classified area pits included depleted, natural, and enriched uranium, thorium, barium, enriched lithium, liquid scintillation vials and beakers, neutron generator tubes and targets, plutonium-contaminated wastes, and plutonium-contaminated weapons test-debris from the Nevada Test Site. Between 1959 and 1962, small quantities of radioactively contaminated inorganic acids and organic solvents ware disposed of in Pit SP-1, located in the southeast comer of the classified area. Wastes disposed of in the unclassified area trenches included construction and demolition materials, contaminated equipment and soils, lead shielding, wood crates, steel drums, shipping casks, cardboard boxes, and dry solids. In 1967, approximately 271,000 gallons of coolant wastewater from the Sandia Engineering Reactor Facility was disposed of in Trench D over a 30day period. Tritium is the contaminant of primary concern at the MWL. Groundwater is approximately 460 ft below the surface of the site.
Regulatory: HSWA Part B Permit.
Environmental Safety And Health: Tritium in the vadose zone is the primary health concern.
Cost Savings Potential (Mortgage Reduction): Capping the landfill would save monitoring dollars by precluding institutional controls for the next 100 years.
Cultural/Stakeholder Concerns: No agreements, but because of the nature and name of the site, the public is very aware.

Consequences Of Not Filling Need: 100 years of institutional control.

Privatization Potential: Unlikely **unless the** landfill is capped.

Current Baseline Technology: Proposed No Further Action (NFA) with Institutional Control in the Phase 2 RFI Report. Institutional controls would include physically controlling access to the disposal site, site surveillance and/or security, environmental monitoring, minor custodial care, deed restrictions, and deed notices for 100 years. If the NFA is not accepted, capping the landfill with the waste in place willbe proposed. Appropriate post-closure monitoring systems would be used for a specified time after closure.

Excavation of the landfill and treatment of the wastes is not a viable option. There is currently no technology available for treating tritium-contaminated wastes. The only option would be to excavate the landfill wastes and containerize them for shipment to a permanent disposal faeility.

Cost: $2M
Waste: None currently.
How Long Will It Take: Two years.

Site Technical Point of Contact: Jerry Peace **(505) 284-2472**
DOE End User/Representative Point of Contact: Mark Jackson 845-6288 (KAO)

[SCFA] [SNL]

- **Return to STCG Overview**
- **Return to: STCG main page**
- **Return to: DOE/AL web rite**

Savannah River Site Technology Needs/Opportunities Statement

Need ID

SR-3006

Date Revised

May 02, 1997

OPS Off&/Site

SR/SRS

Operable Unit (if applicable)

Mixed Waste Management Facility, F&H Groundwater, R&K Reactor Basins

Waste Stream

G&S

Waste Management Unit (if applicable)

Mixed Waste Management Facility, F&H Groundwater, R&K Reactor Basins

Facility

N/A

Site Priority Ranking

ER Priority 10 of 14 (New)

Need Title

Tritium hydrogeological control and/or treatment technologies

Need **Description**

At Savannah River Site(SRS), tritium hydrogeological control and/or treatment of large groundwater plumes is a major technical challenge. There is a great need to develop tritium treatment and hydrogeological control technologies for large groundwater plumes, over 100s of acres; with low hitium concentration of 10,000 to 300,000 pCi/ml in unconsolidated subsurface sediments; i,e., sandy/clayey soil. Currently no treatment technology exist to reduce the tritium concentrations to regulatory limits.

Functional Performance Requirements

Tritium hydrogeological control technology must contain the plume at its current volume and location for at least 12.3 years which is the half life of tritium. Cost effective, efficient hydrogeological control technologies may reduce the risk while tritium decays.

At SRS we are in need of cost effective, efficient tritium treatment technologies to treat large tritium plumes; an average plume covers 150 acres and is 200 ft below the surface. The tritium treatment technology should handle high volumes of contaminated groundwater (average 250 gpm). At SRS, tritium impacts the Savannah River and aquifer feeding drinking water supplies of downstream communities. The cleanup levels must meet the EPA MCLs, and SCDHEC GWPS, and other applicable risk based corrective action levels. Currently, the EPA MCL for tritium is 20 pCi/ml. At SRS, tritium typically occurs in conjunction with other radionuclides, VOCs, and metals. SRS needs a specific treatment process for tritium that can be used concurrently with other contamination remediation processes, and with no/minimal secondary waste.

In addition, tritium treatment processes should protect SRS workers from any chemical and physical hazards, and should minimize risk to the environment.

Schedule Requirements

A full scale pump-and-treat process is scheduled to become operational at F & H Area in 1 QFY 1997. The remedy described in the 1992 SRS RCRA permit provides for recovery of contaminated groundwater via extraction wells and treatment of hazardous constituents and radionuclides(except tritium and nitrates). Tritium contaminated effluent will be pumped and reinjected upgradient.

At the Mixed Waste Management Facility(MWMF), pursuant to a settlement agreement with the State of South Carolina, a RCRA Part B permit application has been submitted. Corrective Action Plan(CAP) will be submitted in FY 1997, with the proposed remedy. Remedial action is expected to start FY 1998.

R&K Reactor Basins are in the characterization stage. Per the FFA, RODs will be submitted by 3Q 1998.

- Timing

Technology need 1-3 years

Problem Description

SRS is the largest producer of tritium in the world. Tritium, a product of SRS operations, has been shown to have the high priority for State regulators due to potential impact on public health of the surrounding population of any radionuclide released by SRS. Tritium has continued to be a source of public concern. In the years between 1952 and 1988, tritium was generated extensively as a surplus by-product of the reactor and separations processes. The accepted practice for eliminating the excess tritium was periodic discharge from plant process water systems into unlined seepage basins, which would allow gradual dispersal of the tritium with other residual contammation, into the surrounding soil. Over the years, subsurface bleeding of the waste water with the regular ground water, combined with the rapid migration rate of tritium, has produced large volumes **of** contaminated water containing low tritium concentrations.

The F&H area consists of 3 unlined earthen basins with a combined capacity of 20.5 million gallons of water. The potential F&H groundwater plume covers 200 acres, and is 150 ft below the surface. The Contaminant of Concerns (COCs) are tritium, alpha, and beta emitting radionuclides, and hazardous metals.

The Mixed Waste Management Facility(MWMF) has been used for management and disposal of radioactive wastes generated by SRS processes for 30 years. There are 3 distinct plumes at the MWMF, each covers approximately 150 acres, and 200 ft below the surface. Contaminant of Concerns(COC) are tritium, uranium, CCL4, Pb, Hg, gross alpha, radium, etc.

ADS No.

515,505

RDS No.

R96A0-093, R96A0-066, R96A0-103

WBS No.

11201060302, 11201060202, 112011902 Lower ER03, 112012002 ER04

PBS No.

ER02-FMB

Justification For **Need**

- Technical

Due to the highly mobile nature of tritium, the tritium contamination encompasses a larger plume, or may appear as a hot spot contaminant in larger plumes. These tritium concentrations are above the EPA MCL guidelines and represent a potential threat to human health and the environment. Currently, no treatment technology exists to reduce tritium to reglatory required limits.

- Regulatory

Current Part B permit regulatory deadlines are the drivers for tritium treatment. Groundwater projects are also driven by settlement agreements with the State of South Carolina. The EPA-MCL for tritium is 20 pCi/ml. No treatment technology exists today that can comply with these requirements.

- Environmental Safety & Health

Tritium treatment and/or hydrogeological control technologies should protect SRS workers from any chemical and physical hazards, and minimize risk to the environment. While guidlines for drinking water specify 20 pCi/ml, EPA realizes that these limits are ultra conservative. EPA is currently reviewing these guidelines to see if they can be raised to as high as 80 pCi/ml, which is higher than the levels in question. Based on this information, the risk to the public is low.

- Cost Savings Potential (Mortgage Reduction)

Potential cost savings are based on baseline pump and reinject technology or for tritium treatment which is estimated at between $11M-$30M over the life of the process.

- Cultural/Stakeholder Concerns

Due to tritium contamination reaching to downstream community water supply systems, stakeholders concern over tritium contamination is extremely high. SCDHEC is putting presure on the Site to find a method for containment or treatment.

- Other

Consequences of Not Filling Need

The consequence of not developing a cost-effective and efficient tritium treatment or hydrogeological control technologies will be an increase in the life cycle cost. Tritium is highly mobile, and plume will spread, which will increase the remediation cost drastically. If hitium treatment and hydrogeological control technologies are not developed, the result could be continous interim removal actions which will increase project life cycle cost, increase the risk of not meeting regulatory commitments, and increase the risk to SRS workers, the public, and the environment.

In addition, regulatory and public pressure will remain, unless the threat to human health and the environment is reduced or eliminated.

Privatization Potential

Tritium contaminated groundwater exists predominantly at DOE facilities, limiting the potential commercial application. However, tritium treatment and hydrogeological control technologies has great potential for application at other DOE facilities, such as Hanford, Nevada Test Site, Oak Ridge, Mound, Brookhavan National Laboratories.

Current Baseline Technology

The current baseline technology for tritium is pump and reinject until tritium contaminated groundwater has decayed to accepable levels. Recently, SRS completed a review of potential tritium treatment technologies and recommended development of 3 additional technologies; storage, Isotope separation and immobilization. The Liquid Phase Catalytic Separation(isotope separation) technology is the favored alternative for further development.

cost

Proposed treatment technologies are expensive to construct and operate. Some of these technologies typically generate large quantities of contaminated secondary waste streams. Total life cycle costs are difficult to assess, but preliminary operating costs for innovative technologies are in the range of $4 to $10 per gallon for tritium treatment.

How **Long Will It Take**

A exact measure of time cannot be provided, but it will exceed 25 years.

End User

Bob Aylward, Technology and Feasibility Studies Manager

Site Technical Pont-of-Contact

Ahmet Suer
Environmental Restoration
Westinghouse Savannah River Company
Bldg 720-2B, Rm 2005
Aiken S.C. 29808
Tel: (803) 952-8306
Fax: (803) 952-6538
ahmet.suer@srs.gov

DOE End User/Representative Point-ofcontact

Les Germany
U.S. Department of Energy
P.O. Box A
Aiken, SC 29802
Tel: (803) 725-8033
Fax: (803) 725-7548
les.germany@srs.gov

Focus Area Responses

Focus Area

Subsurface Contaminants

TTPs

TTP Task(s)

Total Funding

Comment/Response

Focus Area Contact

Principal. Investigator

APPENDIX B

LIST OF PARTICIPANTS AND QUESTIONNAIRE

LIST OF PARTICIPANTS

Darrin Mann, Oak ridge
Kim Hanzelka, Oak Ridge
Greg Burbage, Savannah River Site
Robert Minnick, Savannah River Site
Bob Rabun, Savannah River Site
Norbert Golchert, Argonne National Laboratory
Omar Heath, Maxey Flats
Evan Dresel, Hanford
Vern Johnson, Hanford
Linda Bauer, Mound
Charles Gentile, Princeton Plasma Physics Laboratory
Steve Raftoplulos, Princeton Plasma Physics Laboratory
Brian James, Los Alamos National Laboratory
Terry Buxton, Los Alamos National Laboratory
Dale Tuggle, Los Alamos National Laboratory
Chris Miles, Lawrence Livermore National Laboratory
Allen Grayson, Lawrence Livermore National Laboratory
John Baker, Idaho National Engineering Laboratory
Biays Bowerman, Brookhaven National Laboratory

Thank you for your time and help. Please answer the questions to the best of your knowledge.

Name _____
Title _____
Address _____
_____
_____

Phone number _____
Fax number _____
Internet address _____

1.0 Application Characteristics

1.1 Do you have tritium contaminated water at your site which must be monitored on a regular basis?

1.2 How many streams or contaminated water sources must be separately monitored for tritium?

1.2.1 Please characterize typical streams

a. Normal range of tritium contamination in pCi/L

b. Source of water, e.g., groundwater, building drains, process wastes, mixed low level wastes

c. Other radionuclides, likely to be present and at what levels

d. Are significant quantities of other soft beta emitters such as ^{63}Ni, ^{14}C or ^{129}I likely to be in your samples, and at what levels?

1.3 How frequently is monitoring required and approximately how many samples per week must be processed? (Are any streams monitored continuously?)

1.4 How is level of tritium currently determined and what sample pretreatment purification methods are used to exclude other radioisotopes, if any?

1.5 Is it necessary to track short term changes or peak values in tritium concentration, if so, what ramp rate or typical peak profile vs time must be followed?

1.6 Are you permitted to average sets of sample readings when determining compliance with allowable release limits, if so, over what period of time?

1.7 What remedial options are available if contamination limits exceed acceptable values, e.g., can you perform pump-treat-discharge or control release rates to limit discharge tritium concentrations?

1.8 What is the approximate volume flow rate of water to be monitored?

1.9 Do you have installed a network of wells to monitor groundwater contamination, if so, how many wells are in use?

1.10 Have you observed the formation of scale or surface fouling deposits on pipes carrying tritium contaminated water?

2.0 Commercial Considerations

2.1 How would a submersible probe with the capability to measure tritium be of benefit in meeting the needs of your site?

2.2 Approximately how much does it cost per sample to collect and process samples for tritium using present methods?

Would a continuous tritium monitor allow you to significantly reduce the number of samples being taken?

2.3 What is the turnaround time to obtain contamination data using present methods?

2.4 Are there any waste disposal problems or significant exposure risks created by the use of existing sample collection or analysis, e.g., disposition of contaminated samples mixed with scintillation fluids?

3.0 Basic Performance Characteristics

3.1 The minimum detectable concentration of tritium proposed for the continuous monitor is 2000 pCi/liter (1/10 the EPA Drinking Water Limit) if conflicting radiation from other radionuclides is not present. Would this sensitivity be required to meet your needs?

3.2 What elapsed time between calibration would be acceptable for your application?

3.3 What ramp rate of change in tritium concentration levels does this instrument have to be able to follow for your use?

3.4 What range of concentrations must this instrument be able to measure for your site?

4.0 System Design Features

4.1 How would you classify the following possible system features for your application (mandatory or desirable or not required)?

a. Prefilter with delta-p alarm

b. Flow sensor with low flow alarm

c. Provisions for chemical cleaning

d. Modular digital electronics

e. Automatic alarm on loss of signal output or indicated contamination levels exceeding instrument range

f. Internal check source for instrument response check

g. Corrosion resistant polymer sensor housing

h. Battery back-up power supply rated for 1 hour operation during outage of normal power supply. (Auto supply reset on power supply switchover.)

i. Other recommended features (please list)

5.0 Physical/Mechanical Configuration

5.1 How would you classify the following possible mechanical/physical configuration features for your application (mandatory, desirable, or not required)?

a. Housing designed to fit within 4-inch nominal well casing.

b. Inlet, outlet and electrical leads all connected to top end of housing.

c. Housing and connecting leads submersible.

d. Seismically qualified sensor assembly.

e. Integral venturi-type jet pump or air driven diaphragm pump to force sample fluid through sensor housing (remote mounted drive pump or air supply).

f. Sensor housing rated for 50 psig at 100°F.

g. Other recommended features (please list).

6.0 Electronic Features

6.1 How would you classify the following possible electronic features for your application (mandatory, desirable or not required)?

a. RS-232 Port for Data Logging

b. Analog output signal connection for remote display.

c. Remote computerized adjustment of ratemeter operating modes and parameter setpoints.

d. Sensor to ratemeter permissible distance 50 ft.

e. Line voltage spike/variation protection.

f. Shielding against external electromagnetic noise sources, e.g., welding, microwave transmitters.

g. Other recommended features (please list).

7.0 Operation and Maintenance

7.1 How would you classify the following possible operational features (mandatory, desirable or not required)?

a. Self check diagnostics

b. Modular circuit boards

c. Well pump down prior to sample measurement

d. Return of sample fluid to source

e. Discharge of effluent sample fluid to waste treatment collection tanks

f. Other recommended features (please list).

APPENDIX C

TARGET SPECIFICATION

TARGET SPECIFICATION

Instrument Function : In-situ detector of tritium beta radiation for site characterization or long-term monitoring.

Available Units of Measure	pCi/L
Range	1000 to 3,000,000 pCi/L
Integration Time	≤ 1 hour
Gamma Compensation	For Cs-137 Gamma perpendicular to sensor axis, <+300pCi/L/100mR/h
Display	16 character LCD, Back Lit
Accuracy	± 30% (1 sigma confidence) for tritium concentrations <20,000 pCi/Land ± 25% (1 sigma confidence) for tritium concentrations >20,000 pCi/L
Operating Temperature	5° to 50° C
Temperature (relative to electronics)	± 1 LSD* over range of 0° to 50° C
Noise	± 1 LSD* (long term)
Operating Humidity (for electronics module)	to 95% R.H. (Non-Condensing)
High Level Alarm	Two audio/visual alarms with acknowledge and user configured automatic reset or latching set points are independent and adjustable.
Low Flow Alarm	Audio alarm
Linear Analog Output	Signal to be compatible with standard instrumentation loops
Log Analog Output	Signal to be compatible with standard instrumentation loops
Power Supply	110 or 220 VAC (50-60 Hz) with battery back-up unit rated for 1 hour operation

TARGET SPECIFICATION

Sample Connection..... VCR (vacuum coupling, no o-ring) fittings for liquid sample inlet and outlet (configured to prevent external light from entering cell)

Sampling Rate..... Approximately 1 L/minute

Filtration..... 1 micron glass-fibre filter (or equivalent which will not absorb tritium) on influent liquid sample

Flow sensor..... Thermal sensor equipped with RTD (Resistance Temperature Detector) for flow range 0.5 to 3 L/min with flow alarm contacts

Construction Features.....

- Corrosion resistant stainless steel or polymer sensor housing rated for 50 psig at 100° F (must minimize tritium absorption)
- Borosilicate glass ports
- Inlet, outlet, and electrical leads connect to top end of housing
- Housing and connected leads are submersible
- Integral venturi-type jet pump or air-driven diaphragm pump to force sample liquid through sensor housing
- Return of sample fluid to source

Size.....

- Diameter to fit in 4" schedule 80 pipe
- Length not to exceed 2 m

Electronics.....

- Modular digital electronics in a weather tight enclosure
- Zero check: electronic zero test - push button switch and digital panel meter display
- Analog output signal connection for remote display
- Instrument test: functional check of photodetector, electrometer, signal conditioning and readout electronics - push button switch activated and display of test value
- Remote display: RS-422 connection (up to 1000 ft) to remote display
- Data communications: data acquisition system serial interface with RS-232C or RS-422 connections
- Data storage: all instrument variables retained in EEPROM
- Automatic alarm on loss of signal or indicated contamination levels exceeding instrument range
- Portable data read out device port (e.g. suitable for notebook PC for downloading data)
- Sensor to ratemeter permissible distance 500 ft
- Line voltage spike/variation protection

- Shielding against external electromagnetic noise sources, e.g. welding, microwavé transmitters
- Self check diagnostics
- Modular circuit boards

Optional Features/Accessories .....

- Multi-unit system capability
- Remote computerized adjustment of ratemeter operating modes and parameter set points

* LSD = lowest significant digit

APPENDIX D

SUMMARY OF CHARACTERISTICS FOR FIBERS TESTED

Summary of Fiber Characteristics

FIBER TYPE DESIGNATION	DESCRIPTION
#1	500 μm O.D., polystyrene core with coextruded clad layer of polystyrene doped with 2% concentration of PMP blue fluor. Clad layer 5-19 μm thick
#4	500 μm O.D., DOW 252 polystyrene core with coextruded clad layer of polystyrene doped with 3-HF green fluor. Clad layer 5-10 μm thick. Approx. ½% concentration.
#5	400 μm O.D. polystyrene rod, polymerized and surface doped with PMP blue fluor. Approx. ½% concentration.
#6	750 μm O.D., PMMA extruded core, stretched and solution clad with polystyrene doped with PMP blue fluor at 2% concentration
#7	1000 μm O.D., Green fluor doping throughout core, low index PMMA clad

APPENDIX E

HYBRID PHOTOMULTIPLIER SPECIFICATIONS

12/96

HYBRID PHOTOMULTIPLIER TUBES (HPMT's)

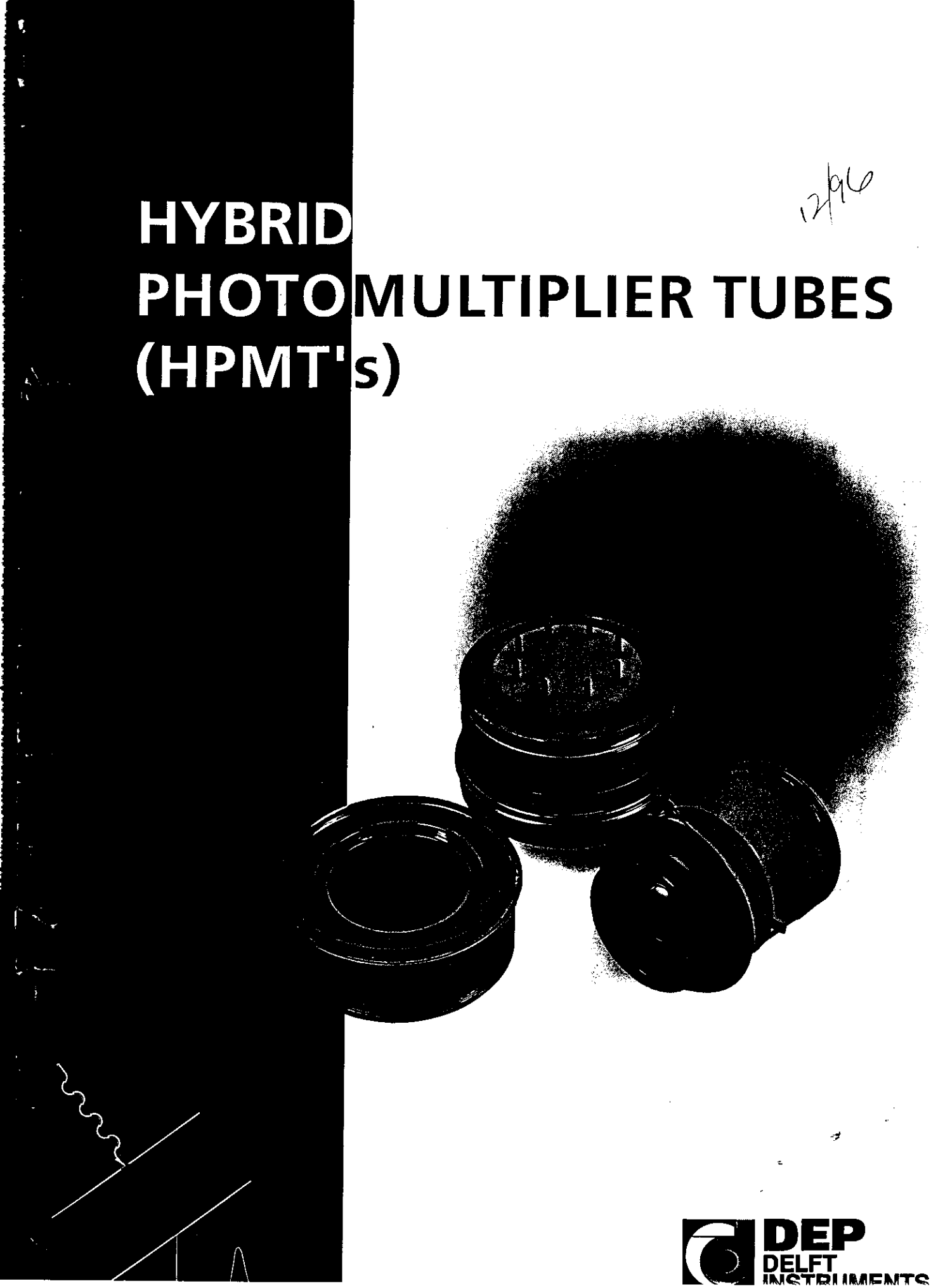

DEP
DELFT
INSTRUMENTS

a new kind of light detector

Introduction

By combining state-of-the-art solid state technology with the latest vacuum photocathode technology, DEP has created a new and innovative range of photodetectors, the DEP Hybrid Photomultiplier Tube (HPMT). These tubes are also known as Hybrid PhotoDiode (HPD). This brochure gives a description of the principle of operation, construction, types and characteristics of the HPMT. The DEP HPMT is very similar to the traditional photomultiplier. as far as customer functions are concerned. However, its unique construction and principle of operation result in many superior performance characteristics. These unique characteristics make the HPMT extremely suitable for high magnetic field and single photon detection applications. Some other fields of application are: high energy physics, astronomy, biology, Laser detection, medical instrumentation like gamma cameras and positron CT, tracer analysis in biochemistry, pollution monitoring, spectroscopy, process control, oil well logging. The DEP. high quality and high performance HPMT offers you a unique possibility to upgrade your system performance!

Tube Structures

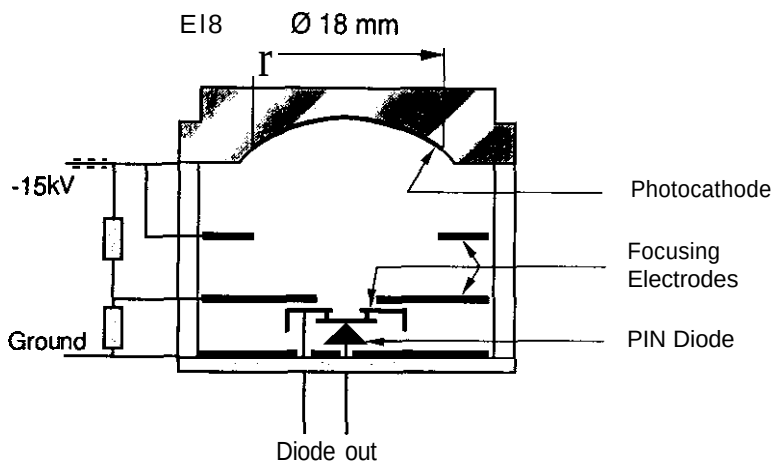

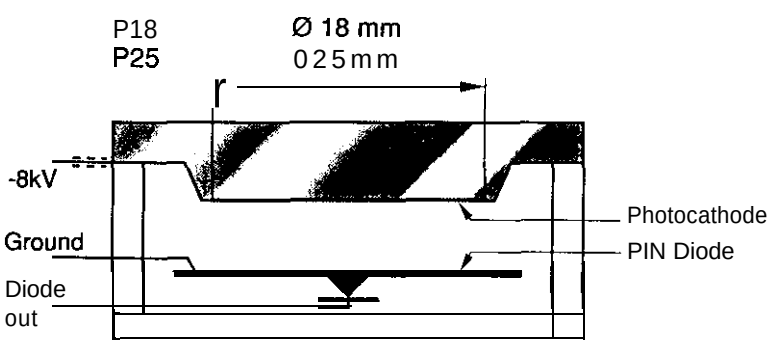

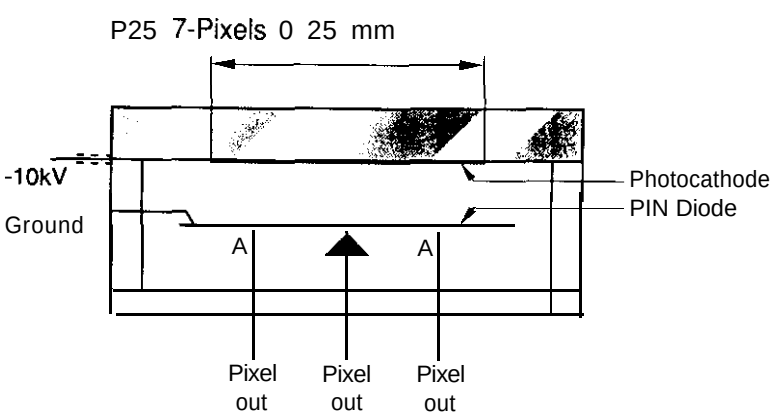

Principle of Operation

Electrostatically Focused HPMT

The E18 electrostatically focused HPMT has an 18mm photocathode on a spherically symmetric shaped window. The photo-electrons that are generated by the incoming photons are focused on a small PIN diode. Two electrodes, each on a negative high voltage, provide the focusing on the diode. The accelerated photo-electrons bombard the backside of the diode and create a number of electron-hole-pairs (typ. 3500 at -15 KV cathode voltage). When the diode is biased in reverse these electron-hole-pairs cause an electric current to flow. This current can be detected and amplified by a charge amplifier or a current amplifier. The advantages of this HPMT are among others very good timing and extremely high photo-electron resolution. Typical applications include astronomy, spectroscopy, scintillation counting, Laser range finding etc.

Proximity Focused HPMT

The P18 and P25 proximity focused HPMT have a photocathode and a PIN diode with an identical sized active area, separated by a small gap. The photo-electrons are accelerated by a high voltage to the diode. Because of the short electron trajectory and the “se of non-magnetic materials this type of HPMT is insensitive for high magnetic fields. The P25 HPMT is available with a single- and multi pixel PIN diode. The single pixel diode is photo-electron bombarded on the junction; the multi pixel diode has seven separated implanted regions and is bombarded on the backside. The multi pixel HPMT provides position sensitivity and can be used in applications where space is limited and a large number of channels is required. Typical applications include the “se in high magnetic fields and position sensitive particle detection.

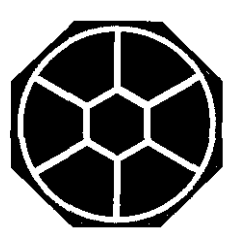

P25 7-Pixels
Diode Layout

Gain

The signal versus acceleration voltage shows a threshold of around 2000 volts. This is the voltage needed for the photo-electrons to penetrate the thin ohmic contact. Above this threshold voltage every 3.6 eV energy increase creates one additional electron-hole pair giving a linear signal amplitude growth with the high voltage. The E18 HPMT with a T-type diode, driven at -15 KV, has a typical gain of 3500 while the P25 HPMT has a gain between 1600 and 2200, depending on the acceleration voltage. Because the HPMT draws virtually no current, the high voltage can be supplied by a miniature high voltage power supply. The stability of the high voltage directly translates to the gain stability of the HPMT.

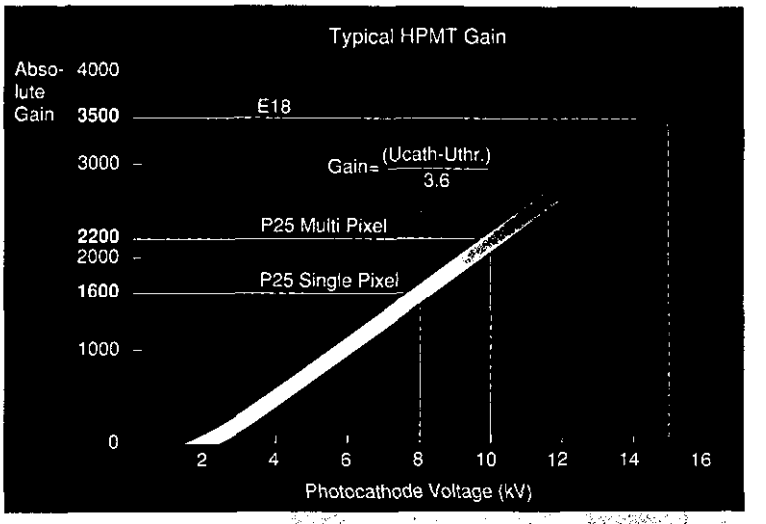

Linearity

The HPMT shows an excellent linear relation between input signal (in photo-electrons) and output signal (in Coulombs). The P25 single pixel HPMT has proven to be linear in charge response over 8 decades of photo-electrons per pulse with nanoseconds long light pulses, starting at the single photo-electron level. The graph shows the HPMT pulse amplitude (red curve) and the collected charge (blue curve). At the 10^6 photo-electrons input level the HPMT pulse response starts to saturate (with a load of 50 Ω). The HPMT charge response however is linear up to more than 10^4 pC corresponding to almost 10^8 photo-electrons.

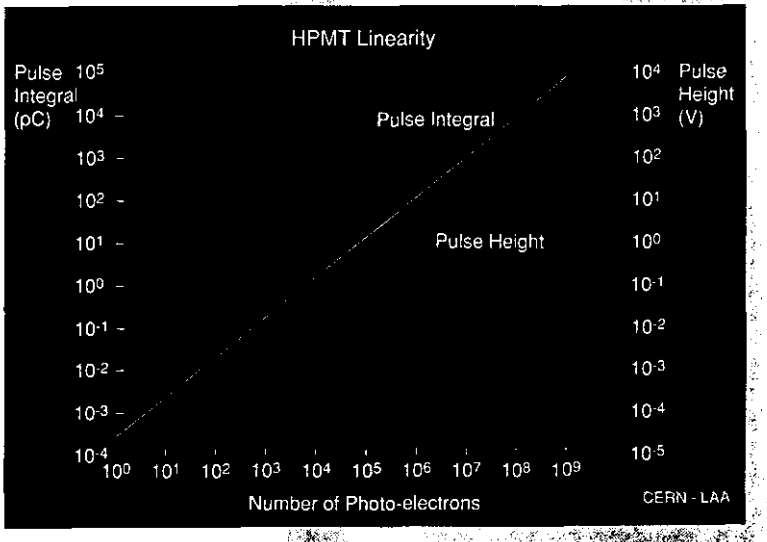

Uniformity

The uniformity of response of the E18 and P25 HPMT lies within the 10% range after a lifetime test of more than 2000 hours at operating voltage and more than 10 Coulombs of delivered signal.

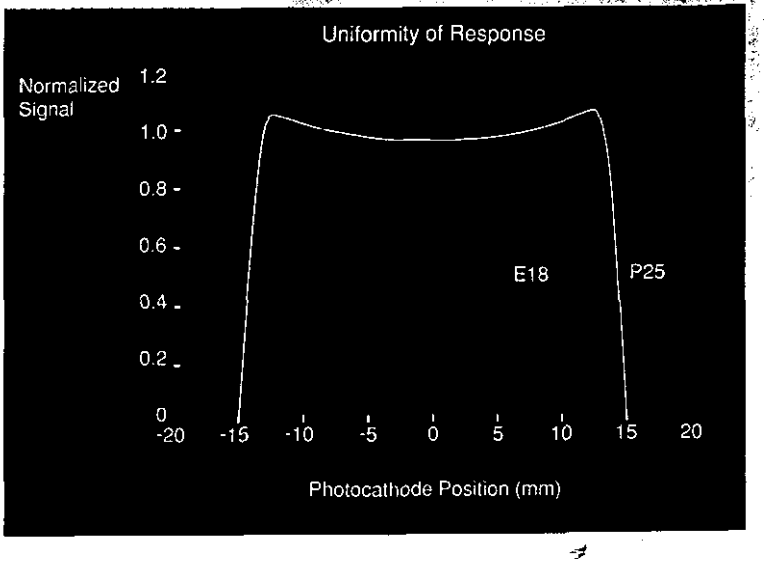

Type	Photocathode Eff Diam (mm)	Photocathode Type	Sensitivity nm	Sensitivity (mA/W) Typ.	Current Gain	Pin Diodes Nr. of Pixels	Pin Diodes Depletion Depth (µm)	Pin Diodes Pixel Capacitance (pF)	Bias Voltage (V) Typ.	Output Pulse** Risetime (ns) Typ.	Output Pulse** Risetime (ns) Max.	Output Pulse** Falltime (ns) Typ.	Output Pulse** Falltime (ns) Max.	Dimensions (mm)	SP Fe
Elec tro Stat cally focu sed	18	S20 on Glass	440	65	3500	1	150	2.3	50	8	10	8	IO	047x40	Gener HPMT
									200	2.5	4	2.5	4	047x40	Fast Tr
									100	4	-	4		047x40	Interna Voltag
		S20-UV on Fused Silica	270 400	70 60	3500	1	150	2.3	100	4	-	4		047x40	UV Sensiti
		s25 on Glass	640 850	40 20	3500	1	150	2.3	100	4	-	4		047x40	Fted Sensiti
		Bialkali on Glass	400 440	80 70	3500	1	150	2.3	100	4	-	4		047x40	Low N Dark c
Prox nity ocu ed	18	Bialkali*** on Glass	400 440	80 70	2600	1	300	100	80	4	7	5	9	Ø37x21	Small F
	25	S20*** on Fiber	440	60	1600	1	300	200	80	6	10	7	12	Ø60x21	Immun Magne
		S20-UV** on Fused Silica	270 400	65 70	1600	1	300	200	80	6	10	7	12	Ø60x21	UV Sensiti
		S20-UV*** on Fused Silica	270 400	65 70	1600	1	300	200	80	6	10	7	12	Ø60x21	Timing
		S20-UV on Fused Silica	270 400	65 70	2200	7	300	1 x20 6 x 3 0	80	6	10	6	IO	360x26	Multi Channe
		S20 on Fiber	440	60	2200	7	300	1x20 6x30	80	6	10	6	10	Ø60x26	Multi Channe

* At Maximum High Voltage
** Measured just below Saturation Level at Maximum Bias Voltage
*** Immune to Magnetic Fields up to 2 Tesla

OPTIONS: High
Built-i
Speci

General Characteristics (cor

Speed

Photon conversion in metal photocathodes has a tim or less and the photo-elect& acceleration of a few field and a linear field has neglectable time spread. T limited by the semiconductor diode characteristics. the capacity of the chip, the bias voltage, the surfac drift time inside the chip and the load resistance. An the specification is therefore the maximum bias vol the very short rise and falltime vs bias voltage.

Specific Features	Type Number	Field of Application
neral Purpose MT	PP0270X	Fluorescence Spectrometers Thickness Meter
st Timing	PP0270Y	Laser Radar Liquid Scintillation Counter Astronomical X-ray Measurement
ernal ltage Divider	PP0270M	Gamma Camera
nsitive	PP0270K	Earth Scattered Light Measurement
d nsitive	PP0270P	GaAs/GaAlAs Laser Detection
v No. of rk Counts	PP0270Z	General Purpose Photon Counter
all Package	PP0350F	Cherenkov Counters, general Photon Detection
nune to gnetic Field	PP0350B	Scintillating Fiber Readout Spagetti Calorimeter
sitive	PP0350D	UV-Scintillating Fiber Readout
ing Diode	PP0350G	Time of Flight Measurement
t i nnel	PP0380C	TOF Counters Cherenkov Counters
ti nnel	PP0380D	Hodoscopes

gh Voltage Power Supply
ilt-in Amplifiers (Charge and Voltage/Current Amplifiers)
ecial Photocathode Sensitivities on Request

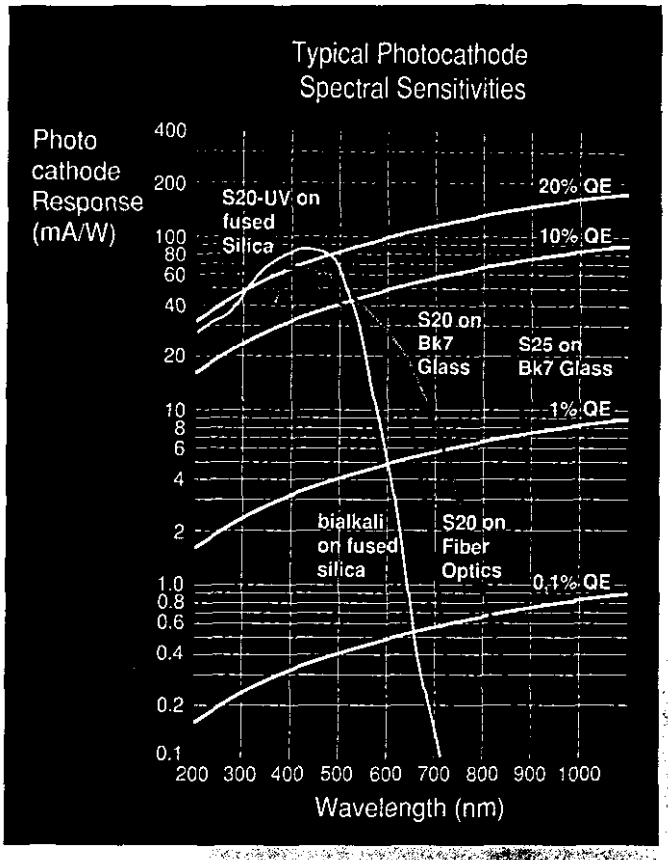

Photocathode Spectral Sensitivities

The graph shows the spectral sensitivity curves of the DEP photocathodes (PC). The S20-UV photocathode process is specially developed for scintillation counting with UV-emitting scintillating fibers. This PC is deposited on a fused silica window. The S20 PC cuts off below 400 nm because of the low transmission of the BK7 glass or fiber window. The bialkali PC was specially developed for applications where a low no. of dark counts is required. The peak sensitivity is typ. 80 mA/W for 400 nm (25% QE)! Special PC sensitivities are available on request.

ont'd)

time scale of pica-seconds ew KV in both a spherical l. The HPMT speed is then s. Determining factors are ace resistance, the charge An important parameter in voltage. The graphs show

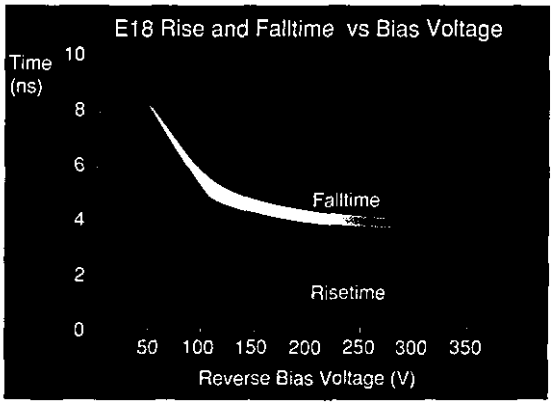

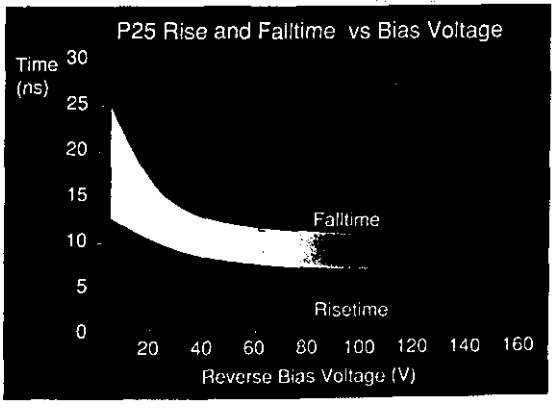

Thanks to an excellent partnership , DEP and Canberra Semiconductor nv in Belgium have been able to combine their skills and technologies which resulted in a series of PIN diodes with excellent characteristics especially for the HPMT application. Two types of diode structures can be distinguished

PIN Diode Structures

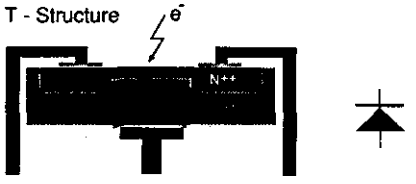

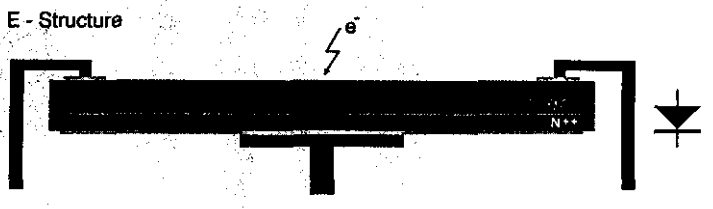

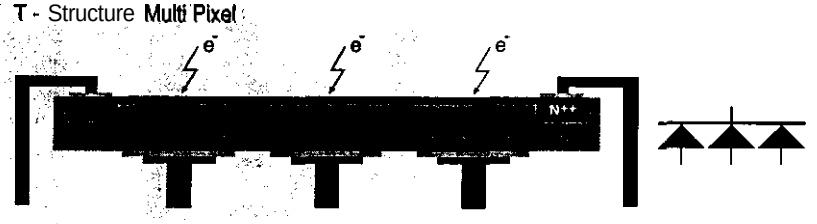

T-Structure

The T-structure PIN diode is a fully depleted Silicon chip. The diode has a P+-junction but is bombarded on the backside (N+-layer). The ohmic contact is ion implanted and is very thin (500 Å) for low electron energy detection. The total thickness of the chip is 150 pm. The transient time is given by the holes velocity and is a function of the electric field (bias voltage) of the diode. Because of the small active surface the diode can be used for detecting fast events (few ns).

E-Structure

The E-structure PIN diode is a partially depleted Silicon ship. The diode is bombarded on the front side (P+-junction). The thickness of the diode is 300 pm. Because of the use in the proximity focused HPMT the active area of the chip is large, compared to the E18 diode. Therefore the capacity of the chip is not extremely low. The transient time of the electrons is shorter than the T-structure. However, the total speed of the diode is depending on the surface resistance and the capacity of the diode (RsxC) which results in a risetime between 5 and 10 ns at maximum bias voltage.

Multi Pixel Diodes

The multi pixel chip contains of seven implanted junctions, fully seperated from each other by a 200 µm wide insulating layer. The ohmic contact is one uniform thin layer. The chip has basically a T-structure (fully depleted, bombarded on the backside) with a thickness of 300 pm.

PIN Diode Equivalent Model

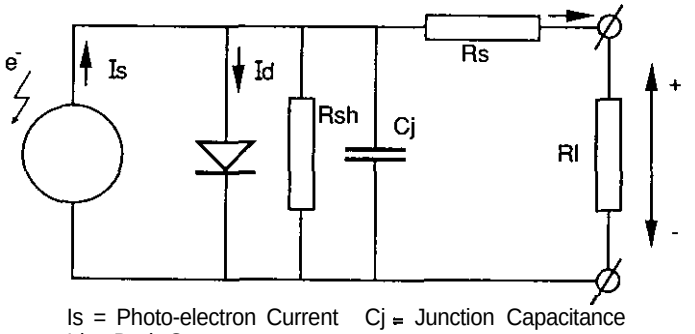

Is = Photo-electron Current
Id = Dark Current
Rsh = Shunt Resistance
Cj = Junction Capacitance
Rs = Series Resistance
Rl = Load Resistance

Specific Characteristics

Single and Multi Photo-electron Counting

The statistical fluctuations of the photo-electron multiplication of the first anode stage of a photo-multiplier are responsible for the intrinsic energy resolution. The best traditional photomultipliers can resolve up to three photo-electron peaks. Because of the high number of electron-hole pairs generated in the anode (PIN diode) of an E18 HPMT the yield of the HPMT anode is roughly 2 orders of magnitude higher than the yield of the first dynode of a PMT and hence the statistical fluctuations are much smaller.

A photo-electron spectrum, detected by an HPMT and recorded via a Multi Channel Analyzer, is shown in the graph. Exited with a scintillating fiber exposed to a Sr-90 source the HPMT resolves more than 14 photo-electron peaks. The second graph compares the contrast function of the HPMT with the contrast function of a PMT. Compared to the PMT the HPMT has a drastically better contrast function. This is the main reason why the HPMT can replace most PMT's in single and multi photon counting applications and will boost up the overall performance of the system.

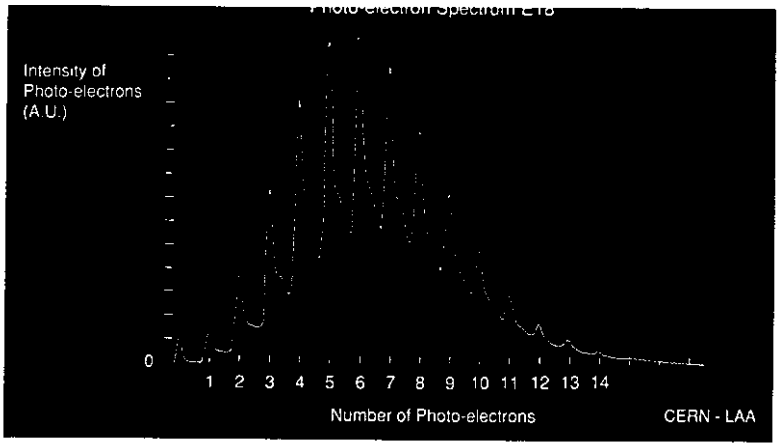

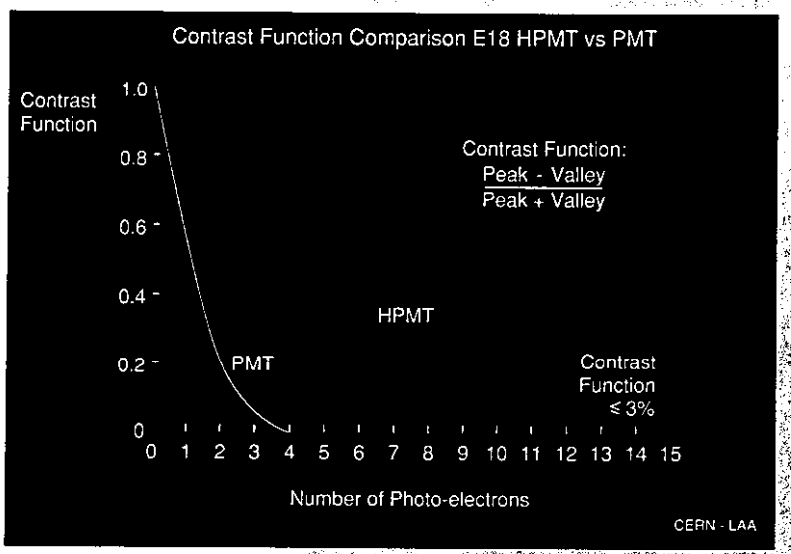

Magnetic Field Behaviour

The P25 HPMT has a small gap between PC and PIN diode. The electric field focuses the p.e.s. on the PIN diode. By applying a strong magnetic field parallel to the electrical field the HPMT shows neglectable variation in the output signal. When the magnetic field forms an angle with the electric field, the photo-electrons still reach the silicon surface with full energy, although in a slightly displaced position and with a variable impinging angle. No signal cutoff is expected unless the photo-electrons are dragged outside of the diode active area.

The graph shows the output signal of the P25 HPMT in a magnetic field up to 1.6 Tesla. Tests with a smaller proximity HPMT have proven that the HPMT behaves correctly in magnetic fields up to 2.5 Tesla. No breakdown is foreseen in higher magnetic fields.

Because of this magnetic field immunity the proximity focused HPMT makes it possible to operate light detectors where magnetic field sensitive PMT's cannot be used.

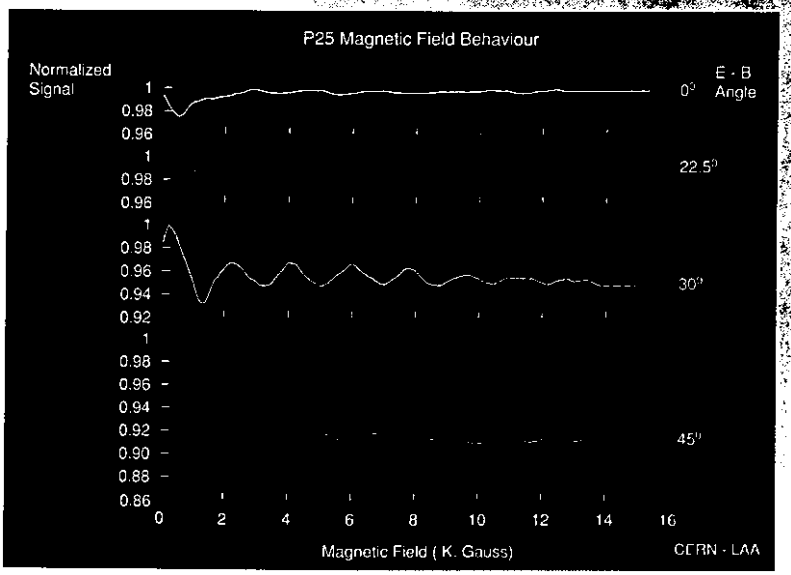

References.

1 R. DeSalvo et al., NIM A315(1992) 375 384, First results on the Hybrid Photodiode Tube.

2 S. Basa et al., NIM A330(1993) 93 99. Test results of the first Proximity Focused Hybrid PhotoDiode Detector Prototypes.

3 C. D'Ambrosoi et al., Ref. CERN-PPE/93-140 (june '93), submitted to NIM. Photoncounting with a Hybrid Photomultiplier Tube.

4 H. Arnaudon et al.. A00 (1993) NIM 00876, Proximity focused Hybrid PhotoDiode characteristics evaluations.

5 C. D'Ambrodio et al.. CERN-PPE/93-218 (dec '93), submitted to NIM, Further results on photon counting with small diameter scintillating fibers.

6 G. Anzivino et al.. CERN-LAA/HC/94-04 (nov '93), presented at the IV International Conference on Calorimetry in High Energy Physics, Isola d'Elba, Italy 19-25 Sept 1993. Recent Developments of the HPD.

7 R. J. Schomaker, presented at the XV European Symposium on Opto Electronics, Paris France, 25.27 April 1994, Performance of the Hybrid Photomultiplier Tube (HPMT).

8 G. Anzivino et al.. CERN-LAA/HC/94-20 (July '94), presented at the VI Pisa Meeting on Advanced Detectors. Elba. Italy, 22-28 May 1994. Review of the Hybrid Photo Diode Tube (HPD), an Advanced Light Detector for Physics,

9 L. Boskma et al.. presented at the V International Conference on Calorimetry. Brookhaven, USA, September '94. The DEP Hybrid Photomultiplier Tube.

The HPMT's are developed in collaboration projects with CERN. Important parts were substantially funded by INFN.

154 - 0818A 2/ mrt.1995

DEP WHEN EVERY PHOTON COUNTS

DEP
DELFT
INSTRUMENTS

DEP (B.V. Delft Electronische Producten)
Dwazziewegen 2, Roden
Postbus 60, 9300 AB Roden
The Netherlands
Tel. +31 - (0)50 5018808
Fax +31 - (0)50 5013510
e-mail: sales@dep.nl

DEP

Hybrid photomultiplier tube (HPMT) PP0275C
with S20-UV photocathode on quartz window
and built-in charge pre-amplifier

Date: 16-12-96

DEP Specification	:	184-1621
DEP drawing	:	183-0322
Serial no.	:	C9643114
Quantum efficiency		
@270nm		56 %
@400nm		82 %
Spectral sensitivity	:	curve attached
Dark count rate		10 c/s/cm²
Single photo-electron resolution	:	13 % FWHM plot attached
Operating Voltages		
High Voltage		-10 kV min -15 kV max
Focus		75 % of High Voltage
Diode Bias Voltage		+ 25 V min +175 V max
Pre-amplifier power supply	:	+12 V -12 v

Remarks:

DEP

PC
pp0275

CATHODE SENSITIVITY

nr : C9643114
date : Dec 16 1996

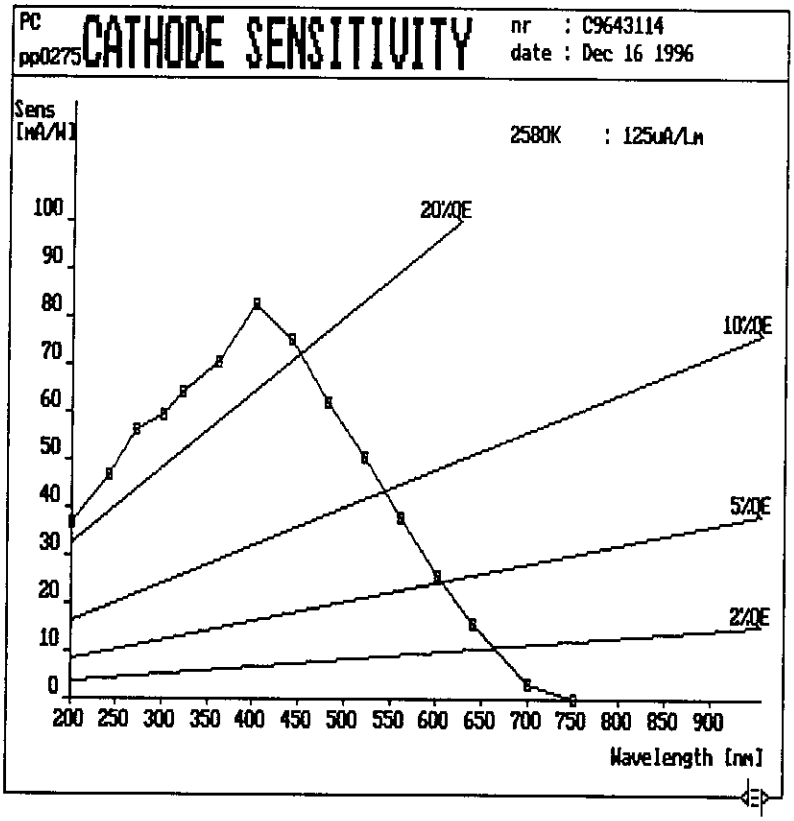

wave-length	radiant sensitivity	QE
200nm	36.6mA/W	22.8%
240nm	47.0mA/W	24.4%
270nm	56.5mA/W	26.0%
300nm	59.6mA/W	24.7%
320nm	64.1mA/W	24.9%
360nm	70.3mA/W	24.3%
400nm	82.4mA/W	25.6%
440nm	75.5mA/W	21.3%
480nm	62.0mA/W	16.1%
520nm	50.6mA/W	12.1%
560nm	37.8mA/W	8.4%
600nm	26.0mA/W	5.4%
640nm	15.8mA/W	3.1%
700nm	3.0mA/W	0.5%
750nm	0.1mA/W	0.0%

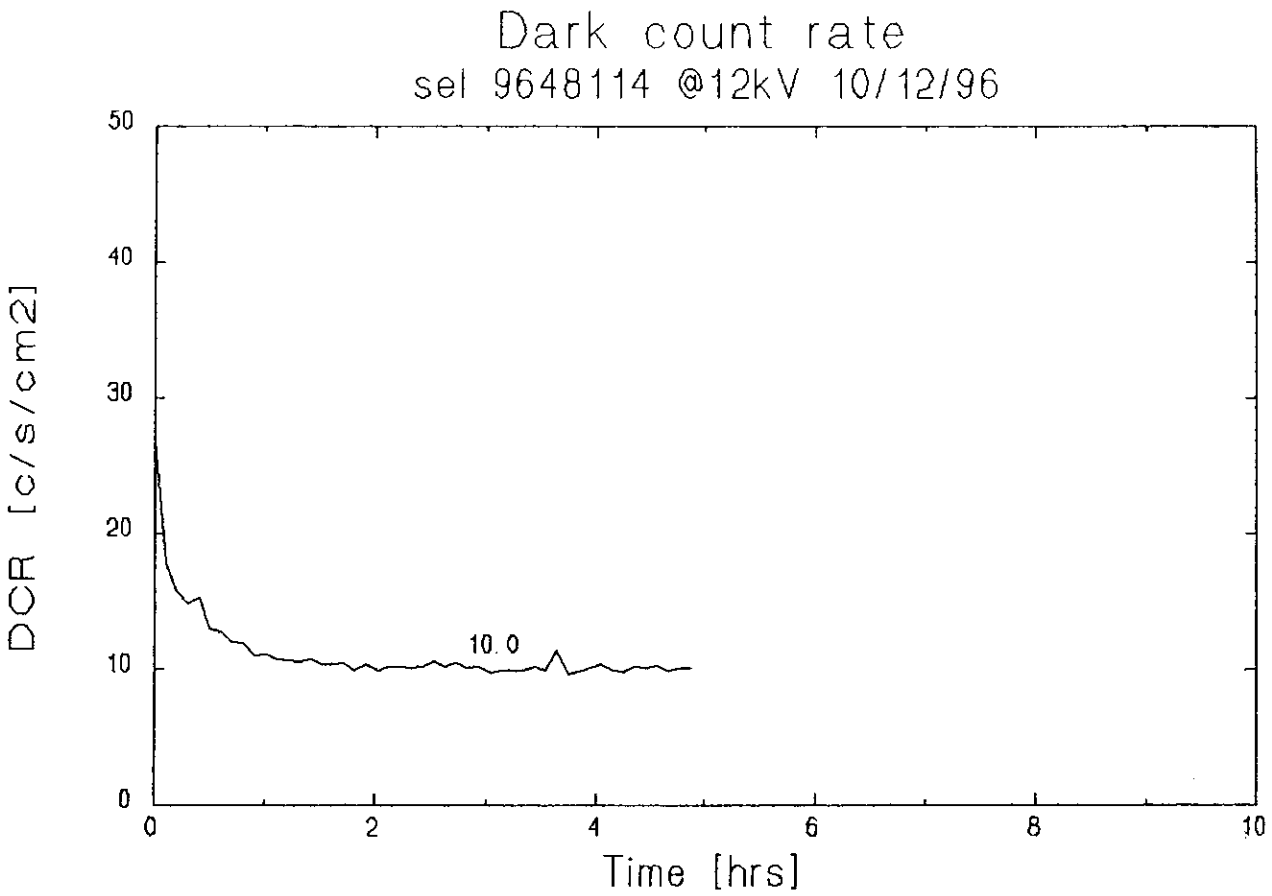
Dark count rate
sel 9648114 @12kV 10/12/96
DCR [c/s/cm2]
50
40
30
20
10
0
0
2
4
6
8
10
Time [hrs]
10.0

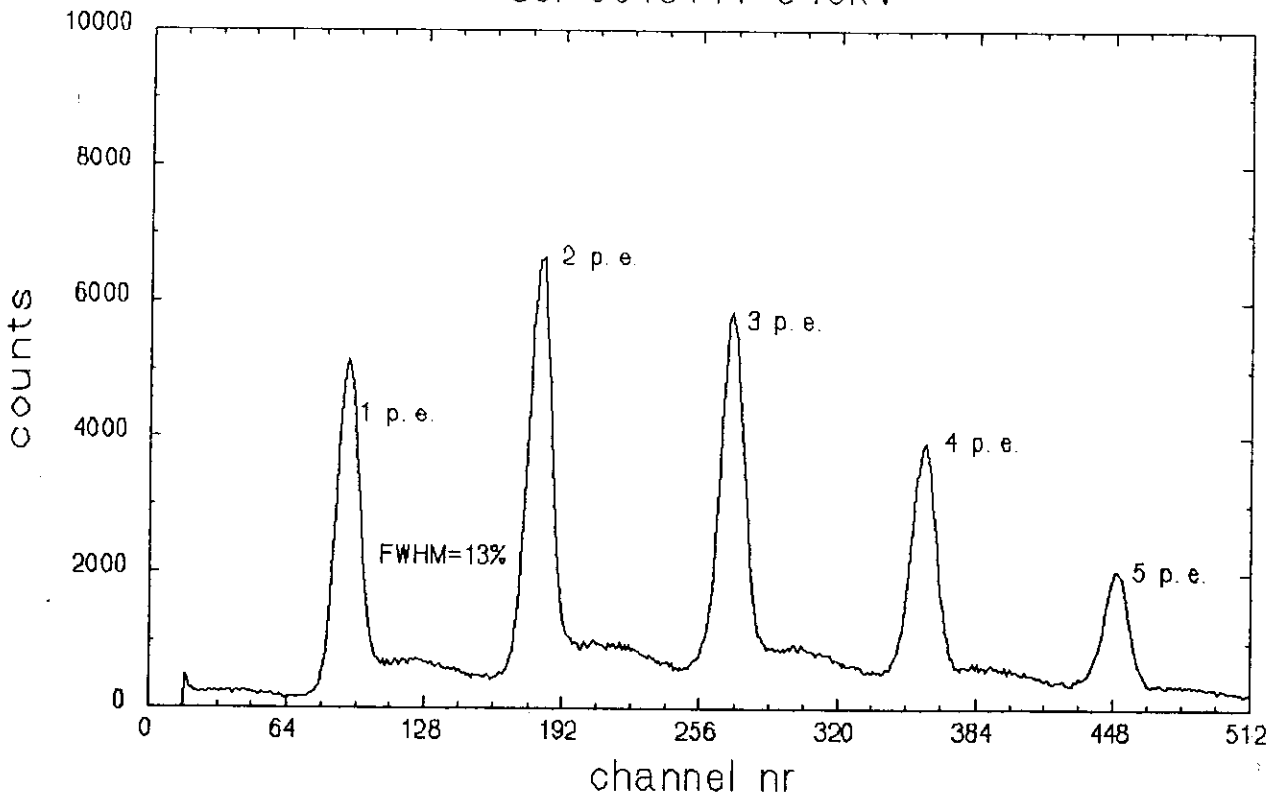
Photo-electron resolution plot
sel 9648114 @15kV
counts
channel nr
1 p. e.
2 p. e.
3 p. e.
4 p. e.
5 p. e.
FWHM=13%
0
2000
4000
6000
8000
10000
0
64
128
192
256
320
384
448
512

PRELIMINARY DATA PRELIMINARY DATA PRELIMINARY DATA

GENERAL DESCRIPTION

The HPMT is a vacuum tube having a SZO photocathode deposited on a fused silica input window, an electron lens that focuses the photoelectrons onto a Silicon PIN diode which is biased in reverse. As a function of their energy, which is determined by the high voltage applied to the photocathode, a number of electron-hole pairs is generated in the silicon causing a reverse current to flow. The diode charge is collected and amplified by a high precision, low noise charge preamplifier. The unit is potted with flying leads for the high voltage and the preamplifier power supply.

MAJOR FEATURES

- single and multi photon counting
- excellent photo-electron resolution
- high gain stnhility
- high QE for UV
- direct charge coupling from diode to pre-amplifier
- extremely low noise pre-amplifier
- compact size
- rigid construction
- no dynode chain, no bleeder required

SPECIFIC DATA

	Minimal	Typical	Maximal	Unit
Useful input diameter		18		mm
Input window: Fused silica				
Photocathode: S20-UV				
optimized for 270 nm				
Cathode sensitivity at: 270 nm	55	60		mA/W
400 nm	65	70		mA/W
Quantum efficiency at: 270 nm	25	28		%
400 nm	20	22		%
# of dark counts at 20°C		100		counts/(sec.cm^2)
Current gain at -15 kV		3500		

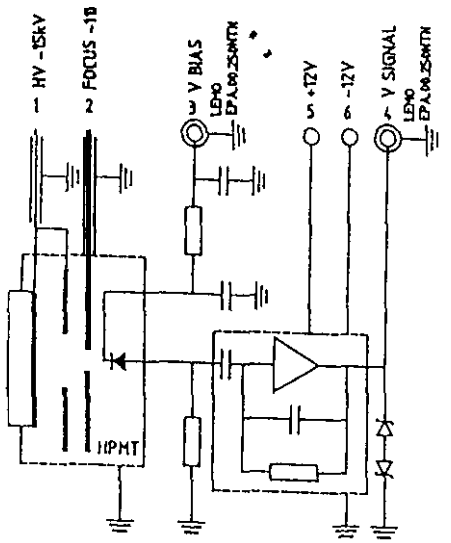

vervallen	vakmanschap:GOEO/FOUT		datum:		
	pers.nr.:		paraaf:		
		'min.	gemeten		max.

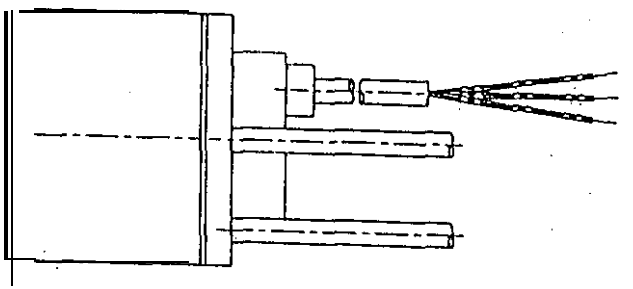

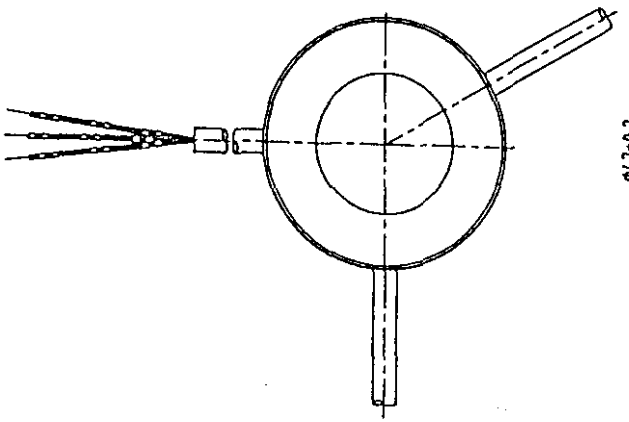

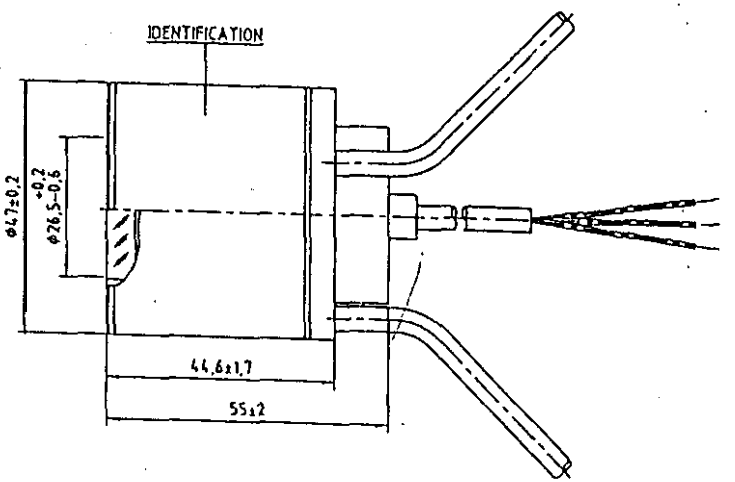

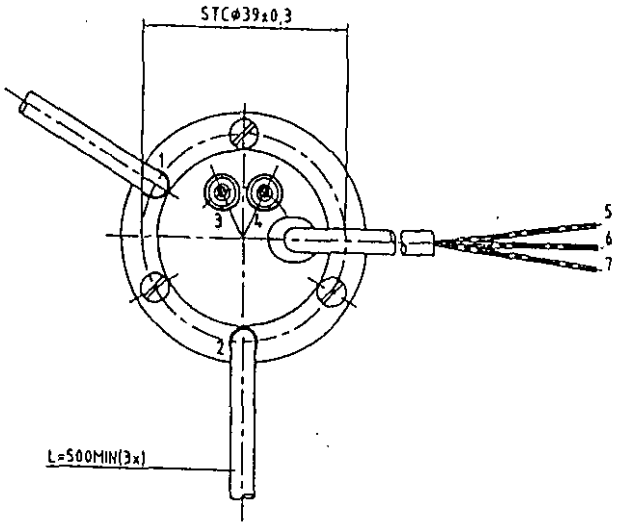

NOTE 1: RED WIRE (COAX) = 1 = HV -15kV
RED WIRE (COAX) = 2 = FOCUS -11kV
CONNECTOR = 3 = V BIAS
CONNECTOR = 4 = V SIGNAL
BROWN WIRE = 5 = +12V (PRE-AMP. POWER SUPPLY)
WHITE WIRE = 6 = -12V (PRE-AMP. POWER SUPPLY)
GROUND = 7 = GROUND / HOUSING

DELFT ELECTRONISCHE PRODUCTEN

aanvlakkansa proj.	schroefdraad DIN 13 6g/6H NEN 3222	ruwheid ISO 1302	materiaal:	get.: JK	A0 15-3-95
glas DIN 3140	vorm- en plaatstol. ISO R1101	maateenheid: mm	schaal: 1:1	gec.:	A1 10-4-96
				gec.:	A2 6-2-96
				gez.:	
				aantal bladen: 1 blad: 1	

FOTOMULTIPLIER PP0275
(PHOTOMULTIPLIER PP0275)

183 0322A2

	Minimal	Typical	Maximal	Unit
Operating Voltage	-10		-15	kV
Coaxial high voltage leads				
Operating temperature	-20		+40	°C
Weight				grams

Uniformity:

The response varies not more than 20% within ø18 mm area when scanned with a 22° aperture beam having a diameter of 1 mm.

PIN diode, T-type:

capacitance		2.24	2.49	pF
total amplifier input capacitance		12		pF
operating voltage (diode bias)	25		100*	V
polarity bias voltage	positive			

*: At higher bias voltage the reverse bias current will increase rapidly and cause damage at values above 1µA.

Pre-amplifier, Low Noise SMD charge amplifier:

Internal bias circuit		
Gain	2	V/pC
	90	mV/MeV(Si)
feedback	1	Gohm
	0.47	pF
power supply	+12 ± 0,0001	V
	-12 ± 0,0001	V
	12	mA

	Minimal	Typical	Maximal	Unit
Overall performance:				
# Of resolvable photo-electron peaks		14		
Output pulse rise time		50		ns
Noise:				
FWHM (1st photo-electron peak)		12	16	%
Equivalent Noise Charge (ENC)		420		e^- FWHM
		180		e^- RMS
		1.5		KeV(Si)
Dynamic range		t.b.s.		photo-electrons
Output impedance		50		ohms

All data was measured with the DEP PP0100Y HPMT High Voltage Power Supply at 15KV operating voltage

APPENDIX F

PHOTOMULTIPLIER SPECIFICATIONS

Side On Type Photomultiplier Tubes

28mm (1-1/8") Dia. Types with UV to Visible Sensitivity

Type No.	Remarks	Spectral Response: Curve Code	Spectral Response: Range (nm)	Spectral Response: Peak Wavelength (nm)	Photocathode Material	Window Material	Outline No.	Dynode Structure: No. of stages	Socket: Socket Assembly	Maximum Ratings: Anode to Cathode Voltage (Vdc)	Maximum Ratings: Average Anode Current (mA)	Cathode Sensitivity: Luminous Min. (μA/lm)	Cathode Sensitivity: Luminous Typ. (μA/lm)
931A	For visible range, general purpose	350K (S-4)	300 to 650	400	Sb-Cs	K	❶	CC/9	E678-11A■/5 6	1250	0.1	20	40
931B	Bialkali photocathode, high stability	453K	300 to 650	400	BA	K	❶	CC/9	E678-11A■/5 6	1250	0.1	30	55
1P21	Low dark current variant of 931A	350K (S-4)	300 to 650	400	Sb-Cs	K	❶	CC/9	E678-11A■/5 6	1250	0.1	20	40
R105	High gain and low dark current variant of 931A				Sb-Cs	K	❶	CC/9	E678-11A■/5 6	1250	0.1	25	40
R105UH	High gain variant of R105				Sb-Cs	K	❶	CC/9	E678-11A■/5 6	1250	0.1	30	50
1P28	For UV to visible range, general purpose	350U (S-5)	185 to 650	340	Sb-Cs	U	❶	CC/9	E678-11A■/5 6	1250	0.1	20	40
R212	High gain and low dark current variant of 1P28				Sb-Cs	U	❶	CC/9	E678-11A■/5 6	1250	0.1	20	40
R212UH	High sensitivity variant of R212				Sb-Cs	U	❶	CC/9	E678-11A■/5 6	1250	0.1	30	50
R1527	Low dark current bialkali photocathode	456U	185 to 680	400	LBA	U	❶	CC/9	E678-11A■/5 6	1250	0.1	40	60
*R4220	High sensitivity variant of R1527	456U	185 to 710	410	BA	U	❶	CC/9	E678-11A■/5 6	1250	0.1	80	100
R106	Variant of R212 with synthetic silica window	350S (S-19)	160 to 650	340	Sb-Cs	Q	❶	CC/9	E678-11A■/5 6	1250	0.1	20	40
R106UH	High gain variant of R106				Sb-Cs	Q	❶	CC/9	E678-11A■/5 6	1250	0.1	30	60
1P28A	Extended-red variant of 1P28	351U	185 to 700		Sb-Cs	U	❶	CC/9	E678-11A■/5 6	1250	0.1	25	60
R372	Red-enhanced bialkali photocathode	451U	185 to 730	410	BA	U	❶	CC/9	E678-11A■/5 6	1250	0.1	40	70
*R3788	High sensitivity bialkali photocathode	452U	185 to 750	420	BA	U	❶	CC/9	E678-11A■/5 6	1250	0.1	100	120
*R4332	Variant of R3788 with synthetic silica window	458S	160 to 750	420	BA	Q	❶	CC/9	E678-11A■/5 6	1250	0.1	100	120
*R2693	Transmission-mode bialkali photocathode	430U	185 to 650	375	BA	U	❷	CC/9	E678-11A■/5 6	1250	0.1	30	50

Unit: mm

❶ 931A, 931B, 1P28, R3788, etc.

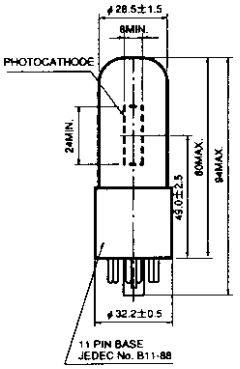

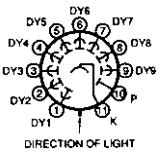

TPMSA0001EA

❷ R2693

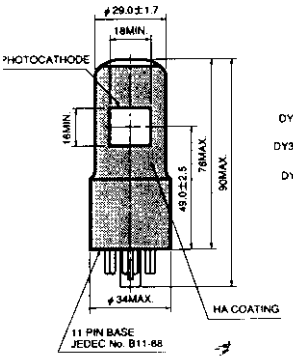

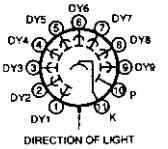

TPMSA0007EA

(at 25℃)

Cathode Sensitivity			K	L	Anode Characteristics			M					A
Blue (5-58) Typ. (μA/lm)	Red / White Ratio Typ.	Radiant Typ. (mA/W)	Anode to Cathode Supply Voltage (Vac)	Anode Sensitivity Luminous Min. (A/lm)	Anode Sensitivity Luminous Typ. (A/lm)	Anode Sensitivity Radiant Typ. (A/W)	Current Amplification Typ.	Anode Dark Current (After 30 min.) Typ. (nA)	Anode Dark Current (After 30 min.) Max. (nA)	Time Response Rise Time Typ. (ns)	Time Response Electron Transit Time Typ. (ns)	Notes	Type No.
5.0	—	48	1000 ⑩	50	400	4.8×10^{5}	1.0×10^{7}	10	50	2.2	22		931A
7.1	—	60	1000 ⑩	50	600	6.6×10^{5}	1.1×10^{7}	5	50	2.2	22	UV glass window type: R1516	931B
5.0	—	48	1000 ⑩	50	250	3.0×10^{5}	6.25×10^{6}	1	5	2.2	22		1P21
5.0	—	48	1000 ⑩	50	400	4.8×10^{5}	1.0×10^{7}	2	10	2.2	22		R105
5.5	—	60	1000 ⑩	1000	1500	1.8×10^{6}	3.0×10^{7}	1	10	2.2	22		R105UH
5.0	—	48	1000 ⑩	20	400	4.8×10^{5}	1.0×10^{7}	5	50	2.2	22		1P28
5.0	—	48	1000 ⑩	50	300	3.6×10^{5}	7.5×10^{6}	1	10	2.2	22		R212
5.5	—	60	1000 ⑩	1000	1500	1.8×10^{6}	3.0×10^{7}	1	10	2.2	22		R212UH
6.4	—	60	1000 ⑩	200	400	4.0×10^{5}	6.7×10^{6}	0.1	2	2.2	22	Photon counting type: R1527P : 10cps Typ.	R1527
8.0	—	70	1000 ⑩	1000	1200	8.4×10^{5}	1.2×10^{7}	0.2	2	2.2	22	Photon counting type: R4220P : 10cps Typ.	R4220*
6.5	—	48	1000 ⑩	100	300	3.6×10^{5}	7.5×10^{6}	1	10	2.2	22		R106
7.0	—	60	1000 ⑩	1000	1500	1.5×10^{6}	2.5×10^{7}	1	10	2.2	22		R106UH
6.5	—	56	1000 ⑩	50	300	2.8×10^{5}	5.0×10^{6}	5	50	2.2	22		1P28A
6.5	0.02	61	1000 ⑩	200	500	4.3×10^{5}	7.1×10^{6}	5	50	2.2	22		R372
10.0	0.01	90	1000 ⑩	500	1200	9.0×10^{5}	1.0×10^{7}	5	50	2.2	22		R3788*
10.0	0.01	91	1000 ⑩	500	1200	9.1×10^{5}	1.0×10^{7}	5	50	2.2	22	QE40% Typ. (at 210nm)	R4332*
7.0	—	62	1000 ⑩	100	300	3.7×10^{5}	6.0×10^{6}	0.5	5	1.2	18	Photon counting type: R2693P : 15cps Typ.	R2693*

HAMAMATSU FINAL TEST SHEET

PHOTOMULTIPLIER TUBE TYPE : R2693P

CUSTOMER : BABCOCK & WILCOX QUANTITY 1 pce.

Serial Number	(1) Cathode Luminous Sens. μA/lm	(2) Anode Luminous Sens. A/lm	(3) Anode Dark Current nA	(4) Cathode Blue Sens. μA/lm Blue	(5) Applied Voltage V	(6) Dark Counts cps	
EA1378	51.8	357.0	0.29	6.60	820	5.6	

NOTES

(1)(2)(4) Light source : Tungsten filament lamp operated at 2856K.
(2)(3) Overall supply voltage : 1000 (V)
Voltage distribution : The standard voltage distribution ratio listed in the HAMAMATSU photomultiplier catalog.
(3) The bulb of the tube is insulated from ground potential.
(4) Measured with a Corning CS 5-58 blue filter (half stock thickness).
(5)(6) Dark Count and the applied voltage at 1×10^6 Gain.

Date : JANUARY 30, 1997 Temperature : 25 ℃

Approved by : Kawamoto

Head-On Type Photomultiplier Tubes

25mm (1") Dia. Types

A) Type No.	Remarks	Spectral Response: B) Number of Code	Range (nm)	Peak Wave-length (nm)	C) Photo-cathode Material	D) Window Material	E) Envelope No.	F) Dynode Structure: No. of Stages	G) Socket: Socket Assembly	Maximum Ratings: H) Cathode Sensitivity: Luminous: Anode to Cathode Voltage (Vdc)	Anode Current (mA)	Min. (μA/lm)	Typ. (μA/lm)
R1535	For scintillation counting	400K	300 to 650	420	BA	K	❶	L/10	E678-14C*/26	1800	0.1	60	115
*R4998	For visible range, fast time response				BA	K	❹	L/10	E678-12A*	2500	0.1	60	70

25mm (1") Dia. Low Profile Types

R2078	For UV range	201S	160 to 320	240	Cs-Te	Q	❷	CC/10	E678-12A*	2000	0.01	—	—
R1924	For visible range	400K	300 to 650	420	BA	K	❸	CC/10	E678-14C*/23 24 25	1250	0.1	60	90
*R3550	Low noise bialkali photocathode	401K		375	LBA	K	❸	CC/10	E678-14C*/23 24 25	1250	0.1	30	50
R1288	High temperature, ruggedized type	401K			HBA	K	❷	CC/10	E678-12A*	1800	0.02	—	40
R1925	For visible to near IR range	500K (S-20)	300 to 850	420	MA	K	❸	CC/10	E678-14C*/23 24 25	1250	0.1	80	120
*R5070	Prismatic window, multialkali photocathode with high sensitivity	502K	300 to 900		MA	K	❸	CC/10	E678-14C*/23 24 25	1250	0.1	130	230

❶ R1535

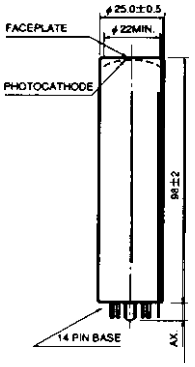

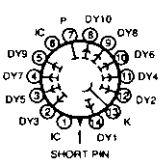

TPMHA0099EA

❷ R2078, R1288

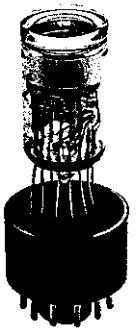

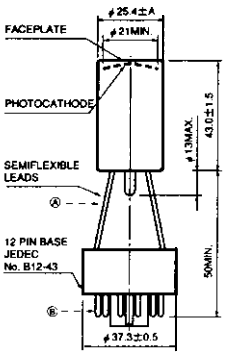

	R2078	R1288
A	0.8	0.5

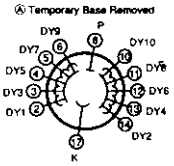

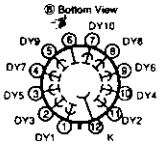

TPMHA0039EA

(at 25°C)

Cathode Sensitivity		K	L	Anode Characteristics M								A
				Anode Sensitivity				Anode Dark Current (After 30 min.)		Time Response		
Blue (CS 5-58) Typ. (μA/lm)	Red/White Ratio Typ.	Radiant Typ. (mA/W)	Anode to Cathode Supply Voltage (Vdc)	Luminous Min. (A/lm)	Luminous Typ. (A/lm)	Radiant Typ. (A/W)	Current Amplification Typ.	Typ. (nA)	Max. (nA)	Rise Time Typ. (ns)	Electron Transit Time Typ. (ns)	Notes	Type No.
11.0	—	88	1500 ⑲	50	300	2.3×10^5	2.6×10^6	10	100	2.4	22		R1535
9.0	—	72	2250 ㉒	100	400	4.1×10^4	5.7×10^6	100	800	0.7	10	Synthetic silica window type : R5320 TTS: 160ps	R4998*
—	—	29ⓐ	1500 ⑱	4×10^3 ⓑ (A/W)	—	1.5×10^4ⓑ	5.0×10^5	0.015	0.1	1.5	14	Dark count: 5cps Typ. 5×10^5, 1500V	R2078
10.5	—	85	1000 ⑱	20	100	9.4×10^4	1.1×10^6	3	20	2.0	19	Photon counting type: R1924P	R1924
6.5	—	60	1000 ⑱	20	100	1.2×10^5	2×10^6	20ⓑ	60ⓑ	2.0	19		R3550 *
6.0	—	51	1500 ⑱	8	15	1.9×10^4	3.8×10^5	0.1	10	1.5	14	Button stem type: R1288-01	R1288
—	0.2	51	1000 ⑱	10	30	1.3×10^4	2.5×10^5	3	20	2.0	19	Synthetic silica window type : R1926	R1925
—	0.25	65	1000 ⑱	20	100	2.8×10^4	4.3×10^5	3	20	2.0	19	28mm dia. type: R5051	R5070 *

100 cps with 300 cps via Telecom 12/13

(Unit: mm)

❸ R1924, R1925. R3550, R5070

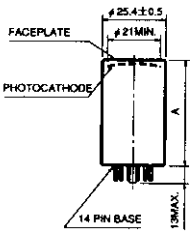

	R5070	Others
A	46±1.5	43±1.5

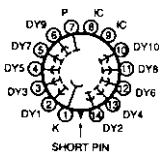

TPMHA0040EA

❹ R4998

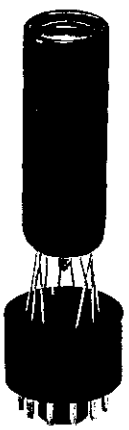

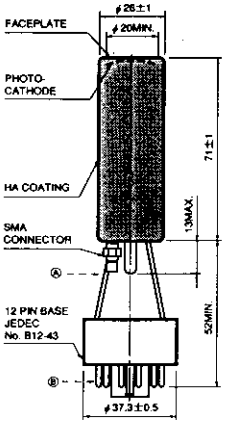

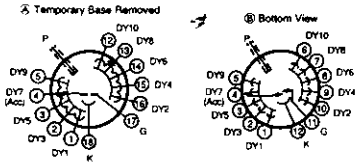

TPMHA0093EA

HAMAMATSU

FINAL TEST SHEET

PHOTOMULTIPLIER TUBE

TYPE : R3550

CUSTOMER BABCOCK E WILCOX

QUANTITY 1 pce.

Serial Number	(1) Cathode Luminous Sens. μA/lm	(2) Anode Luminous Sens. A/lm	(3) Anode Dark Current nA	(4) Cathode Blue Sens. μA/lm Blue			
NA37b7	54.3	183.(	0.03	7.57			

NOTES

(1)(2)(4) Light source : Tungsten filament lamp operated at 2856K.
(2)(3) Overall supply voltage : 1000 (V)
Voltage distribution : The standard voltage distribution ratio listed in the HAMAMATSU photomultiplier catalog.
(3) The bulb of the tube is insulated from ground potential.
(4) Measured with a Corning CS 5-58 blue filter (half stock thickness).

Date : JANUARY 23, 1997

Temperature : 25 ℃

Approved by :

HAMAMATSU

SINGLE PHOTON COUNTING

TUBE TYPE : R3550
SERIAL NO. : NA3757

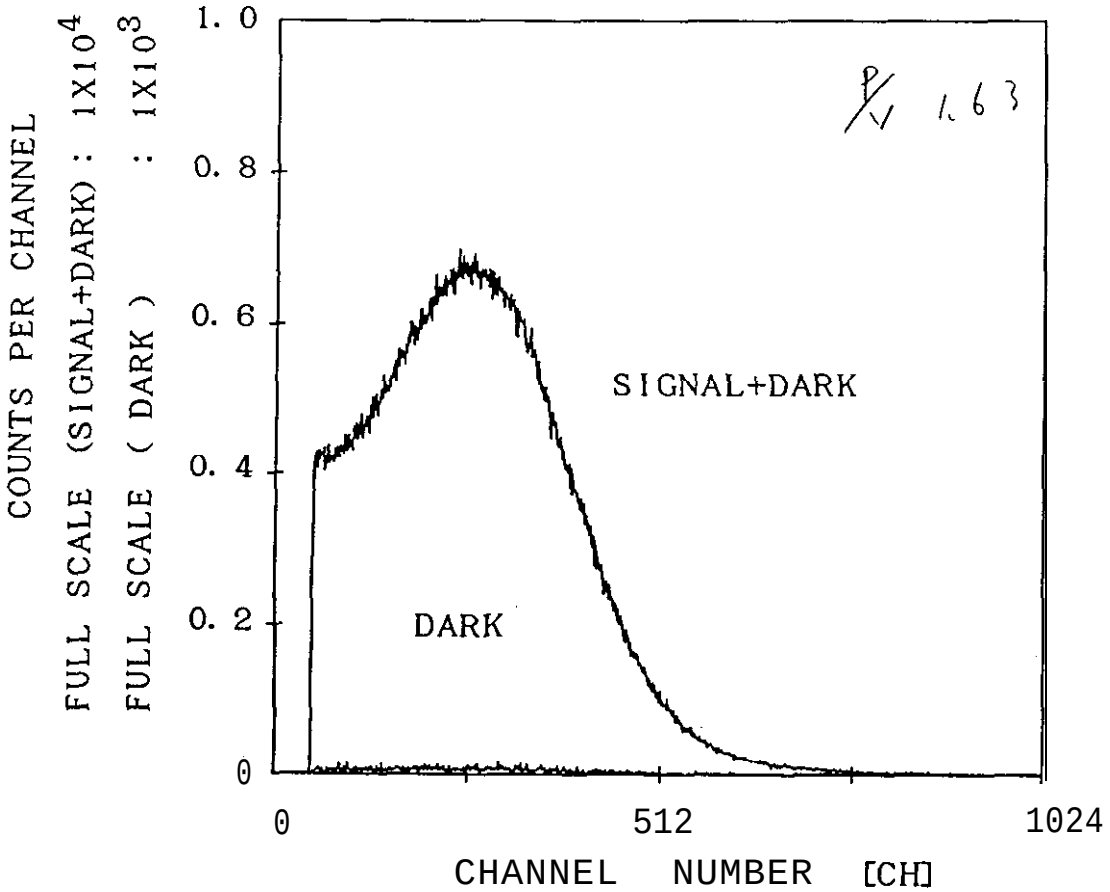

WAVELENGTH OF INCIDENT LIGHT : 400 [nm]
SUPPLY VOLTAGE : 915 M
LOWER LEVEL DISCRI. : 88 [CH]
UPPER LEVEL DISCRI. : 796 [CH]
PHOTON+DARK COUNTS : 10371 [cps]
DARK COUNTS : 11.5 [cps]
LIVE TIME 200 [sec.]
P.H.A. :NAIG-E / PREAMP. :CANBERRA 2005
COMMENT
TEST DATE : DEC./13/ 96
Temperature : 25 [Cl
TESTED BY : H.M

HAMAMATSU

B-20 8.10 10,000

RC - 367 - REV. 4-4-79

PROJECT TITLE 2/11/97 **CALCULATION SHEET**

PROJECT NO. LAJ

SUBJECT R2693P Voltage Divider PAGE _____ OF _____

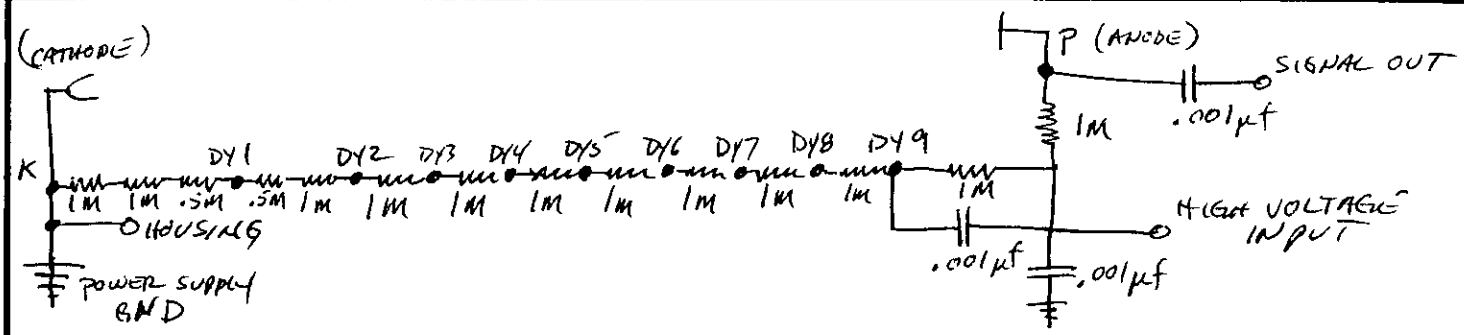

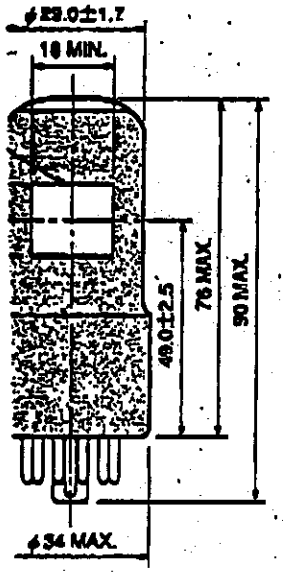

9E
1.B11-65

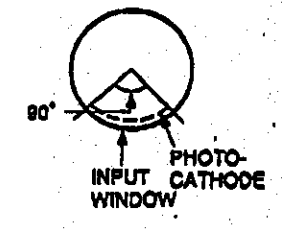

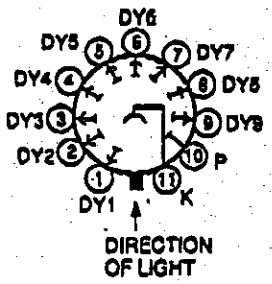

Bottom View

● R2693P

Electrodes	K	Dy1	Dy2	Dy3 .... Dy8	P
Ratio		2.5	1.5	1 1	1

Supply Voltage: 1000Vdc, K: Cathode, Dy: Dynode, P: Anode

PERFORMED BY _____ DATE _____ CHECKED BY _____ DATE _____
(ASME CODE APPLICATIONS ONLY)

REF. DRAWING NO. _____ REF. LOG BOOK PAGE _____

APPENDIX G

TEST PLAN DETAILS

TEST PLAN

To provide the experimental data required for design of the prototype, six series of tests are planned. The six series will address the following issues:

- magnitude of fiber efficiency, p
- stability of fiber response
- thresholding
- coincidence counting
- fiber absorption coefficient, k
- sensitivity to other radionuclides, N_{INT}

Each of these test series is discussed in detail below.

FIBER EFFICIENCY - TEST SERIES A

Objective - The objective of Series A is to experimentally determine p for each of the experimental fiber types.

Approach

Figure 1 shows the components of the set-up required for Series A. A bundle of fibers will be encased in a Teflon tube and interfaced at one end with the HPMT. The bundle assembly will be flooded to various levels with tritiated water of known activity. The output pulses from the HPMT will be input to pulse height analyzer (PHA).

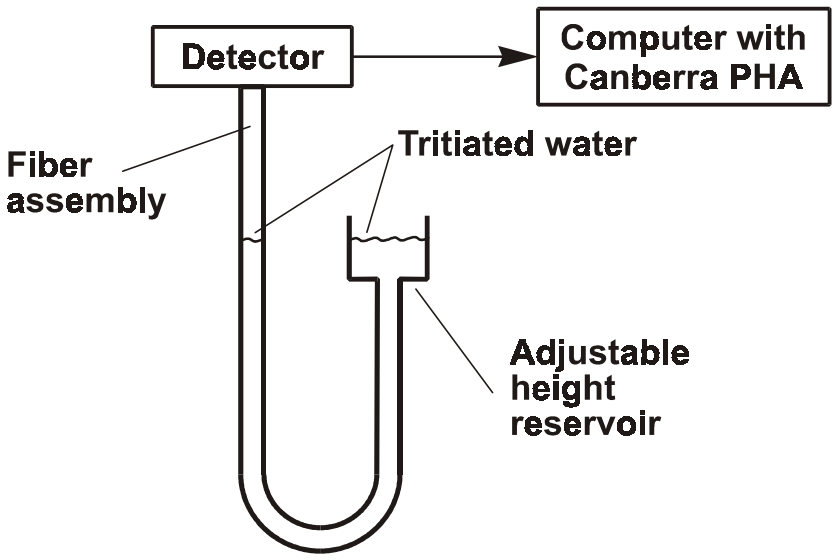

Figure G-1. Setup for Test Series A

The fiber bundles will consist of fibers whose length is L = 50 cm. A bundle of each type of fiber will be prepared and tested. Pulse height spectra will be recorded for fiber immersion lengths of 15, 25, 35, and 45 cm. The "dark count" pulse height spectra will also be recorded.

The integral of the pulse height spectrum over all heights gives the total number of counts which is

$$\int_0^\infty P(h)dh = Ct \qquad (1)$$

where t is the time over which counts are recorded. Integrating the spectrum therefore provides C. Using the experimentally measured value of C in Equation (7.28) the only unknowns are p and k. In Test Series E, we shall independently measure k. Using the Series E value of k, Equation (7.28) can be solved for p.

Since we shall be making measurements of C for four different fiber immersion lengths, k could also be determined from the Series A data. However, the length resolution is not as good as can be obtained in the Series E approach.

TEST SERIES B - STABILITY

Objective - Evaluate the effect of extended water immersion on the response repeatability of the fibers.

Approach

The experimental setup will be the same as in Series A except that the bundle length will be only 15 cm. Three assemblies of each fiber type will be prepared. Pulse height spectra will be recorded for each assembly when first fabricated and again after 10, 20, and 40 days. Between readings, the three assemblies for a given fiber type will be stored as follows:

- one in water at 120 deg. F
- one in water at 60 deg. F
- one in air at room temperature

The assemblies stored in air will act as a control, while the two water-soaked assemblies will be subject to change due to the water.

TEST SERIES C - THRESHOLDING

Objective - To determine the improvement in signal-to-noise ratio possible by optimizing the counter threshold.

Approach

Figure 2 is a block diagram showing the major components of the set-up. The same fiber assemblies used in Test Series A will be used here. The C3866 converts mV level pulses from the detector to 5V pulses that are directly input to a counter. The counter is an 8254 chip resident on a computer plug-in card. The C3866 provides a tunable threshold that allows rejection of all input pulses below the threshold level.

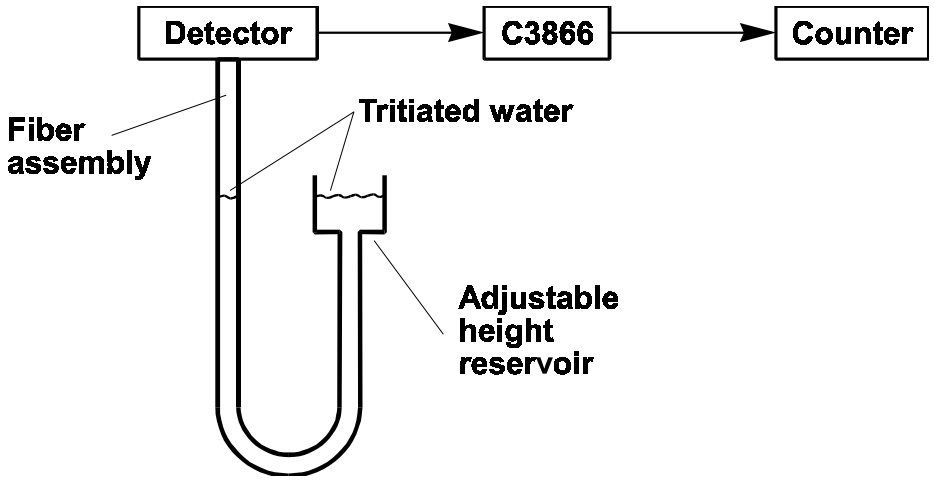

Figure G-2. Set-up for Test Series C

The procedure will be to

- measure the dark-noise count rate as a function of threshold level.
- measure the count rate with the fibers exposed to tritiated water as a function of threshold level.
- calculate from the above measurements the signal-to-noise ratio as a function of threshold to determine the threshold level that optimizes the ratio.

Measurements will be made for each of the three detectors and at three different immersion levels for each of the different fiber types.

TEST SERIES D - COINCIDENCE

Objective - To determine the signal-to-noise ratio that can be achieved by employing coincidence counting between detectors at each end of the fiber bundle.

Approach

Figure 3 is a block diagram showing the major components of the set-up. The thresholds on the two C3866 chips will be set at the optimal levels determined in Series C. The 10 nsec pulses from the outputs of the C3866 chips will first be extended in length to 1) make them compatible with input to the 8254 chip counters, and 2) to simplify the coincidence timing requirements. The delay coil is simply a length of coax cable that provides the proper phasing between the signals from the two detectors. The pulse stretcher for the HPMT signal will be adjustable up to 100 µsec. The length of this pulse is the coincidence window.

The stretched pulses from the two detectors will be input to counters as well as being sent together into an AND gate. The AND gate will output a pulse only when both detectors output a pulse during the coincidence-window time.

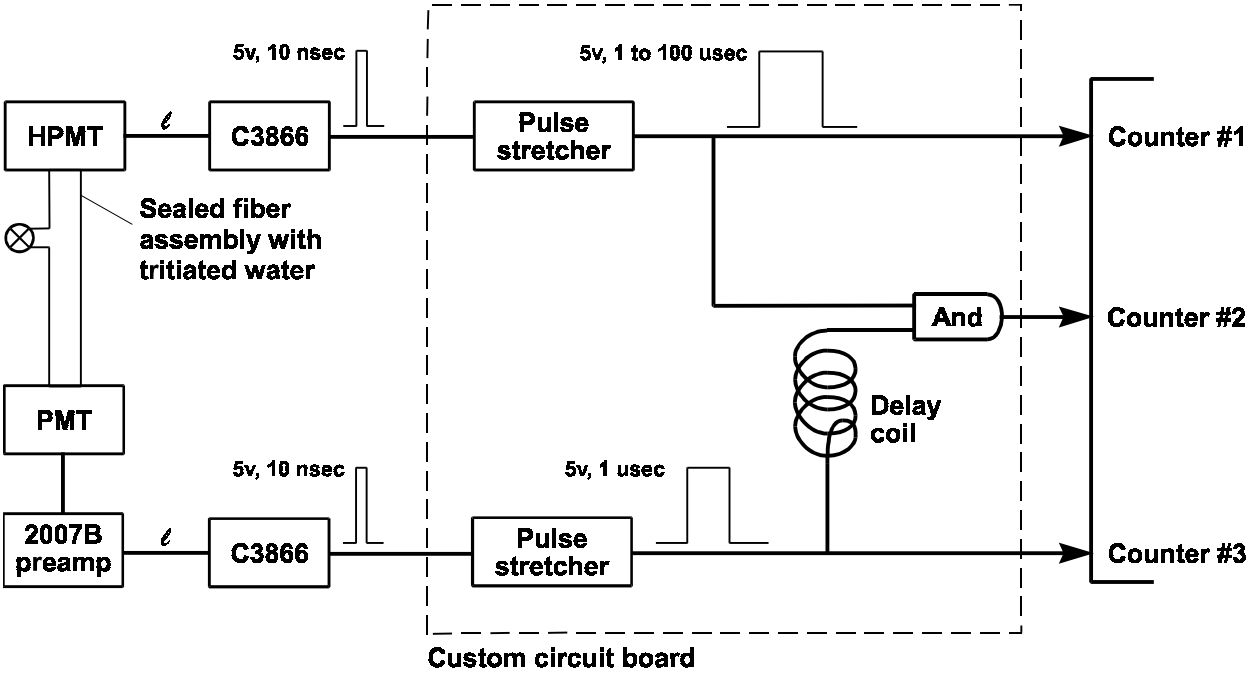

Figure G-3. Set-up for Test Series D

Two different fiber assemblies will be prepared for each fiber type. One assembly will be short (approximately 15 cm fiber length) and the others will be long (approximately 50 cm fiber length).

The procedure will be to record for each fiber assembly

- HPMT counts
- PMT counts
- coincidence counts

for both

- shutter closed (dark counts)
- shutter open to fiber

for coincidence windows of

- 1 µsec
- 10 µsec
- 100µsec

TEST SERIES E - ABSORPTION COEFFICIENT

Objective - Determine the "effective absorption coefficient", k, for each of the fiber types.

Approach

Figure 4 shows the major components of the set-up. The pulsed N_2 laser illuminates the fiber at a right angle to the fiber axis. The 337 nm N_2 laser light is converted by the scintillating dye to photons (characteristic of the dye) that are trapped in the fiber and transmitted to the entrance of the monochromator. The Princeton Instruments analyzer is an electronic spectrometer employing a 700+ element intensified detector.

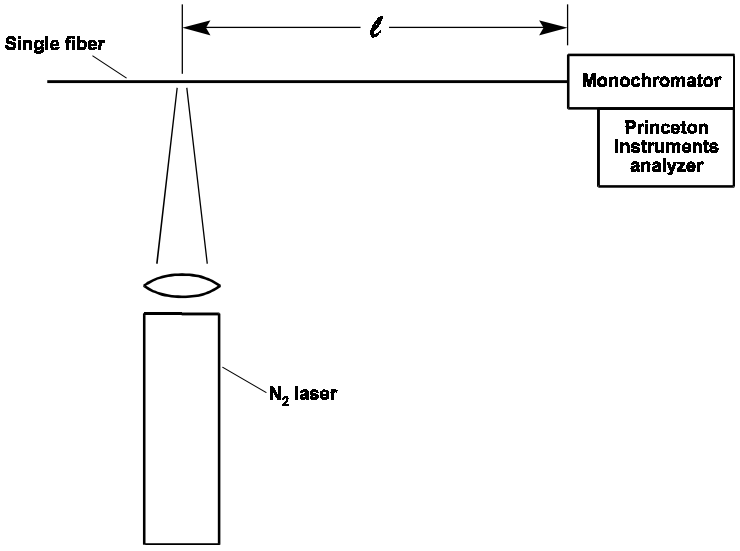

Figure G-4. Set-up for Test Series E

The procedure will be to record spectra of the light delivered to the monochromator for monochromator-to-illumination-point distances

ℓ = 10, 20, 30, 40, 50, 75, and 100 cm.

For each type of fiber, spectra will be recorded for three different fibers.

Each recorded spectrum is a plot of intensity as a function of wavelength. Since the losses are exponential, we can write

$$I(\lambda)d\lambda = I_o(\lambda)\, e^{-k(\lambda)\ell}\, d\lambda \tag{2}$$

And the transmission between ℓ and a point 10 cm from the monochromator is

$$T(\lambda) = \frac{I_o(\lambda)\, e^{-k(\lambda)\ell}}{I_o(\lambda)\, e^{-k(\lambda)10}} = e^{-k[\ell-10]} \tag{3}$$

The effective transmission, i.e. the transmission averaged over all wavelengths, is

$$T = \frac{\int T(\lambda)d\lambda}{\int d\lambda} \equiv e^{-k[\ell-10]} \tag{4}$$

Where k is the effective (averaged over all λ) absorption coefficient. After T (λ) is determined, this data will be used in Equation (4) to find a "best fit" value for k.

Note that k is a constant for small values of ℓ but decreases as ℓ increases. The effective absorption coefficient will be calculated from Equation (4) using values of T (λ) calculated from Equation (3) using the recorded spectral data.

SERIES F - INTERFERENCES

Objective - determine the extent to which the fibers respond to radiation from species other than β's from ^3H.

Approach

Rationale: We have not yet determined what other species and corresponding activity levels are likely to be present in the water samples for which the target tritium monitor is intended. For these preliminary interference tests we have chosen a range of radiations for which we have sources on hand.

Figure 5 is a block diagram showing the components of the set-up.

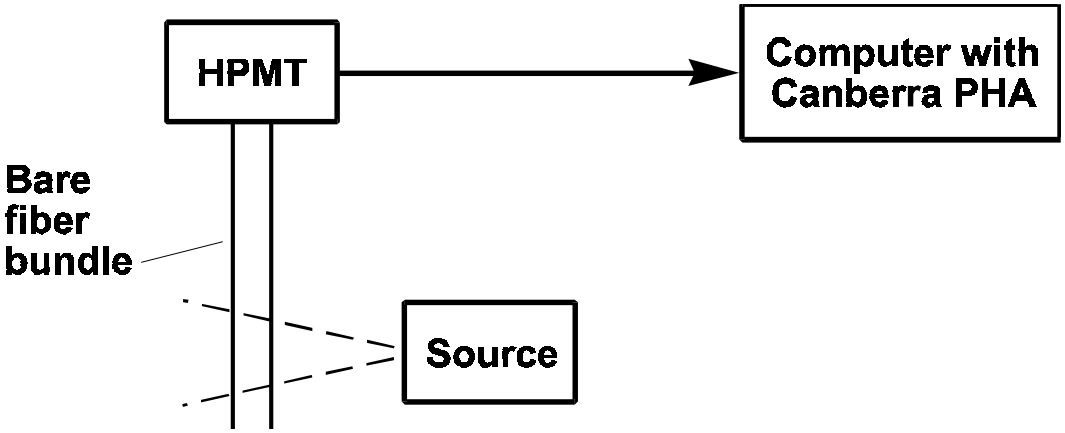

Figure G-5. Set-up for Test Series F

The data will, as in Series A, be pulse height spectra. Sources used will be:

5.44/5.49 MeV α particles from Am-241
546 KeV β particles from Sr-90
622 KeV λ's from Cs-137
59.6 KeV λ's from Am-241

APPENDIX H

CERTIFICATION SHEET ON TRITIATED WATER

CERTIFICATE OF CALIBRATION
BETA STANDARD SOLUTION

Radionuclide	H-3	Customer:	ALLIANCE PHYSICS AND MEASUREMENTS
Half Life:	12.35 ± 0.1 years	P.O.No.:	9701081
Catalog No.:	7000-0014	Reference Date:	1 February 1997 12:00 PST.
Source No.:	553-67	Contained Radioactivity:	0.9432 mCi
		Contained Radioactivity:	34.90 MBq

Description of Solution

a. Mass of solution:	1012 g in 1 liter bottle	
b. Chemical form:	Tritiated water in water	
c. Carrier content:	Not applicable	
d. Density:	0.9982	g/ml @ 20°C.

Radioimpurities

None detected

Radioactive Daughters

None

Radionuclide Concentration

0.9320 µCi/g

Method of Calibration

Weighed aliquots of the solution were assayed using a liquid scintillation counter.

Uncertainty of Measurement

a. Systematic uncertainty in instrument calibration:	±	3.0%
b. Random uncertainty in assay:	±	1.8%
c. Random uncertainty in weighing(s):	±	0.5%
d. Total uncertainty at the 99% confidence level:	±	3.5%

NIST Traceability

This calibration is traceable to the National Institute of Standards and Technology.

Leak Test(s)

See reverse side for Leak Test(s) applied to this source.

Notes

1. IPL participates in an NIST measurement assurance program to establish and maintain implicit traceability for a number of nuclides, based on the blind assay (and later NIST certification) of Standard Reference Materials (As in NRC Regulatory Guide 4.15).

Ann M. Hunn

QUALITY CONTROL

28 Jan 97

Date Signed

ISOTOPE PRODUCTS LABORATORIES
1800 N. KEYSTONE STREET
BURBANK, CALIFORNIA 91504
818·843·7000 FAX 818·843·6168

APPENDIX I

EFFECT OF WATER ON β ENERGY

Introduction

Precontract measurements of fiber efficiency were done by laying the fibers onto a surface of known tritium-beta activity. Because of the proximity, it was assumed that all emitted betas hit the surface of the fiber.

In planning the fiber evaluation tests for the present contract, we used the fiber efficiency results from the precontract tests to estimate the count rate we would get from a bundle of N fibers immersed in tritiated water of known activity. These estimating calculations assumed an exponential absorption with distance from the fiber of the number of beta particles. However, the loss of energy with distance was ignored. It was assumed that as in the case of the initial measurements (which were made with a very short air path) the average beta energy reaching the fiber would be 6 KeV. Tritium beta particles are emitted with a spectrum of energies up to 18 KeV and an average at 6 KeV.

We consider below the energy loss and its effect on the predicted response.

Analysis

Consider a fiber immersed in tritiated water with a volume activity $F\left(\frac{\text{betas}}{\text{sec}\cdot\text{cm}^3}\right)$. The beta particles are emitted isotropically so the activity per unit solid angle will be

$$G = \frac{F}{4\pi}\left(\frac{\text{beta}}{\text{sec}\cdot\text{cm}^3\text{sr}}\right) \tag{1}$$

Using spherical coordinates, we consider a volume element

$$d\upsilon = r^2 dr\, \sin\theta d\theta d\phi \tag{2}$$

A unit area, α, of the fiber surface subtends a solid angle at the volume element of

$$\Omega = \frac{\alpha\cos\theta}{r^2} \tag{3}$$

where θ is the angle between the direction of the volume element and the normal to the fibers surface.

The differential beta rate, dn, in betas per second incident on the fiber area, α, from the differential volume, $d\upsilon$, in the absence of losses can be written

$$dn = G\Omega d\upsilon \tag{4}$$

Since there is, in fact, an exponential loss of beta particles with distance, we can write

$$dn = Ge^{-\frac{r}{\tau}}\Omega d\upsilon \tag{5}$$

where τ is the characteristic absorption length.

Substituting Equations (1), (2), and (3) into (5),

$$dn = \frac{F\alpha}{4\pi}\frac{\cos\theta}{r^2}e^{-\frac{r}{\tau}}r^2\,dr\sin\theta d\theta d\phi \tag{6}$$

which, upon integration, gives the beta arrival rate as

$$n = \frac{F\alpha}{4\pi}\int_{\phi=0}^{2\pi}\int_{\theta=0}^{\pi/2}\int_{r=0}^{\infty}e^{-\frac{r}{\tau}}\cos\theta\sin\theta\,d\theta d\phi dr \tag{7}$$

The angular integration gives

$$\int_0^{2\pi}d\phi\int_0^{\pi/2}\cos\theta\sin\theta\,d\theta = \pi \tag{8}$$

Which, substituted into Equation (7), gives

$$n = \frac{F\alpha}{4}\int_0^{\infty}e^{-\frac{r}{\tau}}dr \tag{9}$$

Dividing through by the fiber area, α, we get the incident beta flux per unit area as

$$R = \frac{n}{\alpha} = \frac{F}{4}\int_o^{\infty}e^{-\frac{r}{\tau}}dr \tag{10}$$

Equation (10) gives the total beta flux at the fiber. We wish to consider now the energy distribution of the beta particles reaching the fiber.

The energy spectrum for tritium beta decay can be written[1]

$$n'(E')dE' = \text{const}\,(E'+m_ec^2)\,(E'^2+2m_ec^2E')^{1/2}\,(E_{max}-E')^2\,dE' \tag{11}$$

1 I. Kaplan, Nuclear Physics, Addison Wesley Publishing Co., Inc., Reading, MA, 1995, p 306.

where m_e is the rest mass of the electron

E_{max} = 18 KeV is the maximum energy in the distribution

and n'(E') dE' is the number of emitted beta particles, whose energy is between E' and E'+dE'.

If we use Equation (12) to normalize the spectrum, we eliminate the constant in Equation (11) and can put the results in terms of the fraction of the beta particles within the energy range

$$n(E')dE' \equiv \frac{n'(E')dE'}{\int_0^{E_{max}} n'(E')dE'} \tag{12}$$

Since F is the total number of beta particles over the entire energy range, the number within the range from E' to E'+dE' is

$$n'(E')dE' = n(E')dE'\ F \tag{13}$$

Beta particles emitted within energy E' do not reach the fiber surface with that same energy due to losses suffered during passage through the intervening water.

Energy loss by a nonrealistic charged particle per unit length of its path in a given substance can be expressed as[2]

$$\frac{-dE}{dr} = \frac{4\pi e^4 N}{m_e v^2} Z \ell n\left(\frac{2m_e v^2}{I}\right) \tag{14}$$

where e is charge of the beta particle
v is the speed of the particle
Z is the atomic number of the substance
N is the electron density of the substance
and I is the average excitation potential of the substance.

Since the maximum energy of the tritium betas is 18 KeV and the rest mass energy of an electron is 511 KeV

$$v_{max}^2 = \frac{18}{511} c^2 = .035c^2 \tag{15}$$

So relativistic effects should be small and Equation (14) should apply.

2 Ibid. p 261

Combining constants, Equation (14) can be expressed

$$\frac{-dE}{dr} = \frac{const}{E} \ell n\left(\frac{2E}{I}\right) \tag{16}$$

The term I is essentially a measure of the energy loss per encounter between the beta and the substance through which it is passing. Assuming that I is small with respect to E, the natural log term of Equation (16) is nearly a constant so that Equation (16) simplifies to

$$-\frac{dE}{dr} = \frac{const}{E} \tag{17}$$

Rearranging and carrying out the integration

$$\int_{E'}^{E(r)} EdE = const \int_{0}^{r} dr \tag{18}$$

we get

$$E^2(r) - E'^2 = const\ r \tag{19}$$

where E' is the energy at the point of emission
and E(r) is the energy after traveling a distance, r, through the water

We determine the constant in Equation (19) by noting that at a distance $r = \rho$, where $\rho \simeq 1\ \mu m$ is the range of the beta particles in water, the energy $E(\rho) = 0$ for even the most energetic of the distribution,

so $$E^2(\rho) = E'^2_{max} + const\,\rho = 0 \tag{20}$$

so $$const = -\frac{E'^2_{max}}{\rho} \tag{21}$$

With Equation (21) in Equation (19), we can express the distance dependence of the energy as

$$E(r) = E'\left(1 - \frac{E'^2_{max}}{E'^2 \rho} r\right)^{1/2} \tag{22}$$

Combining Equations (22) and (13) into (10), we can express the energy spectrum of the beta particles incident on the fiber as

$$R(E)dE = \frac{1}{4}\int_{o}^{\infty} n(E')dE' F e^{-\frac{r}{\tau}} E'\left(1 - \frac{E'^2_{max}}{E'^2 \rho} r\right)^{1/2} dr \tag{23}$$

Finally, incorporating Equations (11) and (12) into (23), and using the numerical values for rest energy and maximum energy, we get

$$R(E)dE = \frac{F}{4}\int_{o}^{\infty}(E'+511)\,(E'^{2}+1022E')^{1/2}\,(18-E')^{2}\,E'\left(1-\frac{18^{2}}{E'^{2}\rho}r\right)^{1/2} e^{-\frac{r}{\tau}}\,dr \qquad (24)$$

Equation (24) gives the energy spectrum of the betas that reach the fiber surface. The average energy is given by

$$\overline{E} = \frac{\int E\,R(E)dE}{\int R(E)dE} \qquad (25)$$

A lotus spreadsheet was set up to numerically integrate Equations (24) and (25). Figure I-1 is a printout showing the format of the spreadsheet and the equations used. Figure I-2 summarizes the results.

The calculated results presented in Figure I-2 are dependent on the assumed values for the range in water and are affected by the assumption made to simplify the energy loss equation. Nevertheless, it is clear that the loss of energy through the water is a significant factor that cannot be ignored.

FILENAME: BETARNGN.WK4

2	B	C	D	E	F	G	H	I	J	K	L	M	N	O	P	Q	R	---	AY	AY
3																		---		
4				r=	0.95	0.95	0.95	0.95	r=	0	0	0.05	0.05	0.1	0.1	0.15	0.15	---	1	1
5	@SUM(B9..B60)			@SUM(E9..E60)			@SUM(I9..I60)			@SUM(L9..L60)		@SUM(N9..N60)		@SUM(P9..P60)				---		
6	62113036		NORMALIZE	6.06884				0			6.069		4.371		3.309		2.508	---		0
7						E(r)=E												---		
8	"n(E')dE"	E'	n(E')dE'	E'n(E')dE'			E	En(E)dE		E	En(E)dE	E	En(E)dE	E	En(E)dE	E	En(E)dE	---	E	En(E)dE
9	0	0	0.000	0.000	-308	0	0	0		0	0	0	0	0	0	0	0	---	0	0
10	1770959	0.5	0.029	0.014	-308	0	0	0		0.5	0.014	0	0	0	0	0	0	---	0	0
11	2366332	1	0.038	0.038	-307	0	0	0		1	0.038	0	0	0	0	0	0	---	0	0
12	2733514	1.5	0.044	0.066	-306	0	0	0		1.5	0.066	0	0	0	0	0	0	---	0	0
13	2971613	2	0.048	0.096	-304	0	0	0		2	0.096	0	0	0	0	0	0	---	0	0
14	3121762	2.5	0.050	0.126	-302	0	0	0		2.5	0.126	0	0	0	0	0	0	---	0	0
15	3206551	3	0.052	0.155	-299	0	0	0		3	0.155	0	0	0	0	0	0	---	0	0
16	3240360	3.5	0.052	0.183	-296	0	0	0		3.5	0.183	0	0	0	0	0	0	---	0	0
17	3233233	4	0.052	0.208	-292	0	0	0		4	0.208	0	0	0	0	0	0	---	0	0
18	3192655	4.5	0.051	0.231	-288	0	0	0		4.5	0.231	2.01	0.103	0	0	0	0	---	0	0
19	3124472	5	0.050	0.252	-283	0	0	0		5	0.252	2.97	0.149	0	0	0	0	---	0	0
20	3033420	5.5	0.049	0.269	-278	0	0	0		5.5	0.269	3.75	0.183	0	0	0	0	---	0	0
21	2923447	6	0.047	0.282	-272	0	0	0		6	0.282	4.45	0.209	1.9	0.089	0	0	---	0	0

B9= (C9+511)*(C9^2+2*511*C9)^0.5*(18-C9)^2*(C$10-C$9)

D9= +B9/B6

E9= +C9*D9

F9= (C9^2-18^2*F$4)

G9= +F9*@IF(F9<0,0,1)

H9= +G9^0.5

I9= +H9*$D9

60	0	18	0.000	0.000	16.2	16.2	4.02	0		18	0	17.5	0	17.1	0	16.6	0	---	0	0

Figure I-1. Spreadsheet Format Used to Integrate Eqs. (24) and (25)

SUM	SUM	SUM
1.02	1.02123	6.11

E[avg]	1.003 Kev	6.00 Kev

r	E[avg]	Rdr	E[avg]Rdr	E'	RE'dr
0.00	6.0688	0.05	0.3034	6.00	0.30
0.05	4.3713	0.05	0.2079	6.00	0.29
0.10	3.3089	0.05	0.1497	6.00	0.27
0.15	2.5082	0.04	0.1079	6.00	0.26
0.20	1.8870	0.04	0.0772	6.00	0.25
0.25	1.4122	0.04	0.0550	6.00	0.23
0.30	1.0764	0.04	0.0399	6.00	0.22
0.35	0.7839	0.04	0.0276	6.00	0.21
0.40	0.5743	0.03	0.0192	6.00	0.20
0.45	0.3960	0.03	0.0126	6.00	0.19
0.50	0.2793	0.03	0.0085	6.00	0.18
0.55	0.1886	0.03	0.0054	6.00	0.17
0.60	0.1198	0.03	0.0033	6.00	0.16
0.65	0.0673	0.03	0.0018	6.00	0.16
0.70	0.0383	0.02	0.0010	6.00	0.15
0.75	0.0196	0.02	0.0005	6.00	0.14
0.80	0.0086	0.02	0.0002	6.00	0.13
0.85	0.0029	0.02	0.0001	6.00	0.13
0.90	0.0005	0.02	0.0000	6.00	0.12
0.95	0.0000	0.02	0.0000	6.00	0.12
1.00	0.0000	0.02	0.0000	6.00	0.11
1.05	0.0000	0.02	0.0000	6.00	0.10
1.10	0.0000	0.02	0.0000	6.00	0.10
1.15	0.0000	0.02	0.0000	6.00	0.09
1.20	0.0000	0.02	0.0000	6.00	0.09
1.25	0.0000	0.01	0.0000	6.00	0.09
1.30	0.0000	0.01	0.0000	6.00	0.08
1.35	0.0000	0.01	0.0000	6.00	0.08
1.40	0.0000	0.01	0.0000	6.00	0.07
1.45	0.0000	0.01	0.0000	6.00	0.07
1.50	0.0000	0.01	0.0000	6.00	0.07
1.55	0.0000	0.01	0.0000	6.00	0.06
1.60	0.0000	0.01	0.0000	6.00	0.06
1.65	0.0000	0.01	0.0000	6.00	0.06
1.70	0.0000	0.01	0.0000	6.00	0.05
1.75	0.0000	0.01	0.0000	6.00	0.05
1.80	0.0000	0.01	0.0000	6.00	0.05
1.85	0.0000	0.01	0.0000	6.00	0.05
1.90	0.0000	0.01	0.0000	6.00	0.04
1.95	0.0000	0.01	0.0000	6.00	0.04
2.00	0.0000	0.01	0.0000	6.00	0.04
2.05	0.0000	0.01	0.0000	6.00	0.04
2.10	0.0000	0.01	0.0000	6.00	0.04
2.15	0.0000	0.01	0.0000	6.00	0.03
2.20	0.0000	0.01	0.0000	6.00	0.03
2.25	0.0000	0.01	0.0000	6.00	0.03

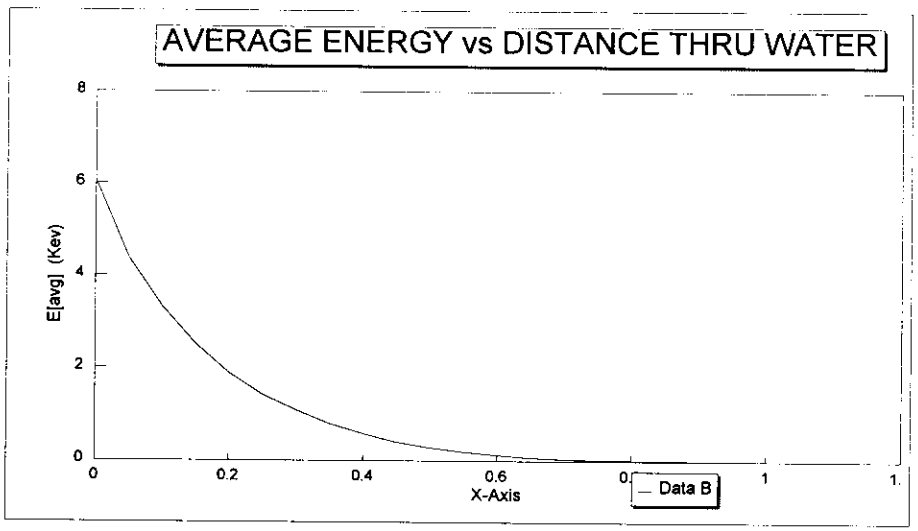

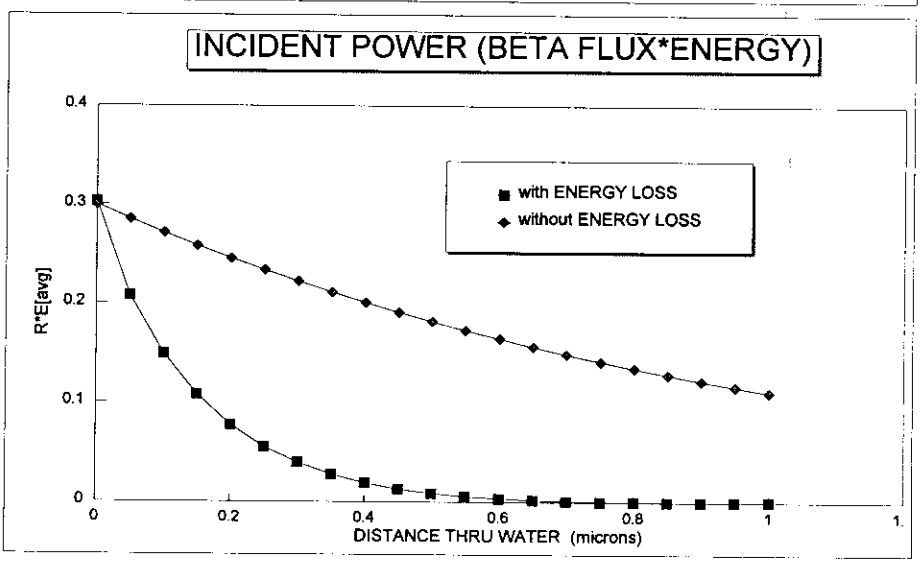

Figure I-2. Results From Numerical Integration of Eqs. (24) and (25)